國立交通大學

多媒體工程研究所

碩 士 論 文

光束構成法之腦部活動相關性時空造影

Beamformer-based Spatiotemporal Imaging of Correlated Brain Activities

研 究 生：陳乙慈

指導教授：陳永昇　博士

中 華 民 國　九 十 八　年 六 月

光束構成法之腦部活動相關性時空造影
Beamformer-based Spatiotemporal Imaging of Correlated Brain Activities

研 究 生：陳乙慈　　Student：I-Tzu Chen

指導教授：陳永昇　　Advisor：Yong-Sheng Chen

國 立 交 通 大 學

多 媒 體 工 程 研 究 所

碩 士 論 文

A Thesis

Submitted to Institute of Multimedia Engineering

College of Computer Science

National Chiao Tung University

in partial Fulfillment of the Requirements

for the Degree of

Master

in

Computer Science

June 2009

Hsinchu, Taiwan, Republic of China

中華民國九十八年六月

Beamformer-based Spatiotemporal Imaging of Correlated Brain Activities

A thesis presented

by

I-Tzu Chen

to

Institute of Multimedia Engineering

College of Computer Science

in partial fulfillment of the requirements

for the degree of

Master

in the subject of

Computer Science

National Chiao Tung University

Hsinchu, Taiwan

2009

Beamformer-based Spatiotemporal Imaging of Correlated Brain Activities

國立交通大學
研究所碩士班

論文口試委員會審定書

本校 多媒體工程 研究所 陳乙慈 君

所提論文:

光束構成法之腦部活動相關性時空造影

Beamformer-based Spatiotemporal Imaging of Correlated Brain Activities

合於碩士資格水準、業經本委員會評審認可。

口試委員：

指導教授：

所　　長：

中 華 民 國 九十八 年 六 月 十 日

國 立 交 通 大 學

博碩士論文全文電子檔著作權授權書

（提供授權人裝訂於紙本論文書名頁之次頁用）

本授權書所授權之學位論文，為本人於國立交通大學多媒體工程研究所 _____組， 97 學年度第 2 學期取得碩士學位之論文。

論文題目：光束構成法之腦部活動相關性時空造影
指導教授：陳永昇

■ 同意

本人茲將本著作，以非專屬、無償授權國立交通大學與台灣聯合大學系統圖書館：基於推動讀者間「資源共享、互惠合作」之理念，與回饋社會與學術研究之目的，國立交通大學及台灣聯合大學系統圖書館得不限地域、時間與次數，以紙本、光碟或數位化等各種方法收錄、重製與利用；於著作權法合理使用範圍內，讀者得進行線上檢索、閱覽、下載或列印。

論文全文上載網路公開之範圍及時間：

本校及台灣聯合大學系統區域網路	■ 中華民國 100 年 8 月 19 日公開
校外網際網路	■ 中華民國 102 年 8 月 19 日公開

■ 全文電子檔送交國家圖書館

授 權 人：陳乙慈

親筆簽名：陳乙慈

中華民國 98 年 8 月 19 日

國 立 交 通 大 學

博碩士紙本論文著作權授權書

（提供授權人裝訂於全文電子檔授權書之次頁用）

本授權書所授權之學位論文，為本人於國立交通大學多媒體工程研究所 _____組， 97 學年度第 2 學期取得碩士學位之論文。

論文題目：光束構成法之腦部活動相關性時空造影
指導教授：陳永昇

■ 同意

本人茲將本著作，以非專屬、無償授權國立交通大學，基於推動讀者間「資源共享、互惠合作」之理念，與回饋社會與學術研究之目的，國立交通大學圖書館得以紙本收錄、重製與利用；於著作權法合理使用範圍內，讀者得進行閱覽或列印。

本論文為本人向經濟部智慧局申請專利(未申請者本條款請不予理會)的附件之一，申請文號為：_____，請將論文延至____年____月____日再公開。

授 權 人：陳乙慈

親筆簽名：陳乙慈

中華民國 98 年 8 月 9 日

國家圖書館
博碩士論文電子檔案上網授權書

（提供授權人裝訂於紙本論文本校授權書之後）

ID:GT079657508

本授權書所授權之論文為授權人在國立交通大學多媒體工程研究所 97 學年度第 2 學期取得碩士學位之論文。

論文題目：光束構成法之腦部活動相關性時空造影
指導教授：陳永昇

茲同意將授權人擁有著作權之上列論文全文（含摘要），非專屬、無償授權國家圖書館，不限地域、時間與次數，以微縮、光碟或其他各種數位化方式將上列論文重製，並得將數位化之上列論文及論文電子檔以上載網路方式，提供讀者基於個人非營利性質之線上檢索、閱覽、下載或列印。

※ 讀者基於非營利性質之線上檢索、閱覽、下載或列印上列論文，應依著作權法相關規定辦理。

授權人：陳乙慈

親筆簽名：陳乙慈

民國 98 年 8 月 19 日

中文摘要

大部分的研究都同意腦部的神經元會集體有著同步的活動特徵。過去的研究指出時序上的相關性與腦部區域間的溝通息息相關。在腦磁圖儀與腦電圖儀的研究中，一般會透過神經活動的振盪訊號來研究區域間的功能關聯性。然而，神經活動的時序訊號一般都是包含跨頻帶的資訊，所以從一般性的同步來研究區域間的功能相關性是很重要的。

在這篇論文中，我們提出了一個以光束構成法為基礎的方法來估算腦部活動相關性。透過我們的方法，可以揭露神經互聯網的活動情形。神經互聯網間是利用類似的時序特徵訊號來交換資訊。一但使用者指定了一個區域，我們便可分析該區域中最具代表性的特徵訊號，並找出具有相似特性的區域的分布情況。原則上，將腦中的位置兩兩用我們的方法計算，就可以找出所有可能的神經互聯網。

我們的方法利用最大相關性準則來最大化參考區域和全腦的其他區域的活動相關性。透過這個準則，我們可以用閉形式解的方式正確地解析出訊號源電偶極方向，進而有效的決定對應各個位置的空間濾波器。我們的方法可以計算出相關性分布圖，從這個圖可以看出與參考區域有顯著相關性的腦部區域。

實驗證明了我們的方法確實可以正確的計算出腦部中有相關活動的區域。與過去傳統的腦部定位方法不同的是，我們專注在找出有著與參考訊號類似的時序訊號特徵的腦部皮質區域。除此之外，我們也將方法應用到實際由人腦量測的實驗證明我們方法的可行性。在鏡像神經元實驗中，大多我們找出有相關性的區域都曾在之前情緒處理、臉部感知和鏡像神經原系統的研究中發現。除此之外，我們還可以提供這些與神經互聯網相關的區域在時間上的資訊。

簡言之，我們提出的方法是利用腦磁波來研究腦部活動間的相關性。並建立一個腦部活動動態的時空造影與顯示系統。使用者給定一個神經網路中的區域來當作參考的區域，我們的方法可以推估在每個時間點與參考的區域相關的區域分布情形，進而揭露出這個時間網路的活動情況。

Abstract

It has been widely accepted that neurons in the human brain collectively have synchronous patterns of activities. The past findings have suggested that temporal correlation may relate to the communications between the distributed areas. There are some studies in magnetoencephalography and electroencephalography that analyze the functional connectivity between cortical areas using the oscillatory features of neuronal activity. However, temporal dynamics of neuronal activities is generally consisted of cross-frequency components. Therefore, it is also important to directly investigate the functional connectivity as well as general synchronization.

In this thesis, we have proposed a beamformer-based imaging method of correlated brain activities that can reveal the neural network with similar temporal patterns for information exchange. The method can identify the correlation distribution referred to a specified position, called the reference region. In principle, we can apply our method on all pairs of grid points to identify all possible neural networks of correlated activities.

Our method exploits a maximum-correlation criterion that maximizes the significant level of correlation between the reference region and the entire brain volume. The maximum correlation criterion helps to analytically and accurately determine the dipole orientation in a closed-form manner and thus determine the spatial filter very efficiently for each position. The correlation map can be calculated to reveal cortical regions with significant similarity to the reference position in the brain.

The experiments with simulation data demonstrated that our method can accurately determine the correlated regions. Different from the conventional source localization method, we focus on the areas which have the similar temporal patterns with the reference signal. We demonstrated the applicability of the proposed method on real data. In the mirror neuron experiment, most of the regions we revealed are reported by the previous findings of emotional processing, face perception and the mirror neuron system. Moreover, we can provide the time information about when these regions are correlated to the neural network.

In summary, the proposed method can be used to directly study dynamics of correlation brain areas based on electromagnetic recordings of brain activities. Given the reference region as one of the areas in the neural network, our method can estimate the correlated regions at each time point and thus reveal the dynamic behavior of the neural network.

致謝

碩士班的生活已經結束了，這兩年過得相當充實且快樂。首先我要感謝指導老師陳永昇和陳麗芬老師，你們對於研究的熱忱及不輕放任何細節的態度是對我最好的身教，也謝謝你們非常能容忍像我怎麼盧的人，願意在假日還陪我討論實驗的結果。還有陽明的宏哲大師，謝謝你提供給我這麼好的實驗資料，並在百忙之中與我討論，讓我的論文能夠有個漂亮的句點。

感謝實驗室的學長姐和同學們，與你們相處的日子真是太白癡了。尤其是MEG組的老大慧伶，不論是研究討論、找尋美食、瘋狂玩樂等事，你都是最佳良伴。當然還有一起打拼的夥伴們，公主大人小萱萱、白爛湊熱鬧的發亮二人組、還有假音戰士sheep、來無影去無蹤的育宏，有你們在的日子，實驗室總是熱鬧滾滾，與你們一起湊熱鬧總能讓我打結的腦袋重新恢復運轉。

謝謝學中，有了你的陪伴討論，讓我更能穩定心神，堅定的朝目標邁進。最後要謝謝我的家人，你們對我的支持是讓我前進的最大動力。

E S A
1896

Contents

List of Figures vii

List of Tables ix

1 Introduction 1
- 1.1 Correlated Brain Activities . . . 2
- 1.2 Magnetoencephalography . . . 7
  - 1.2.1 Background . . . 7
  - 1.2.2 Related work of the source activities at cortical level . . . 9
- 1.3 The synchronization phenomena in MEG . . . 11
- 1.4 Thesis scope . . . 13
- 1.5 Thesis organization . . . 13

2 Method 15
- 2.1 Scalar beamformer . . . 16
- 2.2 Imaging of the brain activities correlated to the reference signals . . . 18
- 2.3 Maximum correlation beamformer . . . 19
- 2.4 Reference region . . . 21
- 2.5 Studying the interactions . . . 22

3 Experiment Results 25
- 3.1 Material . . . 26
  - 3.1.1 Anatomical Data . . . 26
  - 3.1.2 MEG Data . . . 26
- 3.2 Data Preprocessing . . . 27
- 3.3 Experiments . . . 29
  - 3.3.1 Simulation data 1 . . . 29
  - 3.3.2 Simulation data 2 . . . 29
  - 3.3.3 Real data - happy mirror neuron . . . 34

4 Discussion **81**
4.1 Simulation data 82
4.2 Real data - happy mirror neuron 82

5 Conclusion **91**

Bibliography **93**

List of Figures

1.1 The partition of the human brain 2
1.2 The broadmann area 3
1.3 The binding problem 4
1.4 Action potential and local field potential 6
1.5 Solution to the inverse problem calculated by MCB algorithm. 11
1.6 The time-frequency map of the estimated sources by maximum contrast beamformer in the experiment of lifting left index finger 12

2.1 The concept about unit-gain and minimum variance constraints in beamformer. 17
2.2 The progress for revealing neural network 23

3.1 happy mirror neuron paradigm 28
3.2 Preprocessing for MEG recordings. 29
3.3 groundtruth 30
3.4 simu1 result 30
3.5 groundtruth 31
3.6 ICA 32
3.7 Result of ICA 33
3.8 Result of Slide Window 34

4.1 filtered signal 83
4.2 face perception and attention systems 84
4.3 the areas of mirror neuron system 86

E S A
1896

List of Tables

3.1 The parameters of maximum contrast beamformer on the happy mirror neuron experiment 35
3.2 time interval 36
3.3 The information of reference region at LIFG on three conditions 37
3.4 The result of the reference region at LIFG on imitation condition 38
3.5 The result of the reference region at LIFG on observation condition 44
3.6 The result of the reference region at LIFG on execution condition 52
3.7 The information of reference region at LIFG on three conditions 62
3.8 The result of the reference region at LIFG on imitation condition 63
3.9 The result of the reference region at LIFG on imitation condition with different threshold 67
3.10 The result of the reference region at LIFG on observation condition 71
3.11 The result of the reference region at LIFG on execution condition 76

4.1 The result of the reference region at LIFG on imitation, observation and execution condition 87

E S A
1896

Chapter 1

Introduction

1.1 Correlated Brain Activities

The brain is the most important component of human to coordinate the other parts of human body, and it is the center of the human nervous system and is the most complex organ in any creature on earth. The human brain has been estimated to contain 10^{12} neurons, of which about 10^{11} are cortical pyramidal cells. These cells pass signals to each other via around 10^{15} synaptic connections [1]. Human brain is often analogized with the most powerful computer, which is compared as 'computer' capable of processing 10^{12} Gigabits of 'information' per second [2]. At the end of the 18th century, the electric brain signal was found. When we perform a task, the neurons at corresponding cortex activate. The entire excited neuron can be thought of as a battery, and the potential difference causes a current flow, therefore the information interchange between the neurons. As neurons become active, they induce changes in blood flow and oxygenation levels.

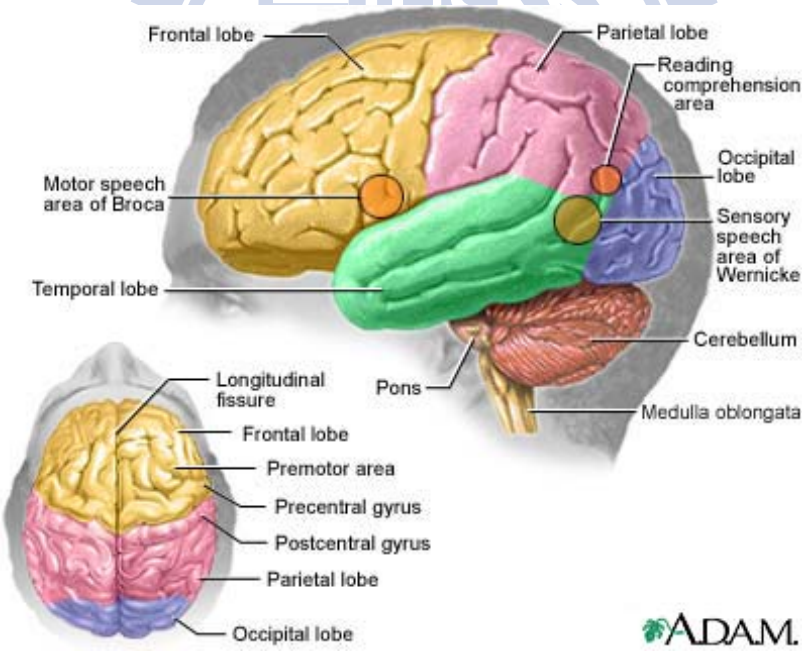

Figure 1.1: The major areas of the human brain - frontal lobe, partial lobe, occipital lobe and temporal lobe.

Our brain can be separate to several parts according to their anatomical structure or the

function which were suggested by past findings. It can be separated to four major area which have one or more specific functions. The major separation is frontal lobe, partial lobe, occipital lobe and temporal lobe as Figure 1.1. The function of the frontal lobe is mainly about thinking, planning, and central executive function, motor execution. Then the function about parietal lobe is known as a somatosensory perception, integration of visual and somatospatial information. And the temporal lobe is charged about the language function, auditory perception and is involved in long term memory and emotion. The last, the occipital lobe work for visual perception and processing.

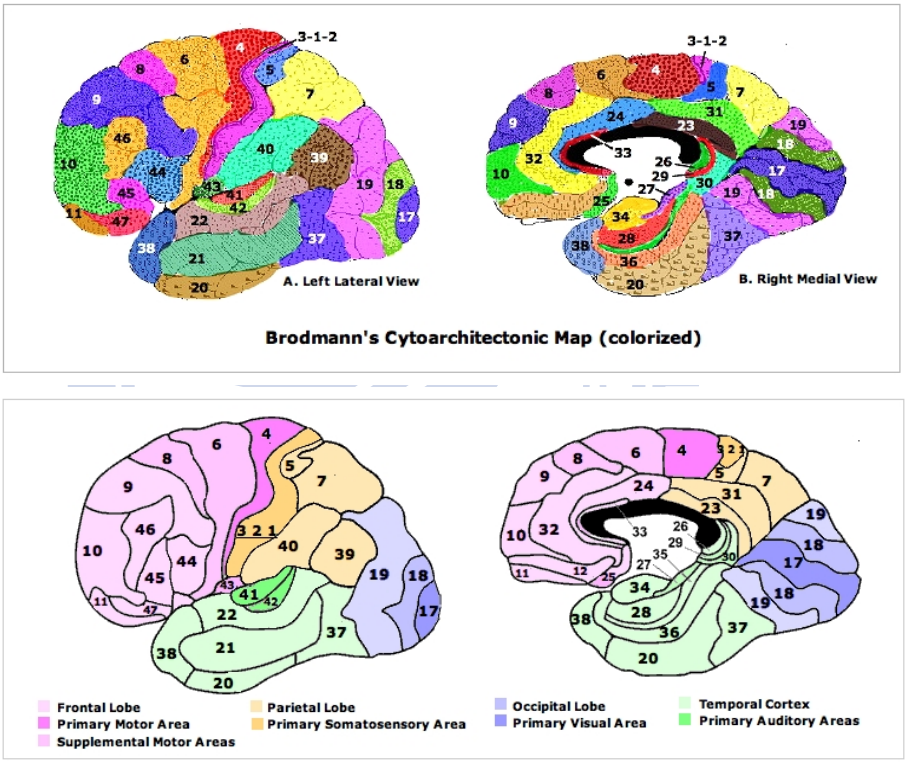

Figure 1.2: The broadmann areas of the lateral and medial side of human brain.

Those major areas introduced above are separated in rough. One of the most common separation is brodmann area as Figure 1.2. It was defined by Korbinian Brodmann. The human brain is separated to 47 areas according to the organization of neurons. However many studies analyze the function of each partition. For example, the broadmann area 45 is well-known broca area which is responsible for speech production.

Even many studies have revealed the functions of the partitions of brain, and traditional research has focused on how neurons represent and the mechanisms. However, human's activities can't accomplish by only activate dependently at just one, two specific areas with one or two times can accomplish the activities. It need the communication between neurons, no matter local communication or long-rance communication, to accomplish a task, even the simple task in our opinion like lifting our finger. The precise coordination of many brain areas is one of the important reasons why our brain own such amazing processing capabilities.

Figure 1.3: Different features are processed by deferent location of the brain, then the brain combine the information to a perception.

For example, the past finding has suggested a so-called "binding problem" that is the problem of combining different features of an object, which are represented in different location in the brain as the Figure 1.3. For multiple objects, it is a particularly complex problem for binding the right features of each object to a representation [3–5]. On the other word, the binding problem is about feature integration, perceptual segmentation, attention, memory, motor control, sensorimotor integration, language processing and logical inference [6]. To handle a cognitive function or perception of and action in a complex environment require the parallel processing of information related to different objects or events. Therefore, neural communication is exiting and important [7].

However, what is the mechanism of the binding problem, or how neuron communicate? Given that the activity evoked by the features comprising an object is distributed,

some mechanism is necessary to identify the members of a representation as belonging together and to distinguish them from other representations that may be present at the same time. what is the mechanism of the binding problem, or how neuron communicate would distinguish it from all other neuronal activity present simultaneously in the cortical network?

The past findings have suggested that temporal correlation may relate the communications and the information flow between the distributed areas [8]. The temporal correlation hypothesis proposes that neural assemblies consist of active neural units that are grouped together based on temporal correlation [9–11]. The temporal binding is that signals of neurons that are to be grouped together are correlated in times. It has been suggested that the binding problem may be solve by a mechanism which exploits the temporal aspects of neuronal activity [9]. The synchronization phenomena predict by temporal binding hypothesis have been documented for several years [6, 11]. In both cortical and subcortical centers, neuron can synchronize their discharge with a precision in the millisecond range [6, 11–13] in sensory-motor system and perceptual and cognitive functions.

Synchronization includes oscillation, phase synchronization and general synchronization where general synchronization is a broad synchronization. Oscillation is a common approach toward modeling such temporal binding to group the neural assemblies. The dynamical linking of different neural structures via oscillatory coupling was demonstrated first by animal experiments [13]. It has also been noticed that responses often exhibit an oscillatory patterning which is best revealed by recording jointly the activity of several adjacent cells [14].

Recording the activity of neurons, it require electrodes to be inserted through the skull into the brain. Such electrodes can record extracellular single-neuron activity, multi-unit activity and local field potential (LFP). Single- and multi-unit activity reflects the action potentials. LFPs represent the aggregate activity of a population of neurons located close to the electrode (spatial average across many neurons) as shown in Figure 1.4, consistent effects across a local population of neurons are enhanced [7,15,16]. For several years, many animal studies report the synchronization phenomena at single neural or LFP levels [6].

On the contrast to invasive modalities, there are several ways to study on brain, through noninvasive imaging of the electrophysiological, hemodynamic, metabolic, and neuro-

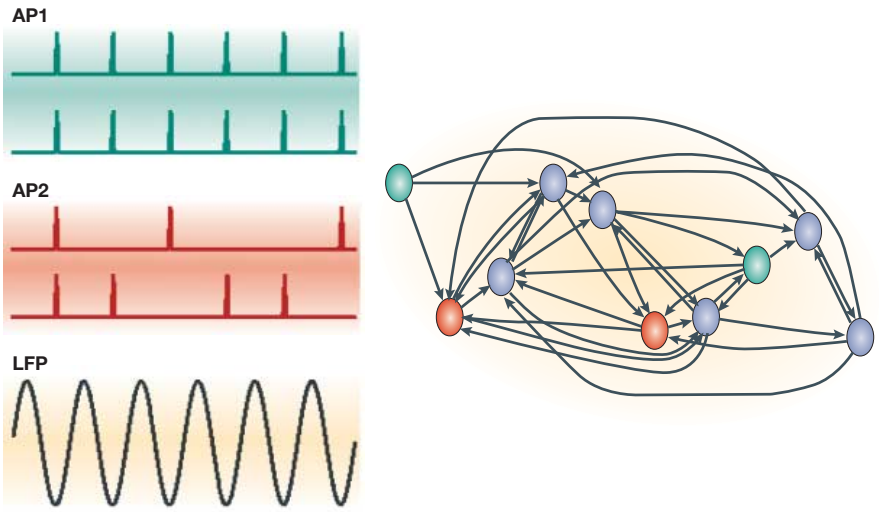

Figure 1.4: Action potentials are AP1 and AP2, and local field potentials (LFPs) are LFP which represent the spatial average of a populations of neurons (right panel) [15].

chemical processes, instead of anatomizing. 'Noninvasive' means without physical harm. There are four major non-invasive modalities, which are Magnetoencephalography (MEG), Electroencephalography (EEG), functional Magnetic Resonance Imaging (fMRI) and Near-Infrared Reflectance Spectroscopy (NIRS). These techniques record a spatial summation of LFPs [15].

The functional magnetic resonance imaging (fMRI), measures blood oxygen level dependent (BOLD) component of the hemodynamic response that is associated with local neural activity with spatial resolution as high as 1-3 mm. Several studies shows some evidence the correlation between LFP and BOLD, and this evidence indicates that the firing activity of a neuronal population will, in general, be proportional to the BOLD response [16]. Therefore, functional magnetic resonance imaging (fMRI) measure the spatial summation of LFPs. Even though it is a very promising approach to investigate the neural activity and the cortico-cortical correlation. However, the temporal resolution is insufficient to observe the details of the communications while the temporal resolution is limited by the relatively slow hemodynamic response, approximately 1s [17].

Another popular non-invasive technique, the scalp MEG/EEG/event-related potential

(ERP), is also thought to reflect the summed electrical effects of excitatory synaptic neurotransmission in large populations of neurons. MEG and EEG are two complementary technique that measure the magnetic induction outside the head and the scalp electric potential those produced by the neuron activities inside the brain. Therefore, the character of higher temporal resolution compared to fMRI allows the studies of the dynamics of neuron network on the order of tens of millisecond. These techniques non-invasively record the neural activity at high temporal resolution; Therefore, they are a proper modality to analyze the neural communication at cortical level.

However, the analysis of neural communication at cortical level based on non-invaseve MEG/EEG need some steps. We introduce the background knowledge in later section1.2 and then introduce how to estimate the cortical neural activity.

1.2 Magnetoencephalography

1.2.1 Background

At the end of the 18th century, the electric brain signal was found. When we perform a task, the neurons at corresponding cortex activate. The entire excited neuron can be thought of as a battery, and the potential difference causes a current flow, therefore the information interchange between the neurons. As neurons become active, they induce changes in blood flow and oxygenation levels, which is imaged by fMRI. fMRI can monitor the hemodynamic changes with spatial resolution as high as 1-3 mm; however temporal resolution is limited by slow hemodynamic changes. Therefore, fMRI has poor temporal resolution compared with MEG and EEG.

MEG and EEG are two complementary technique that measure the magnetic induction outside the head and the scalp electric potential those produced by the neuron activities inside the brain. Therefore, the character of higher temporal resolution compared to fMRI allows the studies of the dynamics of neuron network on the order of tens of millisecond.

Nevertheless, low signal to noise ratio (SNR), and inherent ill-posed problem are two major difficult in the studies of brain functionality by using modality of MEG and EEG. First, electrical brain signal is very tiny compared to the environmental noise. Typical EEG

scalp voltages are on the order of tens of microvolts, and characteristic magnetic induction produced by neural currents is extraordinarily weak, on the order of several tens of femtoTeslas. Therefore, MEG measure induced magnetic field via superconducting quantum interference devices (SQUIDs), a highly sensitive amplifier, inside a magnetically shielded room. So, compared to EEG, MEG has higher signal to noise ratio (SNR). Second, the recording of MEG and EEG are induced by sources distributed the whole head. Even with infinite MEG/EEG sensors, a non-ambiguous solution to source localization of the neuronal activities inside the brain would be possible, let alone the number of electrodes of MEG and EEG sensors usually ten or a few hundreds.

Given the recording of MEG/EEG, the inverse problem involves estimation of the properties of the current sources within the brain that produced these signals. We can acquire the concept of inverse problem from the Bayesian statistic framework.

$$P(x|y) = \frac{P(x)P(y|x)}{P(y)} \tag{1.1}$$

$P(x|y)$ denotes the conditional probability of x given y, also called the posterior probability because it is derived from or depends upon the specified value of y. $P(y|x)$ is the conditional probability of y given x. $P(y)$ is the prior or marginal probability of y, and acts as a normalizing constant. $P(x)$ is the prior probability or marginal probability of x. It is 'prior' in the sense that it does not take into account any information about y. Apply to the MEG inverse problem and let x represent the distribution of the sources inside the brain and y represent the recordings from the MEG/EEG sensors. $P(x|y)$ can describe the inverse problem that to get the distribution of the sources while given MEG recordings. From the Bayesian equation, we can simplify the inverse problem as the form of the right side of the equal sign if we want to know parameters of the source distribution from the recordings. Therefore, $P(y|x)$ is the key to the solution. $P(y|x)$ describes the probability of the recordings when given parameters of the source distribution and that is the forward problem [18, 19].

The inverse problem is to estimate the neuronal activities in the brain based on MEG/EEG recordings [17]. As mention above, involving estimation of the properties of the signal induced by the current source inside the brain help to solve inverse problem. Before we can make such an estimate, we must first understand and solve the forward problem, in

which we compute the scalp potentials and external fields for a specific set of neural current sources.Therefore, the inverse problem can be transformed to the form Eq 1.1. But the inverse problem is a inherent ill-pose problem which has infinite solutions. Lots of algorithms with difference constraint had been proposed to solve the inverse problem.

1.2.2 Related work of the source activities at cortical level

Approximations such as the equivalent current dipole (ECD) model [17, 18, 20, 21], assumptions such as a fixed number of dipoles within an epoch is obtained by the least squares source estimation which is one of the most widely-used method. It finds out he best solution by nonlinear search to minimizing error between the induced electromagnetic field by ECDs and the MEG/EEG recordings. However, It is difficult to decide the prior number of the sources and it may trap in local minimum. Multiple Signal Classification (MUSIC) [22–24] is another kind of method which can avoid trapping in local minimum through by scanning the region of interest and determining the locations with peak projections of forward models in the signal subspace. Minimum Norm Estimation (MNE) [25–27] will estimate the brain activities on the cortical surface, so it set dipole orientation either to be on the tangential plane or normal to the local cortical surface. But the major problem is that because of the minimum norm constraint, the result will tend to emphasize the cortical regions closer to the MEG sensors [28].

Recently, beamformer is one of the most promising solutions to the inverse problem. [29]. Beamformer performs a spatial filter on recordings of MEG/EEG to filter out the signal at the targeted location, acting as a virtual sensor to measure the signal with a specific orientation. Beamformer can obtain the activities of the targeted location and suppress the influence contributed from other sources by imposing the unit-gain constraint and minimum variance criterion. Given a unit dipole with specified position and orientation, we can calculate a spatial filter from the data covariance matrix and the lead field of the dipole. The neuronal activity of the dipole at the specified position can be obtained by applying this spatial filer on the recordings of MEG/EEG. By repeating the procedure for each position inside the brain, we can obtain the neuronal activities of the whole brain.

Two kinds of beamformer, vector-type beamformer [30] and scalar-type beamformer,

have be studied. [31, 32]. The vector-type beamformer decomposes the dipole orientation into three orthogonal components, each one with a fixed orientation. Every component has its own spatial filter calculated individually. Linearly constrained minimum variance (LCMV) [30] is one of the vector beamformer and it sums the results probed on three directions. Only one spatial filter is used for each specific position in scalar-type beamformer. Scalar-type beamformer determines the direction by maximizing the pseudo Z value. Compared to vector-type beamformer, the major advantage of scalar-type beamformer is that the activity distribution is more focal and higher signal-to-noise ratio [32,33]. But using vector-type beamformer is more efficient to calculate the spatial filter because all the procedures involved are deterministic.

In the scalar-type beamformer, only when the dipole orientation is accurate, the effective spatial filter can be calculated. Therefore, it is essential to accurately determine the dipole orientation [33,34]. One way to determine the dipole orientation is to use the normal of cortical surface [34]. But the surface reconstructed very difficultly and the reconstruction deviation will decrease the accuracy of dipole orientation. Only when the estimation error is smaller than ten degrees, the spatial filter determined by the cortical surface normal is feasible [34]. Another way to determine the dipole orientation is to maximize the pseudo Z in the synthetic aperture magnetometery (SAM) method [31] by exhaustively evaluating all the possible candidates. Nonlinear optimization method is more efficient but only can guarantee the suboptimal solution.

Recently, a novel spatial filtering technique, called the maximum contrast beamformer (MCB), was proposed by Chen et al [35]. This MCB method has the advantages of good output SNR and focal activity distribution as in scalar beamformers, while the dipole orientation is determined accurately and efficiently in a close-form solution. The method exploits a maximum-contrast criterion that maximizes the ratio of the reconstructed neuronal activities in the active state to those in the control state and helps to analytically and accurately determine the dipole orientation in a closed-form manner.

The below is the result of MCB algorithm. There are three simulated sources and their strength and frequency are shown as Figure 1.5 (b), three different sinusoidal signals. Their locations in the cortical area are shown as Figure 1.5 (a). The electromagnetic mapping of brain activities calculated by MCB is shown as Figure 1.5 (c). It can be demonstrated that

the three sources are correctly displayed by comparing Figure 1.5 (a) to Figure 1.5 (c).

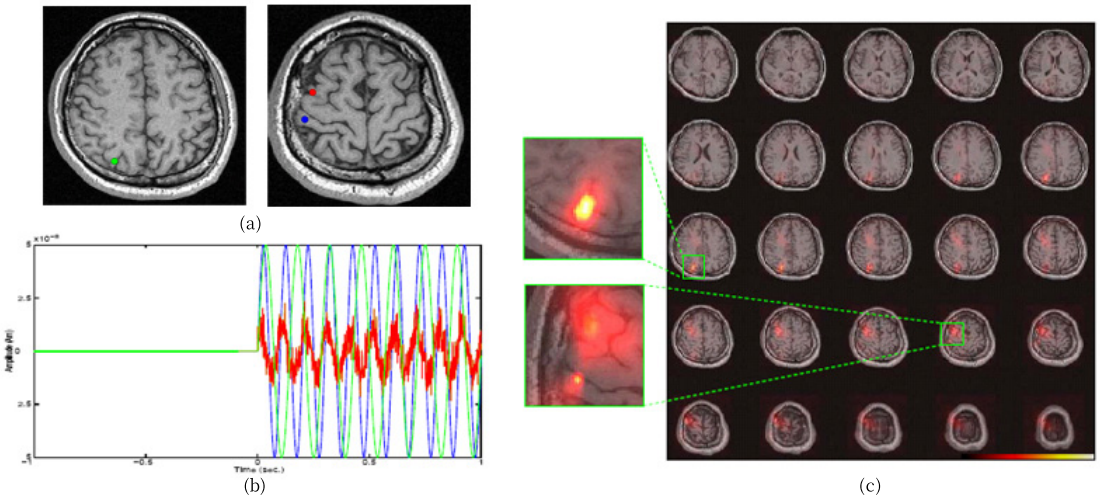

Figure 1.5: This figure shows the MCB result of the simulated data. (a) is the ground truth of this simulated data. (b) is their waveforms. And (c) is the solution to inverse problem calculated by MCB algorithm. [35]

1.3 The synchronization phenomena in MEG

As mention in section1.1, MEG and EEG are non-invasively record a spatial summation of local field potentials with a temporal resolution of millisecond. For several years, most MEG/EEG studies about oscillation for the binding problem analyze at sensor level [36–44]. For example, sleep is conventionally divided into several distinct phases on the basis of the EEG. During slow-wave sleep (SWS), dreaming typically does not occur and the scalp EEG is dominated by high-amplitude, low-frequency oscillations. Most vivid visual dreams take place during the rapid eye movement (REM) phase of sleep, when the scalp EEG shows similar patterns of activity to the waking state, being characterized by high-frequency, low-amplitude signals [45].

Some studies in Magnetoencephalography (MEG) and electroencephalography (EEG) have analyzed the functional connectivity between cortical areas with the oscillatory feature

of neuronal activity using the analysis tool, DICS [15]. In 2001 Gross et al. proposed "dynamic imaging of coherent sources (DICS)" method [46] which image the coherent brain areas using a frequency domain implementation of beamformer inverse algorithm. It can be used for imaging the spatial distribution of power and coherence to a reference signal in a narrow and chosen frequency bands. And the method determines the source orientation by the eigenvector of cross spectral density. The reference signal can be electroencephalographic recording of muscle activities or the activities at a reference area in the brain. And through the phase synchronization analysis can provide the latency information.

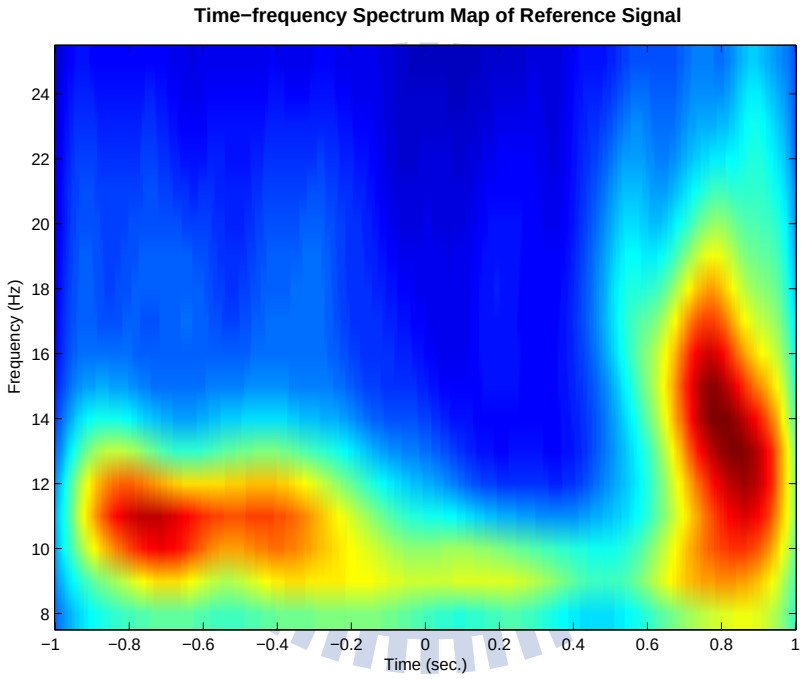

Figure 1.6: The time-frequency map of the estimated sources by maximum contrast beamformer in the experiment of lifting left index finger [35]

However, the method DICS calculate the coherent map in a narrow frequency band. Some tasks may activate on specific frequency band like slow-wave sleep stage, but still some tasks would activate on different frequency band as Figure 1.6. The Figure 1.6 is the time-frequency map of the signal at the significant position calculated by maximum contrast beamformer [35]. Naturally, the neural communication might include multi-frequency

information. It is necessary to develop a new analysis tool to investigate the general synchronization between the cortices directly.

Besides, the dipole orientation estimation is a crucial issue in scalar-type beamformer method [32,33,35]. The spatial filter with a inaccurate orientation fails to correctly estimate the neuronal activities (see the [35] for the theory and the experiment). Therefore, the accurate dipole orientation of the spatial filter to image the cortico-cortical interaction in the brain is necessary. In summary, to study the functional conductivities network which communicate with temporal dynamics needs a new, accurate and effective tool.

1.4 Thesis scope

In this thesis, we propose a beamformer-based imaging method of correlated brain activities that can study the studies of the temporal interaction between different brain cortices by imaging correlation and can reveal the similarity signal pattern. The method can identify the correlation regions to a specific brain region, called reference region. In principle, we can obtain the neural network to apply the method on all pairs of grid points for significant correlation for identifying the neural network of correlated brain region.

Our method exploits a maximum-correlation criterion that maximizes the significant level of correlation between the reference region and other regions inside the brain. Then, the output is the imaging of the brain activities correlated to the reference region. Our method can analytically and accurately determine the dipole orientation in a close-from manner and thus determine the spatial filter efficiently for each position. The correlation map can be calculated to reveal cortical regions with significant similarity to the reference position in the brain.

1.5 Thesis organization

In Chapter 1, we introduced the neural communication phenomena in our brain, the background knowledge of MEG/EEG, the source localization method and the coherence source localization. In later chapter, the method detail would be describe including the

algorithm of beamformer method and the output of our method and the optimal solution of the dipole orientation. In Chapter 3 we showed the experiment setting, preprocessing, and results. In Chapter 3.1, the experiment material, the method of generating simulation data, the paradigm of mirror neuron experiment would be describe. In Chapter 3.2, the process of data preprocessing would be depicted. Then, the experiment results of the simulation data and real data from the mirror neuron experiment are in Chapter 3.3. In Chatper 4, we discussed the results in previous chapter. In Chapter 4.1, we discussed the results of the simulation data and the merit of proposed method. Then the results of the real data from mirror neuron experiment would be discussed in Chapter 4.2. In the last Chapter 5, we concludes our method and the advantage.

Chapter 2

Method

2.1 Scalar beamformer

The Sarvas forward model estimate the recordings when given some dipoles in the brain. If there are k dipoles in the brain, at a certain instance, the estimated recordings $\mathbf{m}$ at time point t equals the summation of the productions of each gain matrix and its corresponding dipole moment at time point t:

$$\mathbf{m} = \sum_{r=1}^{k} \mathbf{L_r} \mathbf{d_r} \tag{2.1}$$

where $\mathbf{d_r}$ locating at $\mathbf{r}$ is the dipole moment and $\mathbf{L_r}$ is the corresponding gain matrix which can be derived from the forward model. Then, $\mathbf{m}$ is the summation of the effects by every source dipoles in the brain. Without of losing generality, we represent the source dipole in the Cartesian coordinate system such that $\mathbf{d_r}$ is a 3×1 vector and its elements represent x, y, z components of $\mathbf{d_r}$ respectively:

$$\mathbf{d_r} = \begin{pmatrix} \mathbf{d}_{\mathbf{r}x} \\ \mathbf{d}_{\mathbf{r}y} \\ \mathbf{d}_{\mathbf{r}z} \end{pmatrix}$$

and therefore, $\mathbf{L_r}$ is a $N \times 3$ matrix.

Then, we separate the dipole moment $\mathbf{d_r}$ into orientation $\mathbf{q} = \mathbf{d_r}/\|\mathbf{d_r}\|$ and magnitude parts $\mathbf{s} = \|\mathbf{d_r}\|$ The Equation 2.1 derive to

$$\mathbf{m} = \sum_{r=1}^{k} \mathbf{L_r} \mathbf{d_r} \tag{2.2}$$

$$= \sum_{r=1}^{k} \mathbf{G_r}(\mathbf{d_r}/\|\mathbf{d_r}\|)\|\mathbf{d_r}\| \tag{2.3}$$

$$= \sum_{i=1}^{k} \mathbf{L_r} \mathbf{q} \mathbf{s}. \tag{2.4}$$

Therefore, we define a unit dipole with parameter $\theta = \{\mathbf{r}, \mathbf{q}\}$, where $\mathbf{r}$ is the dipole location and $\mathbf{q}$ is the dipole orientation, and $\mathbf{l}_\theta$ is the lead field vector of the unit dipole. The lead field vector is the predicted measurement of N MEG sensor with the unit dipole with $\mathbf{q}$ orientation. $\mathbf{l}_\theta$ is calculated by

$$\mathbf{l}_\theta = \mathbf{L_r} \mathbf{q} \tag{2.5}$$

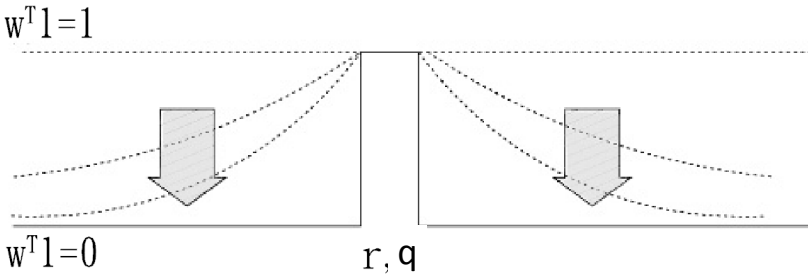

Figure 2.1: With unit-gain constraint, the spatial filter at the location of the target source$(\mathbf{r}, \mathbf{q})$ will preserve the most strength and impress the contribution form other sources by minimum variance constraint.

The MEG recordings $\mathbf{m}(t)$ is decomposed into three components

$$\begin{aligned} \mathbf{m}(t) &= \mathbf{m}_\theta(t) + \mathbf{m}_\delta(t) + \mathbf{n}(t) \\ &= \mathbf{m}_\theta(t) + \mathbf{m}_n(t) \end{aligned} \tag{2.6}$$

where $\mathbf{m}(t) = \mathbf{l}_\theta \mathbf{s}_\theta(t)$ denotes the magnetic field originated from the source with parameter θ, $\mathbf{m}_\delta(t)$ denotes the magnetic field originated from all other sources, $\mathbf{n}(t)$ is the noise, and $\mathbf{m}_n(t)$ denotes the combination of the noise and the magnetic recordings originated from all other sources.

Scalar MEG beamformer performs spatial filtering on recordings to set apart the signals of the location of interest and the others. For a dipole source with parameter θ, the output signal of the beamformer $y(t)$ is acquired by

$$y(t) = \mathbf{w}_\theta{}^t \mathbf{m}(t) \tag{2.7}$$

which approximates the source signal $s_\theta(t)$ of the dipole. To achieve this goal, the spatial filter $\mathbf{w}_\theta$, a $N \times 1$ column vector, can be decided by the unit-gain constraint and minimum variance. With these constraints, the strength of output signal $y(t)$ can be identical with the source strength $s_\theta(t)$ while nulling the contribution of the other sources. We can get the concept about unit-gain and minimum variance constraints from Figure 2.1.

As the following equation,

$$\begin{aligned} y(t) &= \mathbf{w}_\theta{}^t \mathbf{m}(t) \\ &= \mathbf{w}_\theta{}^t \mathbf{m}_\theta(t) + \mathbf{w}_\theta{}^t \mathbf{m}_n(t) \\ &= s_\theta(t) \mathbf{w}_\theta{}^t \mathbf{l}_\theta + \mathbf{w}_\theta{}^t \mathbf{m}_n(t) \\ &= s_\theta(t) + \mathbf{w}_\theta{}^t \mathbf{m}_n(t) \end{aligned} \tag{2.8}$$

the source signal $s_\theta(t)$ can retrieve by applying unit-gain constrain, $\mathbf{w}_\theta{}^t \mathbf{l}_\theta = 1$, and we still have to reduce the leakage of all other sources, $\mathbf{w}_\theta{}^t \mathbf{m}_n(t)$. This is equivalent to minimize the variance of $y(t)$. Therefore, the optimal spatial filter $\hat{\mathbf{w}}_\theta$ can be calculated by

$$\hat{\mathbf{w}}_\theta = \arg\min_{\mathbf{w}_\theta} E\{|y(t) - E\{y(t)\}|^2\} + \alpha \|\mathbf{w}_\theta\|^2 \quad subject \quad to \quad \mathbf{w}_\theta{}^t \mathbf{l}_\theta = 1 \tag{2.9}$$

where E represents the expectation value and α represents the parameter of Tikhonov regularization. Here α is a parameter to restrict the norm of $\hat{\mathbf{w}}_\theta$, corresponding to the shape of beamformer spatial filter. Substituting the Equation (2.8) into Equation (2.9), we can solve the equation by Lagrange multipliers and obtain the optimal solution of $\hat{\mathbf{w}}_\theta$

$$\begin{aligned} \hat{\mathbf{w}}_\theta &= \arg\min_{\mathbf{w}_\theta} \mathbf{w}_\theta{}^t (\mathbf{C} + \alpha \mathbf{I}) \mathbf{w}_\theta \quad subject \quad to \quad \mathbf{w}_\theta{}^t \mathbf{l}_\theta = 1 \\ &= \frac{(\mathbf{C} + \alpha \mathbf{I})^{-1} \mathbf{l}_\theta}{\mathbf{l}_\theta{}^t (\mathbf{C} + \alpha \mathbf{I})^{-1} \mathbf{l}_\theta} \end{aligned} \tag{2.10}$$

where $\mathbf{C}$ is the $N \times N$ covariance matrix of the MEG recordings $m(t)$ and $\mathbf{I}$ is the $N \times N$ identity matrix.

2.2 Imaging of the brain activities correlated to the reference signals

For each dipole source in location $\mathbf{r}$ with fixed orientation $\mathbf{q}$, we can use equation Equation 2.10 to obtain the spatial filter, and further compute the dipole activities by using equation Equation 2.7. Once we apply the procedure mentioned above individually to each position of head region, we can acquire the activities of whole head.

Although there are many kinds of activities in brain, we are only interested in the brain activities which correlating to the source signals at reference region. But through the spatial filter calculated from Equation 2.10 we may obtain strong non-interested activities in the filtered outputs. What we focus on is the correlation level to the reference signal. Therefore, we proposed a method to calculate the imaging of the brain activities correlated to the targeted signals. In contrast to the conventional Beamforming methods which provide statistical maps to reveal the regions having significant neuronal activities, we calculated the correlation between source signal and reference signal.

$$\begin{aligned} R_\theta &= \frac{E\{|\mathbf{w}_\theta{}^t \mathbf{m}_c(t)\mathbf{a}(t)|\}}{E\{|\mathbf{w}_\theta{}^t \mathbf{m}_c(t)|^2\}^{\frac{1}{2}} E\{|\mathbf{a}(t)|^2\}^{\frac{1}{2}}} \\ &= \frac{\{\mathbf{w}_\theta{}^t E\{|\mathbf{m}_c(t)\mathbf{a}(t)|^2\}\mathbf{w}_\theta\}^{\frac{1}{2}}}{\{\mathbf{w}_\theta{}^t \mathbf{C}_m \mathbf{w}_\theta\}^{\frac{1}{2}} E\{|\mathbf{a}(t)|^2\}^{\frac{1}{2}}} \\ &= \frac{\{\mathbf{w}_\theta{}^t \mathbf{C}_{am} \mathbf{C}_{am}{}^t \mathbf{w}_\theta\}^{\frac{1}{2}}}{\{\mathbf{w}_\theta{}^t \mathbf{C}_m \mathbf{w}_\theta\}^{\frac{1}{2}} E\{|\mathbf{a}(t)|^2\}^{\frac{1}{2}}} \end{aligned} \tag{2.11}$$

$\mathbf{a}(t)$ is the reference signal at the reference region which is chosen by users. Appropriate strategies for the selection of the reference region are introduces and illustrated in Chapter 2.4. The $\mathbf{C}_{am}$ is the $N \times 1$ cross-covariance matrix between MEG recording $\mathbf{m}(t)$ and reference signal $\mathbf{a}(t)$. And $\mathbf{C}_m$ is the $N \times N$ covariance matrix. Therefore, the value of R_θ indicates the significant level of similarity between the dipole activities with parameter θ and the reference region at the targeted position $\mathbf{r}$ with dipole orientation $\mathbf{q}$.

There are three covariance matrix involved in the beamformer-based process, that is $\mathbf{C}$, $\mathbf{C}_{am}$ and $\mathbf{C}_m$. The matrix $\mathbf{C}$ is used to calculate the spatial filter and the time interval of $\mathbf{m}(t)$ should be large enough to obtain a reliable result. The matrix $\mathbf{C}_{am}$ is used to calculate the correlation value between the interval of $\mathbf{m}_c(t)$ and the interval of the reference signal $\mathbf{a}(t)$.

2.3 Maximum correlation beamformer

The solution of $\hat{\mathbf{w}}_\theta$ is derived with parameter $\theta = \{\mathbf{r}, \mathbf{q}\}$. Because we calculate the activities of whole head by scanning all of the position in the brain, the position parameter

$\mathbf{r}$ is set to be each position. Then we can obtain the correlation level to the reference region in the entire brain.

However, the orientation parameter $\mathbf{q}$ is difficult to determine. As Chapter 1.3 describe, the accurate dipole orientation $\mathbf{q}$ of the spatial filter extremely influence the accuracy of the spatial filter. Therefore, instead of exhaustive search, we propose a optimal closed-form solution to decide the dipole orientation. By substituting Equation 2.5 to Equation 2.10, we can separate parameter $\mathbf{q}$.

$$\begin{aligned} \hat{\mathbf{w}_\theta} &= \frac{(\mathbf{C}+\alpha\mathbf{I})^{-1}\mathbf{L_r q}}{\mathbf{q}^t\mathbf{L}_\mathbf{r}^t(\mathbf{C}+\alpha\mathbf{I})^{-1}\mathbf{L_r q}} \\ &= \frac{\mathbf{A_r q}}{\mathbf{q}^t\mathbf{B_r q}} \\ where \quad \mathbf{A_r} &= (\mathbf{C}+\alpha\mathbf{I})^{-1}\mathbf{L_r} \quad and \quad \mathbf{B_r} = \mathbf{L}_\mathbf{r}^t\mathbf{A_r} \end{aligned} \tag{2.12}$$

$\mathbf{A_r}$ and $\mathbf{B_r}$ are depend only on the parameter position $\mathbf{r}$, We determine the optimal dipole orientation $\hat{q}$ which can maximize the correlation between the source signal s_θ and the reference signal. By substitute Equation 2.12 into Equation 2.11 and maximin the correlation value, we obtain the optimal $\hat{\mathbf{q}}$:

$$\begin{aligned} \hat{\mathbf{q}} &= \arg\max_{\mathbf{q}} \left(\frac{(\mathbf{w}_\theta{}^t\mathbf{C}_{am}\mathbf{C}_{am}{}^t\mathbf{w}_\theta)^{\frac{1}{2}}}{(\mathbf{w}_\theta{}^t\mathbf{C}_m\mathbf{w}_\theta)^{\frac{1}{2}}E\{|\mathbf{a}(t)|^2\}^{\frac{1}{2}}} \right)^2 \\ &= \arg\max_{\mathbf{q}} \frac{\mathbf{q}^t\mathbf{A}_\mathbf{r}^t\mathbf{C}_{am}\mathbf{C}_{am}{}^t\mathbf{A_r q}}{\mathbf{q}^t\mathbf{A}_\mathbf{r}^t\mathbf{C}_m\mathbf{A}_{\mathbf{r_q}}\mathbf{q}} \\ &= \arg\max_{\mathbf{q}} \frac{\mathbf{q}^t\mathbf{P_r q}}{\mathbf{q}^t\mathbf{Q_r q}}, \end{aligned} \tag{2.13}$$

in which the term $E\{|\mathbf{a}(t)|^2\}^{\frac{1}{2}}$ is a scalar so it can eliminated. $\mathbf{P_r} = \mathbf{A_r}{}^t\mathbf{C}_{am}\mathbf{C}_{am}{}^t\mathbf{A_r}$ and $\mathbf{Q_r} = \mathbf{A_r}{}^t\mathbf{C}_m\mathbf{A_r}$ are 3×3 matrix. The solution of Equation 2.13 is the eigenvector corresponding to the maximum eigenvalue of the matrix eigenvalue of the matrix $\mathbf{Q}_\mathbf{r}^{-1}\mathbf{P_r}$. Because these two matrices, $\mathbf{Q_r}$ and $\mathbf{Q}_\mathbf{r}^{-1}\mathbf{P_r}$ are both 3×3 matrix, we can solve the matrix inverse problem and the eigne problem in a closed-form manner.

2.4 Reference region

In principle, applying the method as above on all pairs of grid points for significant correlation can identity the neural network of correlated brain region; However, it requires large amount of computation. The work can be reduced if we can pick at least one member of the neural network. Picking a suitable reference region is a important issue in our method. Four strategy for selecting the reference regions were listed.

I. The prior information of physiological

A reference region is defined by prior knowledge from the results of others functional imaging studies or anatomical structures or neural pathways.

II. The region of significant activities

A reference region is defined from the source area of strongest activities. For example, the peak in the F-value map of maximum contrast beamformer.

III. The specific signal pattern - independent component

A reference region is defined from the mixing matrix of independent component analysis (ICA). ICA is proposed to solve the problem of blind source separation. It can decompose the input into several independent components, as $\mathbf{X} = \mathbf{MS}$. Given input $\mathbf{X}$, it can calculate $\mathbf{S}$, which contains independent components, under the assumption that the estimated sources $\mathbf{S}$ are as statistically independent as possible. $\mathbf{M}$ is the mixing matrix.

Applying ICA on MEG recordings, it will decompose some independent component. Each column of the mixing matrix is the topography of the respective independent component. We can choose the independent component as reference signal according to the topography, and calculate the cortico-sensor correlation.

2.5 Studying the interactions

We can calculate for significant correlation between other brain areas and the reference region through the introduced analyze method which derive the spatial filter as Equation 2.12, calculate the correlation map through Equation 2.11, and obtain the optimal dipole orientation through the maximum criterion as Equation 2.13.

If we want to analyze the dynamic correlation map of the neural network, we can just choose a short time interval of the reference signal for calculating because the reference region may involve in the neural network just a short time. Besides, the reference signal $\mathbf{a}(t)$ and part of the MEG measurement $\mathbf{m}_c(t)$ can choose different time interval to calculate. For example, we choose 100 to 200 ms of the source signal as the reference signal and then choose 0 to 100 ms of the MEG measurement $\mathbf{m}(t)$ as the $\mathbf{m}_c(t)$ to calculate the correlation map. Therefore, we can calculate the significant correlation between a time interval of the reference region and different time intervals of the other brain areas. Furthermore, we can obtain the sequential correlation map to the reference region through the successive measurement segment which are overlapping by the user define length.

In summary, to analyze the functional connectivity between the cortices, we can follow the progress as shown in Figure 2.2. At first, user has to choose a reference region which can refer our advise in Chapter 2.4. Second, user can use source localization tool to calculate the source signal of the reference region or use the ICA component, and define a time interval as the reference signal. Third, user apply our method to a segment of MEG measurers calculate the correlation distribution to the reference signal in the entire brain. Then user repeat the third step until all the segments of data have calculated so that user can have the dynamic correlation map to the reference region.

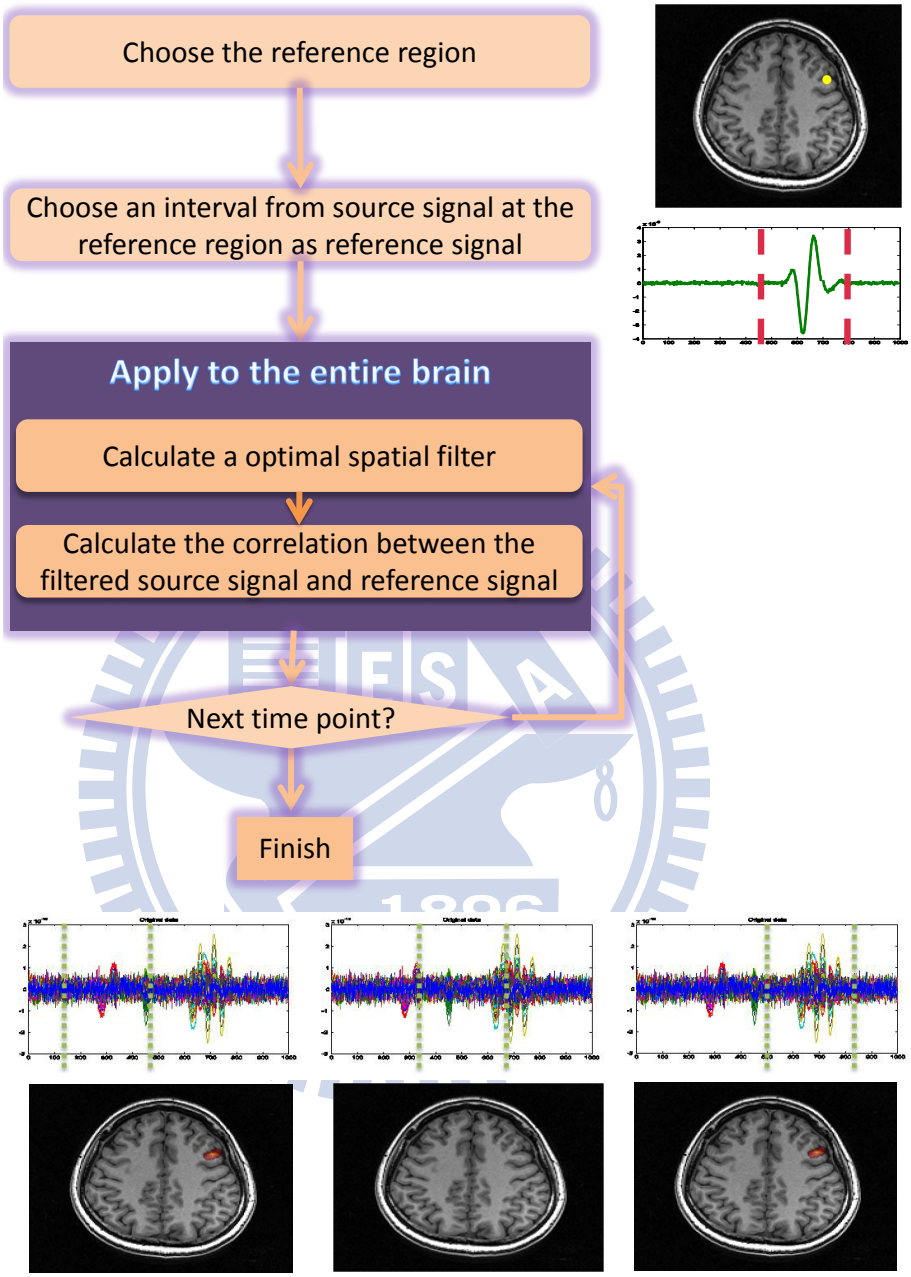

Figure 2.2: First step, user has to choose a reference region. Second step, user can use source localization tool to calculate the source signal of the reference region or use the ICA component, and define a time interval as the reference signal. Third step, user apply our method to a segment of MEG measurers calculate the correlation distribution to the reference signal. Then user repeat the third step until all the segments of data have calculated so that user can have the dynamic correlation map to the reference region.

E S A
1896

Chapter 3

Experiment Results

3.1 Material

To verify the proposed method in Chapter 2, we need the information of the Anatomical Data and the MEG recordings of the magnitude field. There are two kinds of MEG data, including simulation and the real MEG measurement from the experiment of the happy mirror neuron. We will describe some information of these data in the below statements.

3.1.1 Anatomical Data

The Magnetic Resonance Imaging (MRI) images were from the 1.5T GE scanner at the Taipei Veterans General Hospital with TR = 8.672 ms, TE=1.86 ms, FOV = 26x26x10cm^3, matrix size = 256x256, slices = 128, voxel size = 1.02x1.02x1.5mm^3.

3.1.2 MEG Data

Simulations

We simulate the MEG recordings by the forward model in Equation.2.6with given sources as ground truth and add some dipoles acting as noises. There are two kind of noises, background sources and sensor noises. We simulate background sources as random dipoles with zero-mean Gaussian strength and uniformly distributed in the putative sphere of head model. The variances of sensor noises are estimated from the empty room recordings of the MEG system. We also use 1 kHz sampling rate as sampling frequency of the simulated recordings. Before data analysis, we do preprocessing depicted later in Section 3.2

Real MEG measurement

A whole head MEG system at the Taipei Veterans General Hospital (Neuromag Vectorview 306 , Neuromag Ltd., Helsinki, Finland) is used for recording of the minute magnetic field generated by electrical activities within the living human brain. The MEG system is placed in a magnetically shielded room and has capability of 306 channels simultaneous

recording at 102 distinct sites, 24 bits analog to digital conversion, and up-to-8 kHz sampling rate which is sufficient to probe the fast dynamic changes inside human brains.

Experiment paradigm of happy mirror neuron The study focused on the the roles of mirror neuron system for position emotion. Three condition, observation, imitation and execution, were studied. The stimuli were randomized grayscale photographs of faces, depicting neutral and smile, from Taiwanese facial expression image database (http://bml.ym.edu.tw/ download/html/news.htm). The experiment paradigm was shown in Figure3.1. In observation condition stimuli had presented for 700 ms with an inter-stimulus interval (ISI) 1300 ms; Imitation and execution condition with ISI 1500 ms, the stimuli had presented for 2000 ms after a rest block consisting of a fixed cross at the center of the screen. However the stimuli in execution condition were neutral face and neutral face with a fixed cross upon the nose.

Twenty four subjects with no neurological and psychiatric disorder participated in the study. The subjects were introduced to obverse the face in observation condition. In imitation condition they were asked to follow the facial motion of the stimuli. In execution condition, they had to smile when the stimuli with the fixed cross upon the nose wad showed.

The experiment was performed by Hung-Che in brain mapping laboratory of institute of brain science in national yang-ming university.

3.2 Data Preprocessing

The brain signal is comparatively small than the environmental noises. Preprocessing for the recordings to enhance the signal to noise ratio (SNR) is necessary so that further processing would be more smooth going [47]. Generally the experiment will be repeated several times to obtain sufficient amount of recordings. we call the recordings at each time as “trial”. The preprocessing steps we use for MEG recording are stated as below. The first step is to find out the abnormal scale recordings and cut them. Because artifacts, body action and eye blinking produce significant noises, compared to the measurement induced by the electric brain signal while experiment. Hence, we can find out the unusual scale recording to reduce artifact noise on MEG/EEG sensor and electric ocular graph (EOG) channels. The second step is to eliminate the sensor norse. By using signal space projection

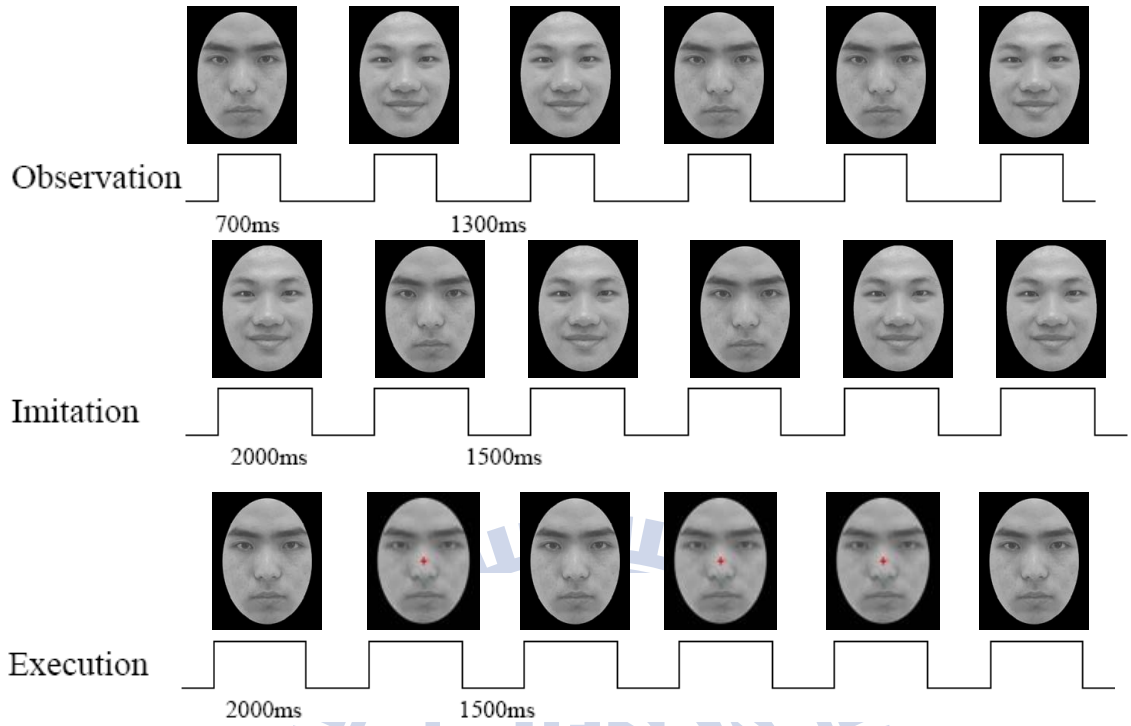

Figure 3.1: The figure was shown the paradigm of happy mirror neuron experiment. The stimuli were face image with random emotion, neutral and happy, on observation and imitation conditions; However, on execution condition, the stimuli were neutral face image as observation and imitation condition and neutral face image with fixed cross upon the nose.

(SSP) [48] we remove the recording those were projected to the individual basis vector of the noise subspace and eliminate from the MEG/EEG measurement. We can obtain the signal space through the noise space which is calculated from emptyroom. By this method, we can transform the measurement to the signal space and reserve them [49]. The third step is to remove unavoidable artifacts such as heartbeat, breath and power line noises. We use bandpass filter to cut them because the artifact of heartbeat and breath is 1 Hz signal, and power line is 60 Hz and its harmonic. The fourth step is to cut down the drift of recordings along with time on each sensor because of the device. By conducting baseline correction, we subtract a baseline estimated by the mean of the recordings at the period which is unaffected by the stimulus, in order to decrease the influence of the noise in the baseline. The preprocessing steps are shown in Figure 3.2

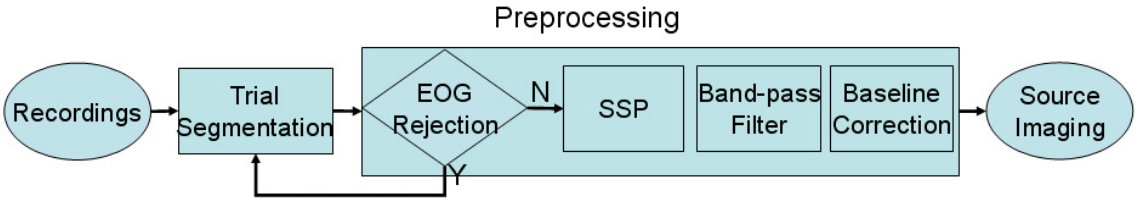

Figure 3.2: This graph shows the all preprocessing steps for MEG recordings. For strengthening SNR, preprocessing for the recordings is necessary. The first step is removing artifacts by finding out the abnormal scale of MEG/EEG recording and EOG channels called artifact rejection. The second step is to eliminate the sensor noise by applying SSP. The next step is applying bandpass filter to cut out the other artifacts which are in specific band like heartbeat and breath and some environmental noises like power line noises. The final step is to conduct the baseline correction to eliminate the drift of recordings. After preprocessing, we can obtain the MEG/EEG recording with higher SNR..

3.3 Experiments

We conduct the simulation to validate our method. Each simulation is added background sources with 3000 random dipoles with the standard deviation of 10 nAm. The variance of sensor noises are estimated form the emptyroom recording of the MEG system.

3.3.1 Simulation data 1

In this simulation, we put a 15 Hz sine wave on the ground truth position (as Figure 3.5). Applying the 15 Hz signal sine wave as the targeted signal, the result of our method is shown in Figure 3.4. The correlation map of the estimated source is focal and significant. The peak exactly locate on the location as the ground truth.

3.3.2 Simulation data 2

Four dipole sources with temporal profiles of sinusoidal were located in three position inside the brain, as shown in Figure 3.5. Strengths of the red, green, and blue profiles

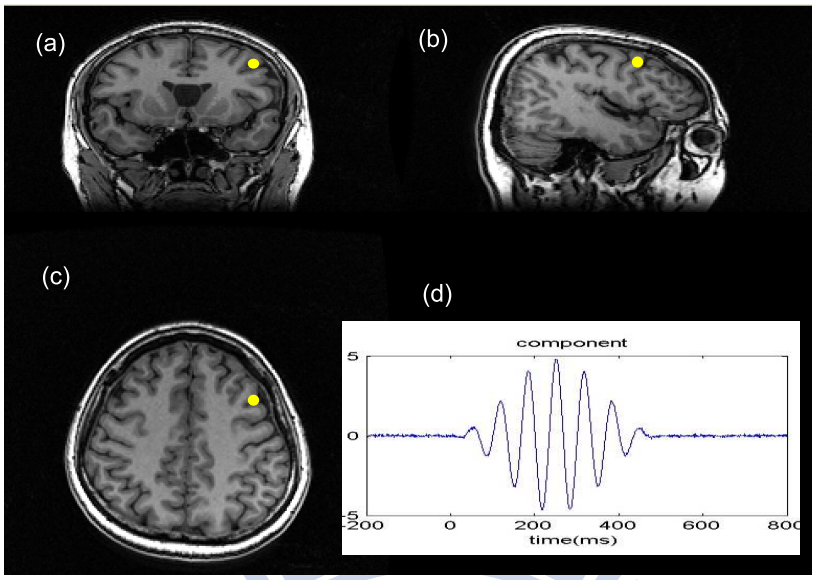

Figure 3.3: (a) the ground truth location in anatomical image of the simulated recordings by coronal view (b) the ground truth location in anatomical image of the simulated recordings by sagittal view (c) the ground truth location in anatomical image of the simulated recordings by transverse view (d) the 15 Hz sine wave temporal profiles

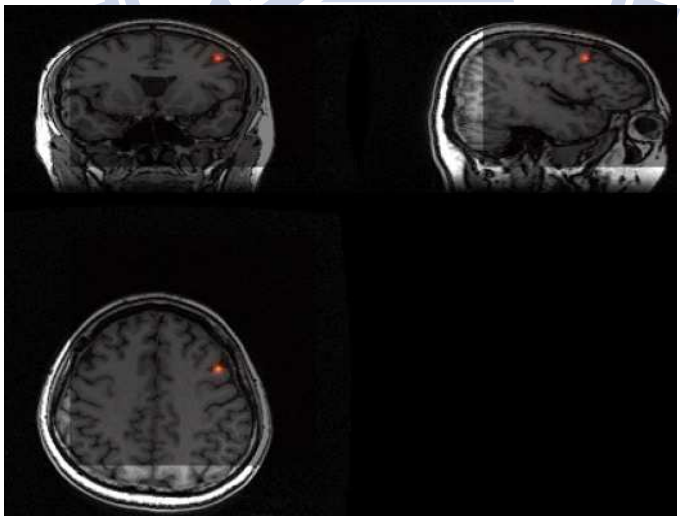

Figure 3.4: Correlation map of the estimated source by out method with the recordings of simulation 1. The significant source are viewed by sagittal, coronal and transverse view.

are all 40 nAm. The profile in the green position is as the red profile at yellow position with 350 ms delay. The orientation of each of the four dipoles was arbitrarily set on the plane tangential to the head sphere. We used (2.6) to compute the simulated MEG signals induced from the four dipole sources, as well as additive background noises from 3000 random dipoles with the standard deviation of 25 nAm.

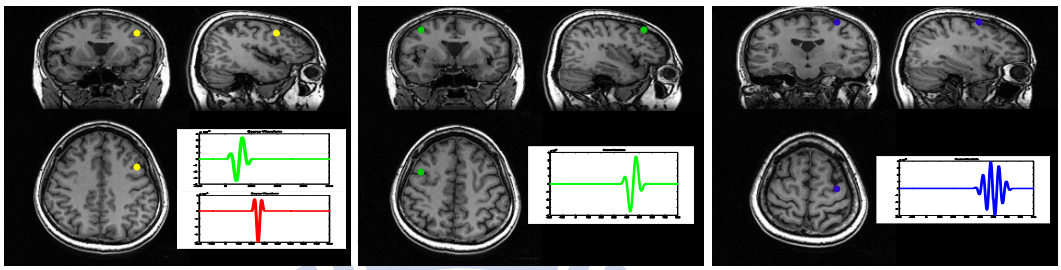

(a) (b) (c)

Figure 3.5: Dipole sources of simulation data contain (a) the first two sources at yellow location with different temporal activities (in red and green), (b) another source at green location with the same temporal activities as the green one at (a), and (c) the last source at the blue location with the temporal activities in blue.

We applied independent component analysis on the simulated measurements to extract components (Figure 3.6) and manually selected four components C1, C2, C3, and C4. Then we calculated and imaged the correlation distribution between each of the selected component and brain activities by (2.11) as shown in Figure 3.7. The correlation map of the estimated source is focal and significant, and the source localization error is 0 mm for all chosen components.

We applied MCB on the simulated recordings to calculate the F-statistic maps which reveal cortical regions with significant difference of activities between the active and control states. Then we chose the filtered signal at the highest F value position from 350 to 550 ms interval as the reference signal. Then we calculated the correlation map between the reference signal and brain activities at different time interval. Figure 3.8(a) shows the correlation map from 0 to 200 ms, and Figure 3.8(b) shows the map from 350 to 550 ms. It is obviously that both maps match the dipole locations at the corresponding time interval.

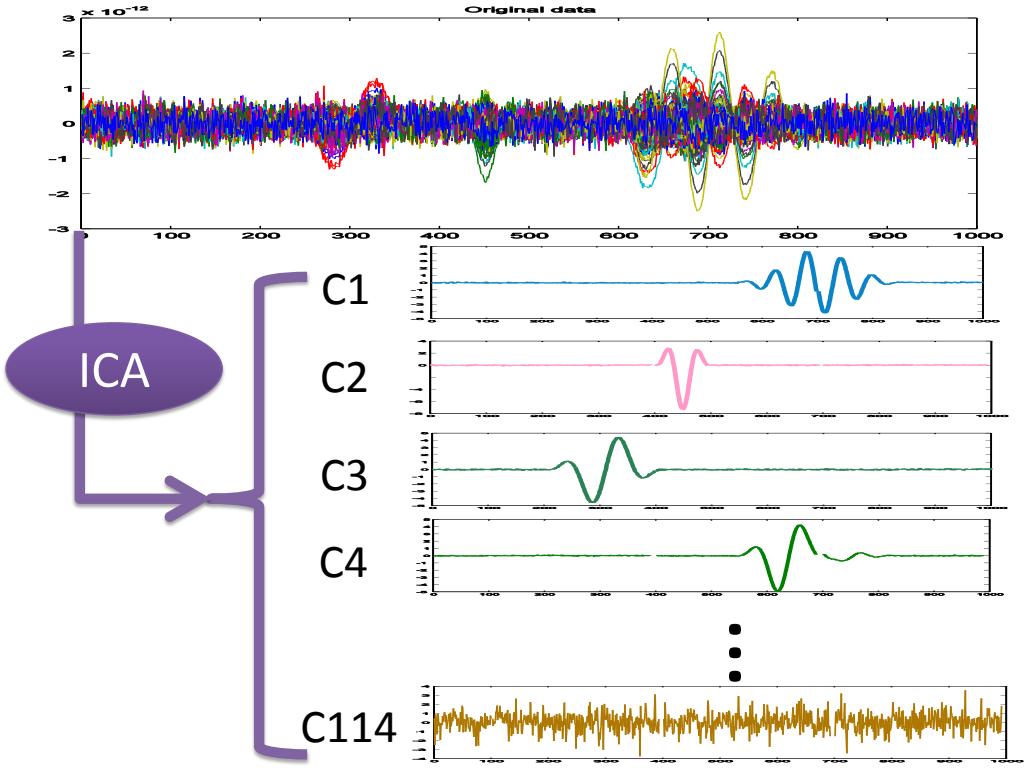

Figure 3.6: The simulated data was decomposed by ICA into 114 components.

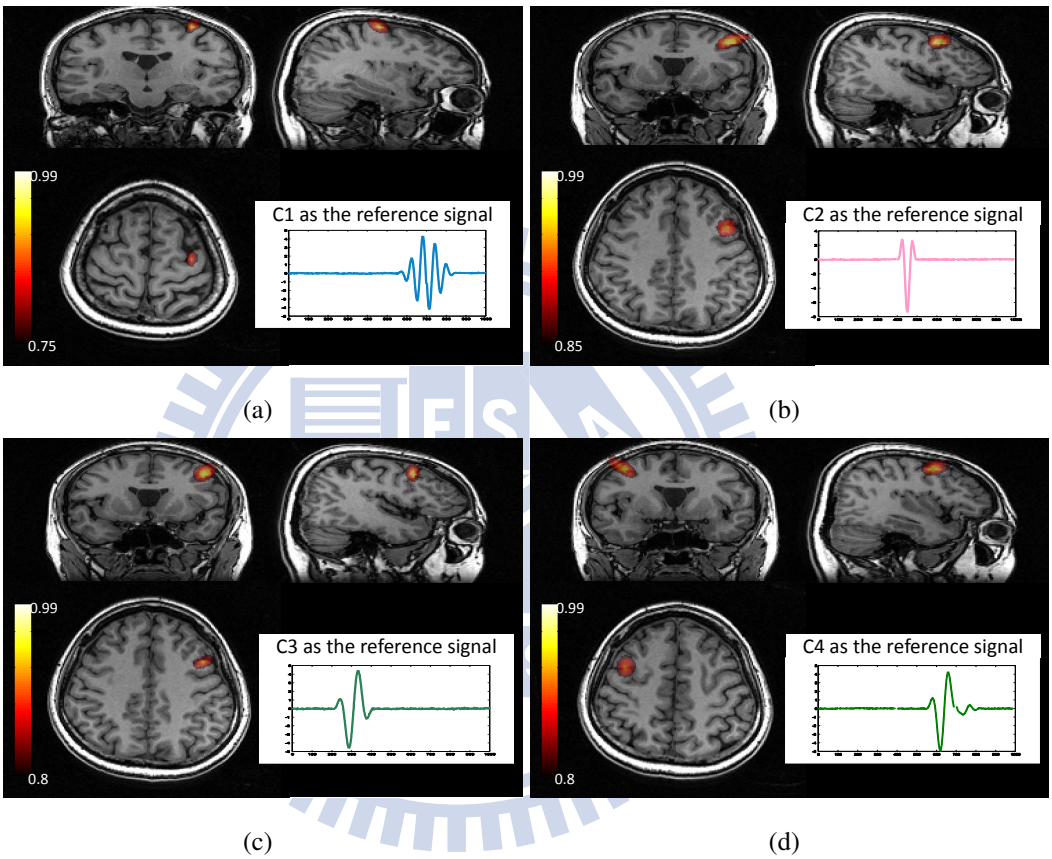

Figure 3.7: The correlation map calculated with the reference signal (a) C1, (b) C2, (c) C3, and (d) C4.

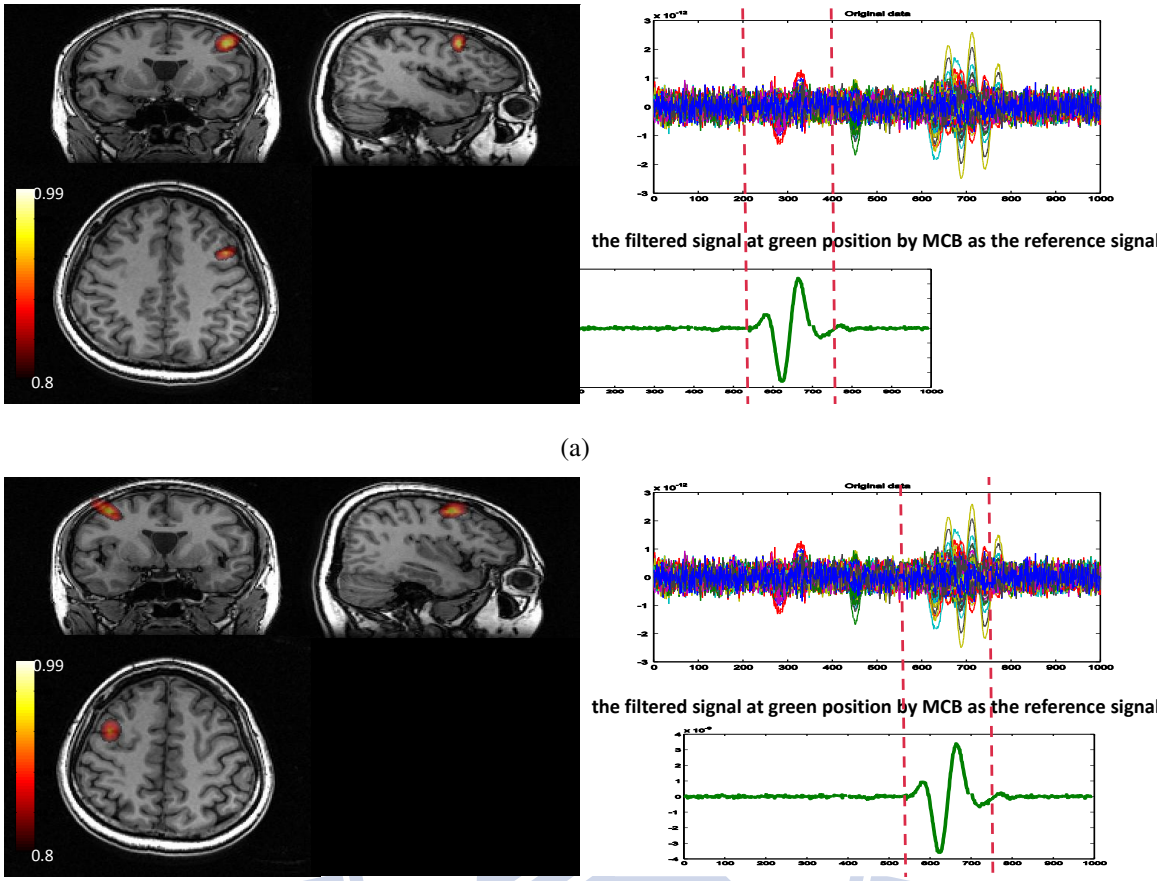

Figure 3.8: The correlation maps calculated with the reference signal filtered by MCB at different time intervals within (a) [0, 200] ms and (b) [350, 550] ms.

3.3.3 Real data - happy mirror neuron

In this experiment, we applied our method on the measurement of two subject with three conditions. We chose seven reference brain regions as reference to find out the highly correlated brain regions and the time between the reference. The seven reference regions were right insula, left inferior frontal gyrus, right inferior frontal gyrus, left amygdala, right amygdala, inferior occipital gyrus and the v1. Those region were suggested highly correlated with mirror neuron system, emotion processing and face perception. That is why we chose them as our reference region. The source signal of those regions were calculated

Table 3.1: The parameters of maximum contrast beamformer on the happy mirror neuron experiment.

the parameter information of MCB	
artifact threshold	6000 fT
electrooculography rejection	0.0002 V
bandpass	2 to 30 Hz
baseline	-200 to 0 ms
tradeoff	0.03
window interval	-50 to 850 ms
control interval	-200 to -100 ms

by MCB, and the time interval of the source signal chosen as the reference signal depended on each reference region and the pattern of the source signal. The parameters of MCB was listed at Table 3.1.

Left inferior frontal gyrus

Subject A

The anatomical position of left inferior frontal gyrus was shown in the first row of the Table 3.3. The axis of the volume was at (56,152,76) voxel. The source signals at the left inferior frontal gyrus of three conditions calculated by MCB was shown in the next row of the Table 3.3. We chose a time interval as reference signal of each condition as shown in Table 3.2; In this reference position, 100 to 200 ms were chosen as reference signal on imitation and observation conditions, and 180 to 280 ms was chosen as reference signal on execution condition.

Imitation condition The results were shown in Table 3.4. We can observe that at

Table 3.2: The referenced time interval of each source signal

	imitate	observation	execution
Right insula	100 to 200 ms	100 to 200 ms	100 to 200 ms
Left inferior frontal gyrus	100 to 200 ms	100 to 200 ms	180 to 280 ms
Right inferior frontal gyrus	50 to 150 ms 50 to 250 ms	140 to 280 ms	120 to 220 ms
Left amygdala	100 to 200 ms	100 to 200 ms	140 to 250 ms
Right amygdala	100 to 200 ms	100 to 160 ms 130 to 280 ms	150 to 250 ms

Table 3.3: The source signal of the left inferior frontal gyrus as reference signal which were calculated by MCB. The first row shows the position of the left inferior frontal gyrus. The next is the source signal of three condition - imitate, observation and execution.

the information of the reference – left inferior frontal gyrus		
the position (56,152,76)		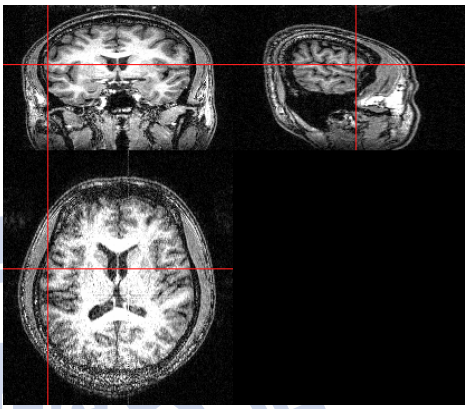
the signal	imitate	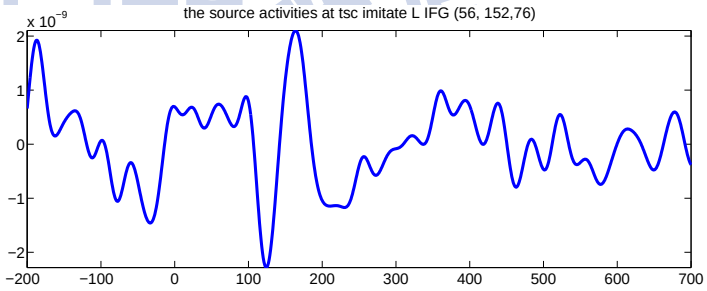
	observation	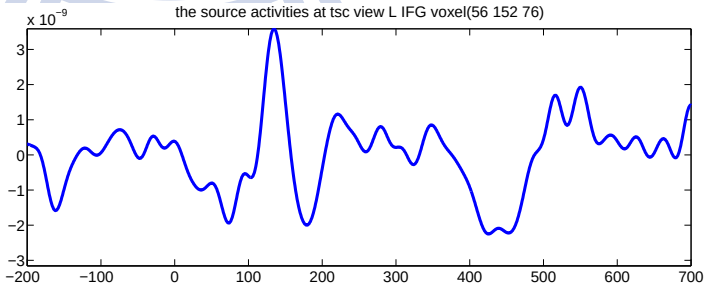
	execution	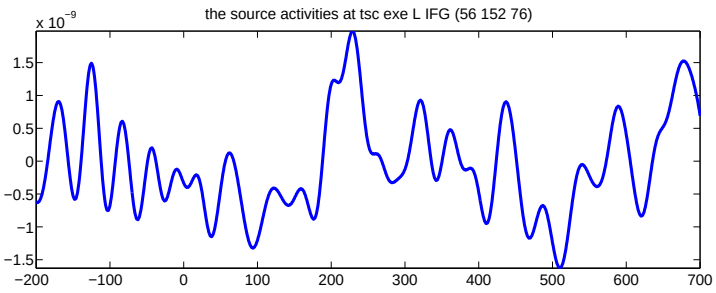

Table 3.4: The correlation map and the significant correlation regions of the reference region at left inferior frontal gyrus on imitation condition at different time interval.

The correlated brain region with left inferior gyrus of various time

70 ms		100 ms		175 ms		240 ms	
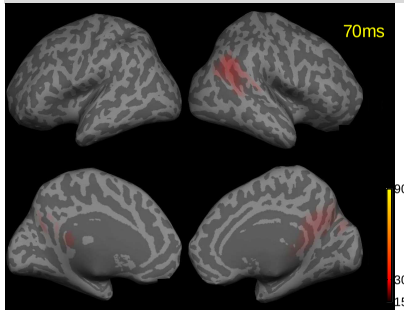		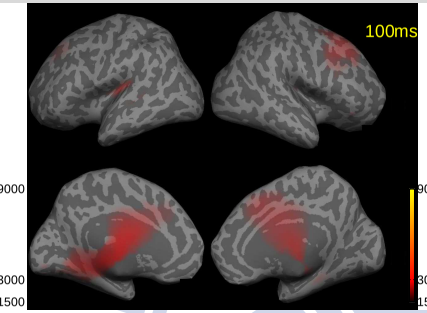		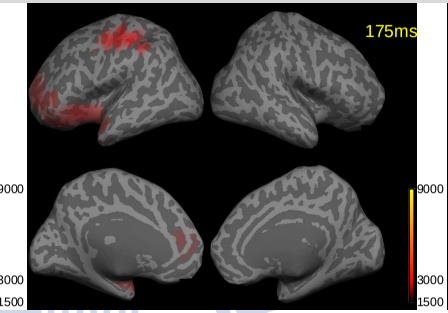		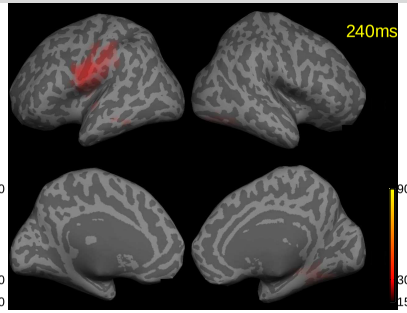	
Left	Right	Left	Right	Left	Right	Left	Right
	angular gyrus		premotor cortex	lateral orbitofrontal cortex central sulcus		facial movement	

385 ms		390 ms		395 ms		400 ms	
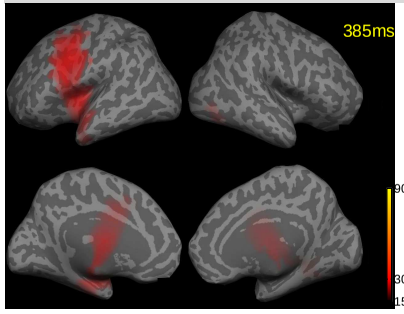		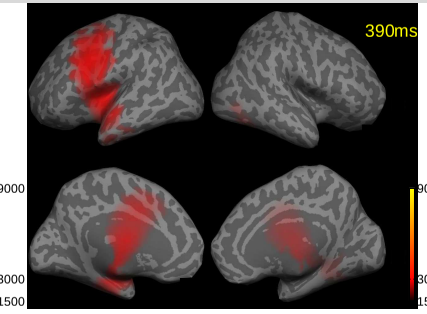		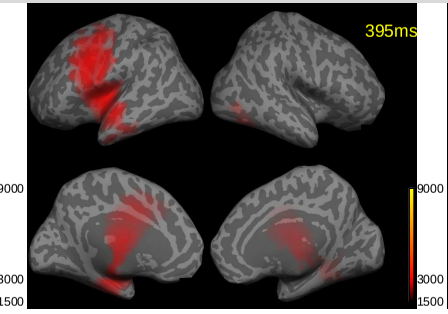		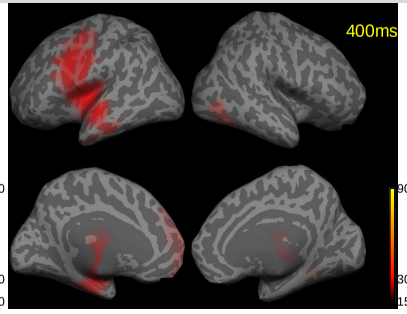	
Left	Right	Left	Right	Left	Right	Left	Right
premotor cortex M1 inferior frontal gyrus middle temporal gyrus		premotor cortex M1 inferior frontal gyrus middle temporal gyrus		premotor cortex M1 inferior frontal gyrus middle temporal gyrus		premotor cortex M1 inferior frontal gyrus middle temporal gyrus anterior prefrontal cortex	

405 ms		410 ms		415 ms		420 ms	
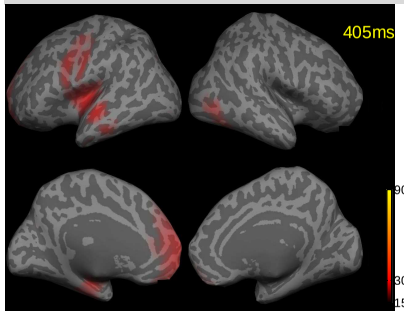		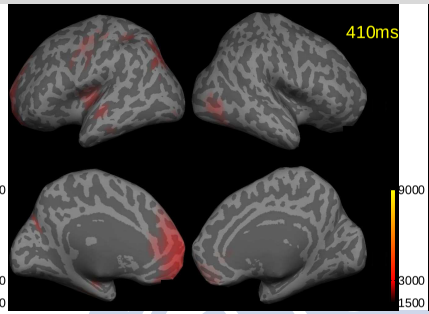		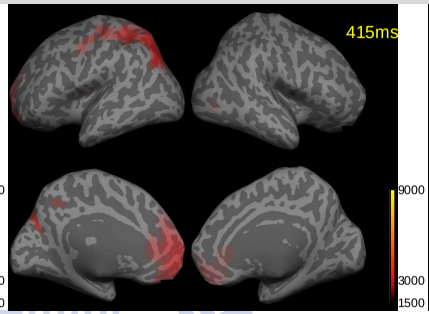		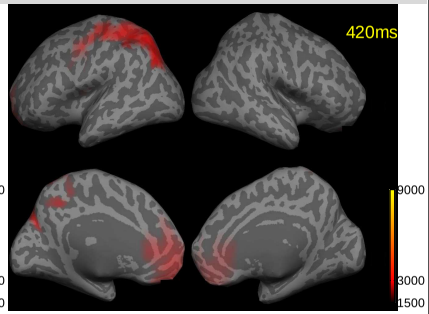	
Left	Right	Left	Right	Left	Right	Left	Right
premotor cortex		anterior prefrontal cortex		orbitofrontal cortex		orbitofrontal cortex	
M1				superior pariatal lobule		superior parietal lobule	
inferior frontal gyrus							
middle temporal gyrus							
anterior prefrontal cortex							

425 ms		430 ms		435 ms		440 ms	
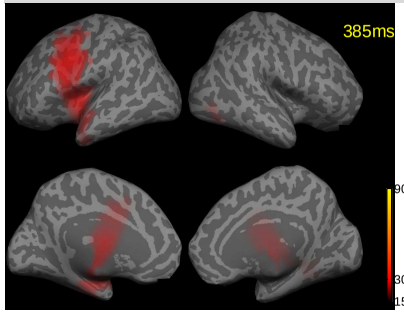		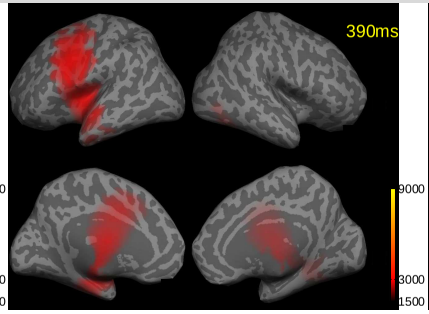		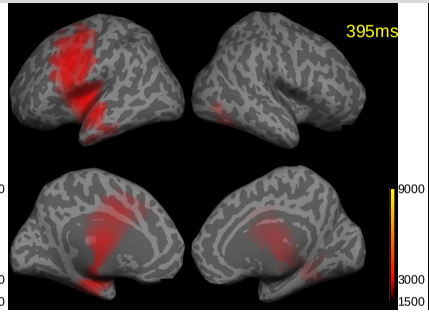		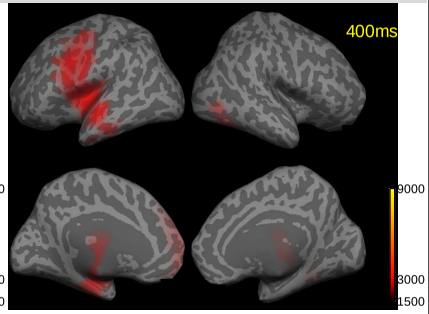	
Left	Right	Left	Right	Left	Right	Left	Right
premotor cortex		premotor cortex		premotor cortex		premotor cortex	
facial movement		facial movement		facial movement		facial movement	
superior temporal sulcus		superior temporal sulcus		superior temporal sulcus		superior temporal sulcus	
amygdala		amygdala		amygdala		middle temporal gyrus	
						amygdala	

445 ms		450 ms		455 ms		505 ms	
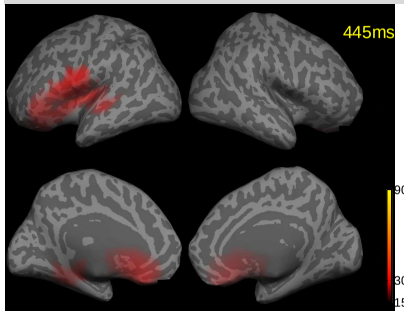		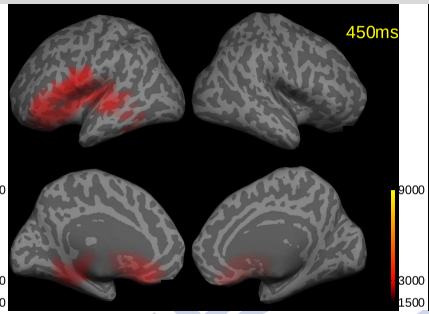		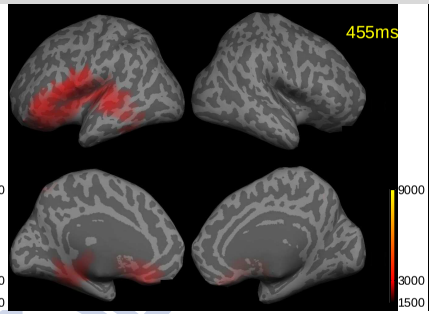		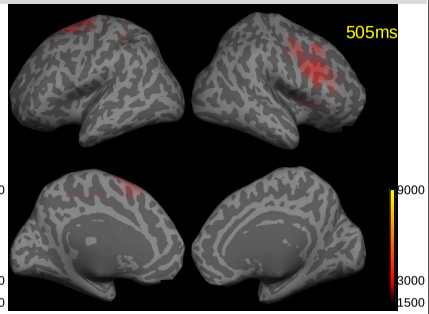	
Left	Right	Left	Right	Left	Right	Left	Right
facial movement		facial movement		facial movement		SMA	premotor cortex
orbitofrontal cortex		orbitofrontal cortex		orbitofrontal cortex			
		superior temporal sulcus		superior temporal sulcus			
				middle temporal sulcus			

510 ms		515 ms		565 ms		585 ms	
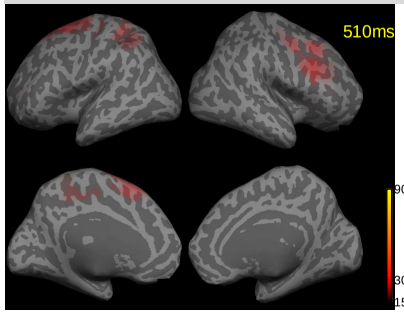		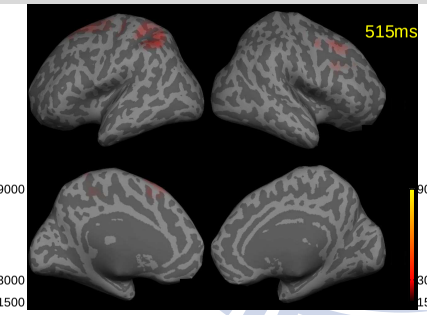		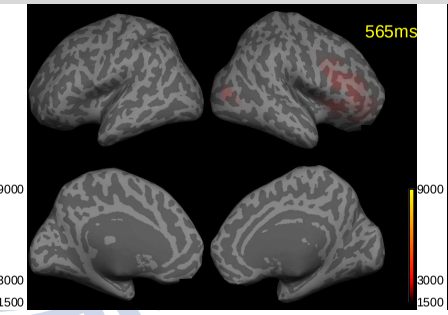		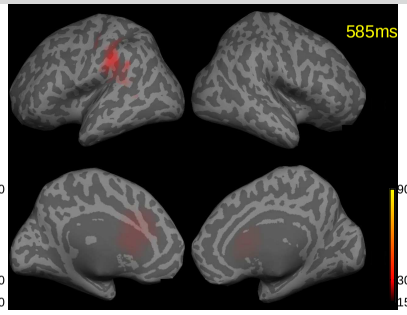	
Left	Right	Left	Right	Left	Right	Left	Right
SMA	premotor cortex	SMA	dorsolateral prefrontal		lateral ventral prefrontal	temporal parietal junction	
superior parietal lobule		superior parietal lobule				inferior parital	

590 ms		610 ms		620 ms		630 ms	
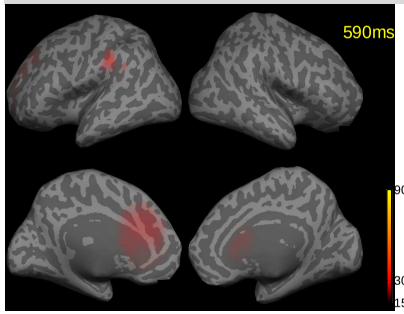		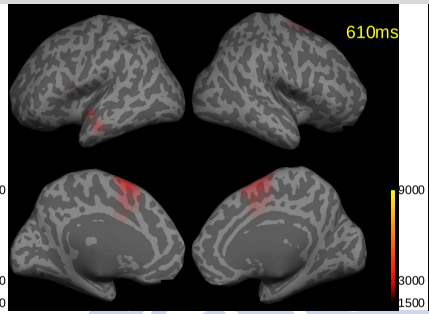		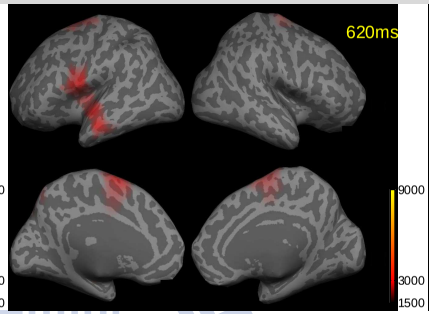		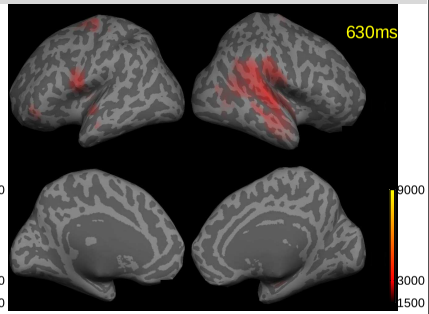	
Left	Right	Left	Right	Left	Right	Left	Right
temporal parietal junction		SMA	SMA	SMA	SMA	inferior frontal gyrus	superior temporal gyrus
anterior cingulate cortex				superior temporal gyrus		SMA	posterior insula cortex
				inferior frontal gyrus			

660 ms		670 ms		675 ms		685 ms	
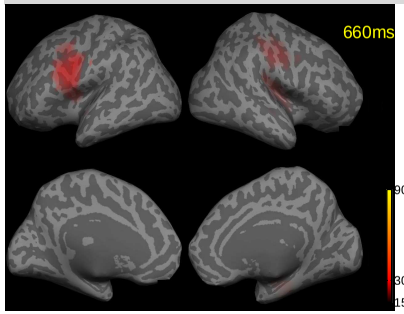		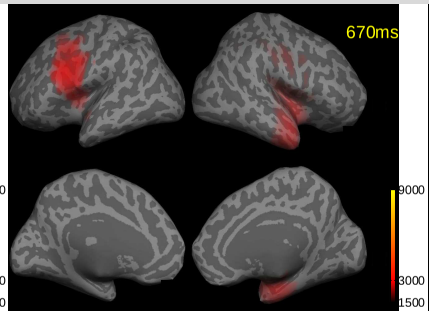		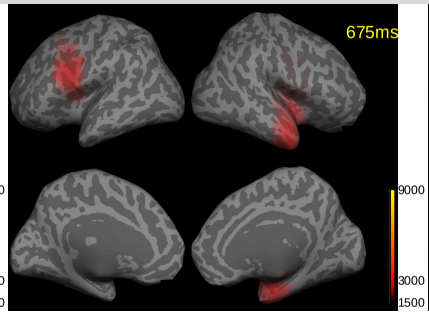		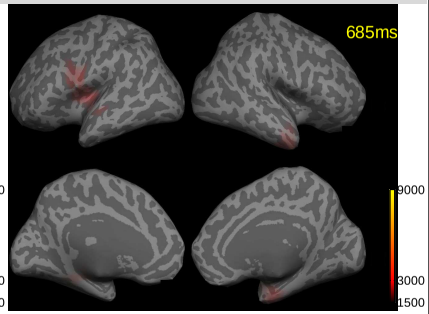	
Left	Right	Left	Right	Left	Right	Left	Right
facial movement	central sulcus	facial movement	central sulcus	facial movement	temporal pole	facial movement	temporal pole
			temporal pole				

690 ms

695 ms

700 ms

Left	Right	Left	Right	Left	Right
facial movement		middle prefrontal cortex		facial movement	
superior temporal sulcus				meddile prefrontal cortex	

Observation condition The results were shown in Table 3.5.

Table 3.5: The correlation map and the significant correlation regions of the reference region at left inferior frontal gyrus on observation condition at different time interval.

The correlated brain region with left inferior gyrus of various time							
95 ms		115 ms		125 ms		140 ms	
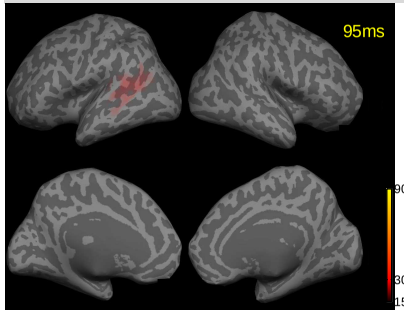		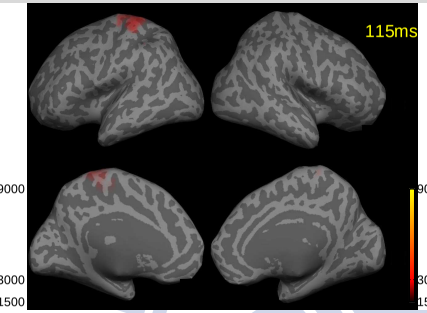		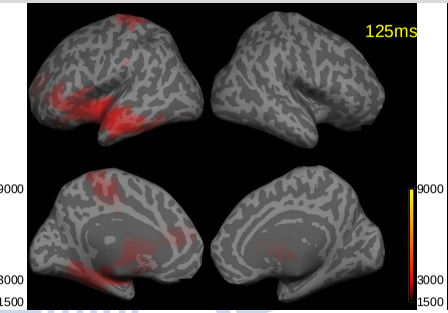		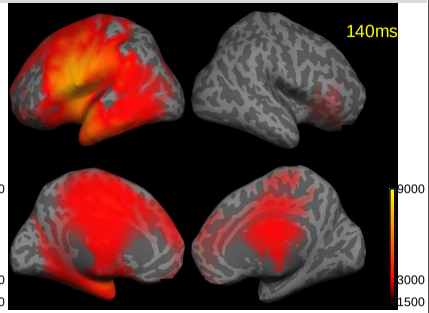	
Left	Right	Left	Right	Left	Right	Left	Right
superior temporal sulcus		central sulcus		central sulcus middle temporal gyrus		inferior frontal gyrus ACC dorsal latteral prefrontal SMA amygdala	inferior frontal gyrus ACC SMA

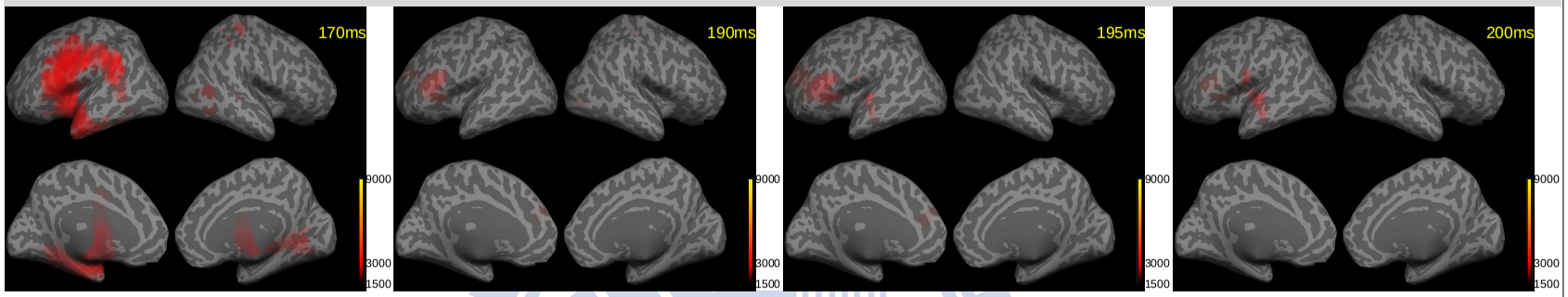

Left	Right	Left	Right	Left	Right	Left	Right
premotor cortex		inferior frontal gyrus		inferior frontal gyrus		inferior frontal gyrus	
M1				dorsolateral prefrontal cortex		superior temporal gyrus	
inferior frontal gyrus				superior temporal gyrus			
temporal pole							
poterior insula							
amygdala							

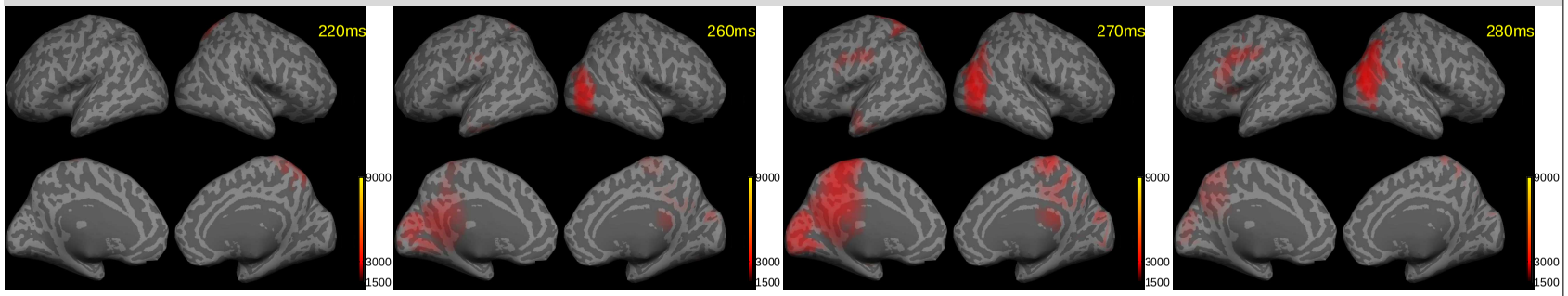

Left	Right	Left	Right	Left	Right	Left	Right
	somatosensory association tex	cor-V1 V2	V2	occipital lobe posterior cingulate cortex somatosensory central sulcus	V2 somatosensory cortex	facial movement occipitalpariatal	V3 posterior parietal cortex

290 ms		320 ms		325 ms		330 ms	
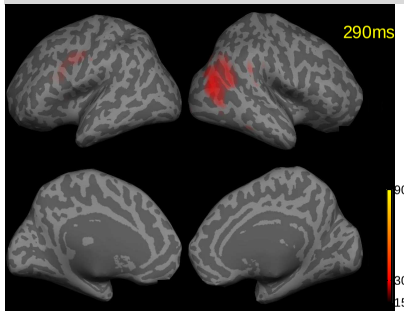		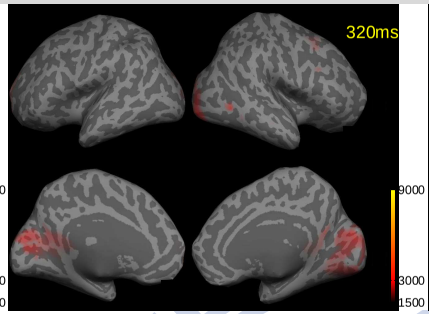		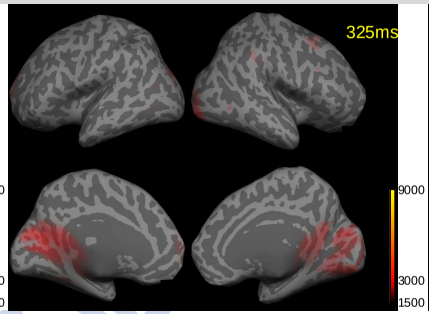		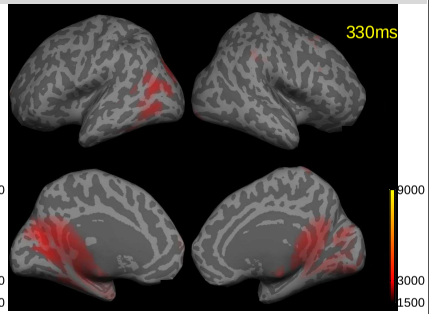	
Left	Right	Left	Right	Left	Right	Left	Right
facial movement	V3	V2	V3 V1	V2 ventral posterior cingulate cortex	V3 V1 ventral posterior cingulate cortex	occipitaltemporal	ventral posterior cingulate cortex

340 ms		345 ms		355 ms		360 ms	
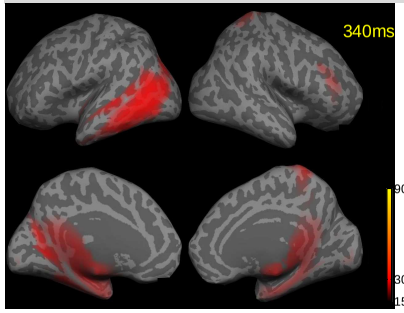		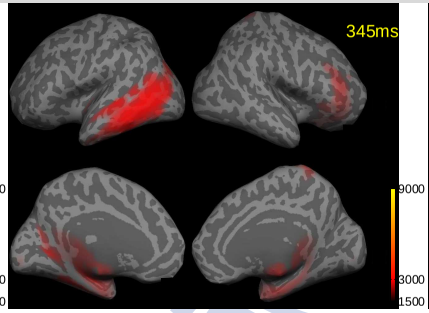		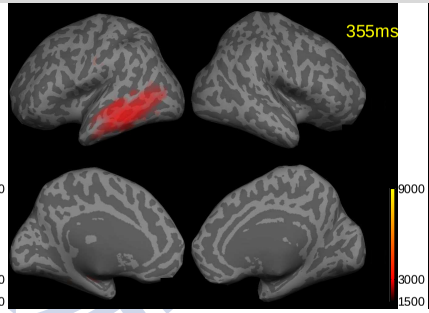		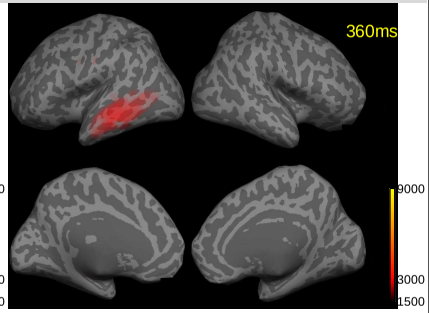	
Left	Right	Left	Right	Left	Right	Left	Right
occipitaltemporal	ventral posterior cingulate cortex inferior temporal gyrus	occipitaltemporal	inferior frontal gyrus inferior temporal gyrus	middle temporal gyrus		middle temporal gyrus	

365 ms		370 ms		375 ms		380 ms	
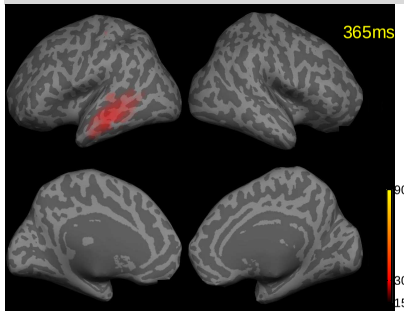		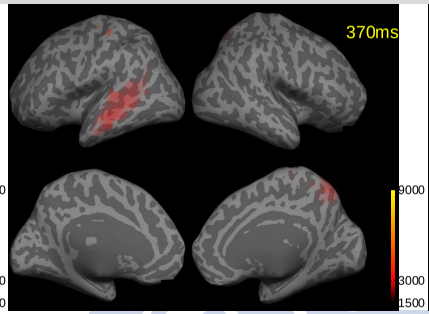		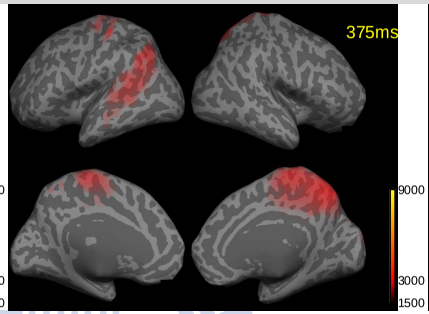		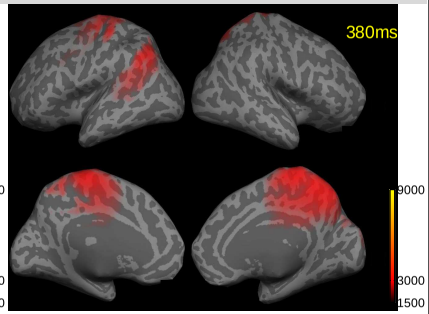	
Left	Right	Left	Right	Left	Right	Left	Right
middle temporal gyrus		superior temporal sulcus	somatosensory gyrus	angular gyrus	somatosensory gyrus	angular gyrus	somatosensory gyrus
				superior temporal sulcus	motor gyrus	temporal parietal junction	motor gyrus
						somatosensory gyrus	
						motor gyrus	

385 ms		390 ms		400 ms		405 ms	
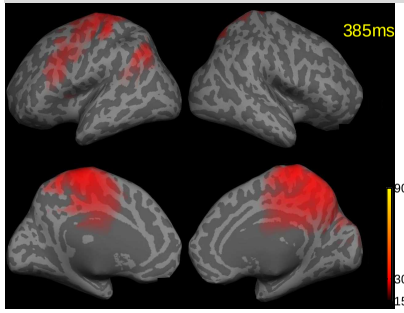		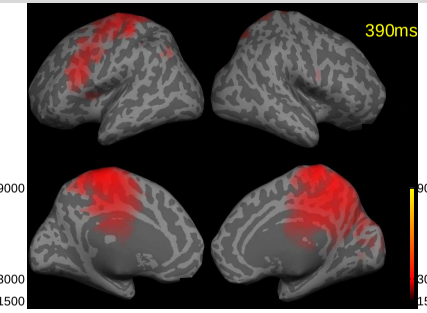		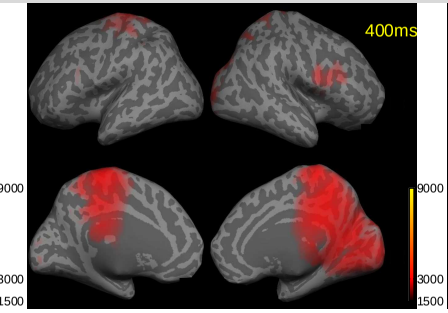		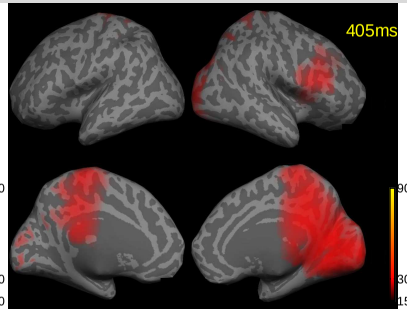	
Left	Right	Left	Right	Left	Right	Left	Right
angular gyrus	somatosensory gyrus	somatosensory gyrus	somatosensory gyrus	somatosensory gyrus	occipital arietal	somatosensory gyrus	inferior frontal gyrus
somatosensory gyrus	motor gyrus	motor gyrus	motor gyrus	motor gyrus	inferior frontal gyrus	posterior cingulate cortex	occipital arietal
motor gyrus	posterior cingulate cortex	premotor	posterior cingulate cortex				
premotor		posterior cingulate cortex					
posterior cingulate cortex		inferior frontal gyrus					
inferior frontal gyrus							

415 ms		425 ms		460 ms		470 ms	
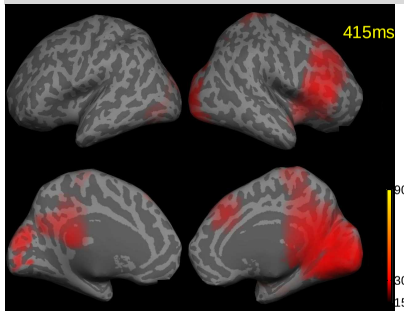		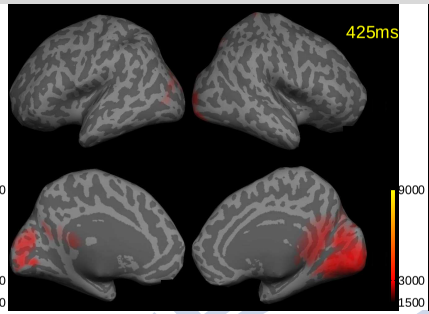		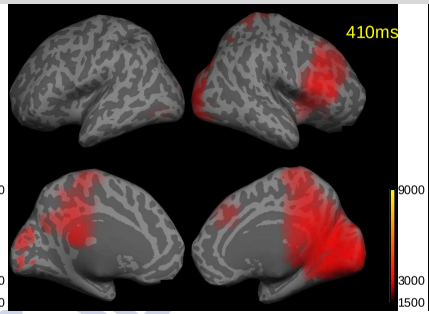		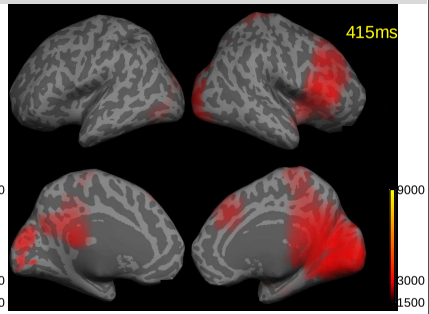	
Left	Right	Left	Right	Left	Right	Left	Right
V1	dorsolateral prefrontal cortex	occipital	occipital	middle temporal gyrus		middle temporal gyrus	
posterior cingulate cortex	inferior frontal gyrus		posterior cingulate cortex			inferior frontal gyrus	
	occipital arietal						

485 ms		490 ms		495ms		500 ms	
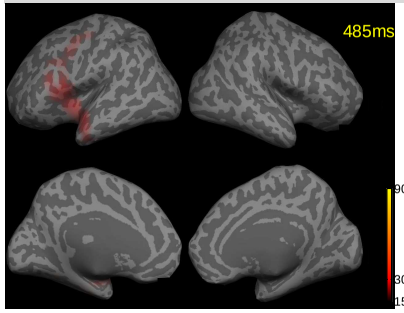		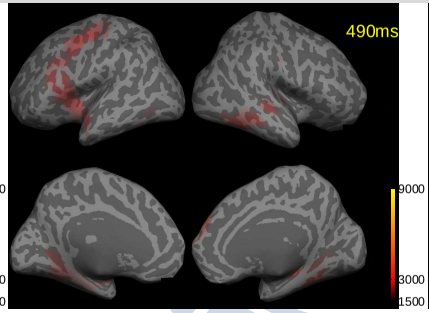		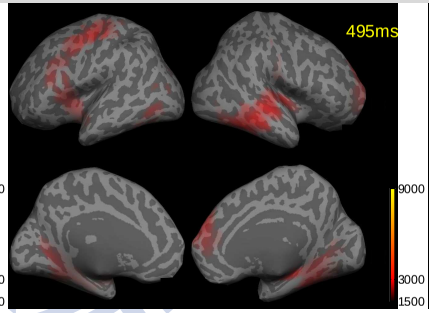		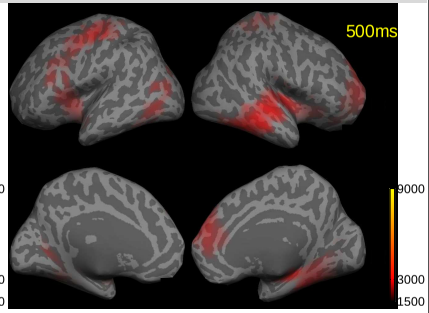	
Left	Right	Left	Right	Left	Right	Left	Right
superior temporal gyrus		inferior frontal gyrus	inferior temporal gyrus	inferior frontal gyrus	inferior temporal gyrus	inferior temporal gyrus	inferior temporal gyrus
inferior frontal gyrus		premotor gyrus		premotor gyrus	middle temporal gyrus	premotor	middle temporal gyrus
premotor gyrus					dorsolateral prefrontal cortex	infeior temporal sulcus	superior temporal sulcus
							dorsolateral prefrontal cortex
							central sulcus

510 ms		515 ms		520 ms		525ms	
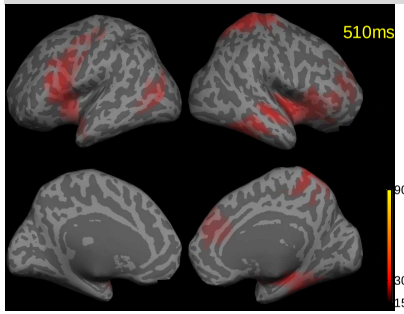		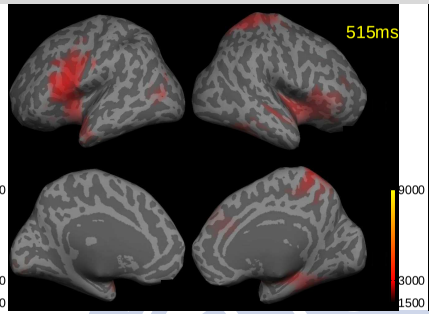		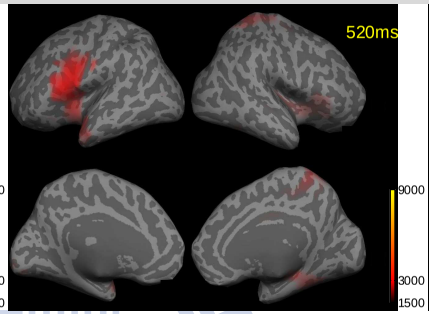		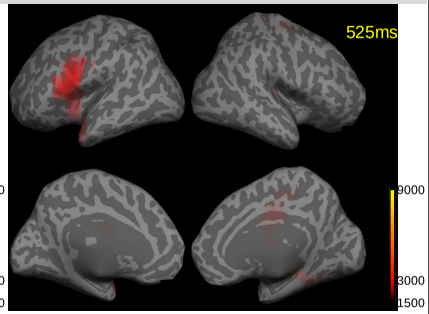	
Left	Right	Left	Right	Left	Right	Left	Right
inferior frontal gyrus	middle temporal gyrus	facial movement	inferior frontal gyrus	facial movement	central sulcus	facial movement	ACC
premotor gyrus	superior temporal sulcus		central sulcus	temporal pole		temporal pole	
superior temporal gyrus	middle prefrontal cortex		amygdala				
	central sulcus						
	amygdala						

530 ms		535 ms		595 ms		605 ms	
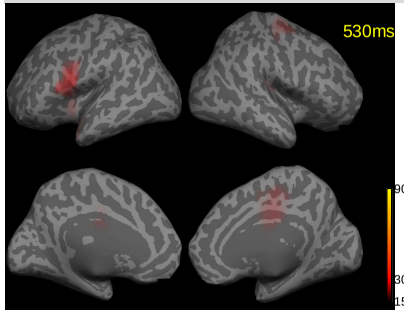		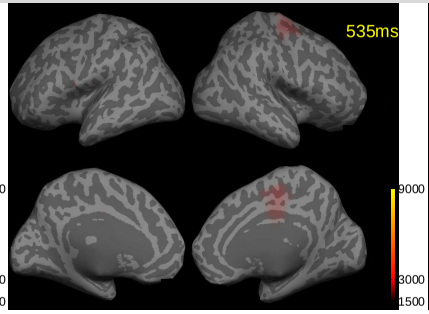		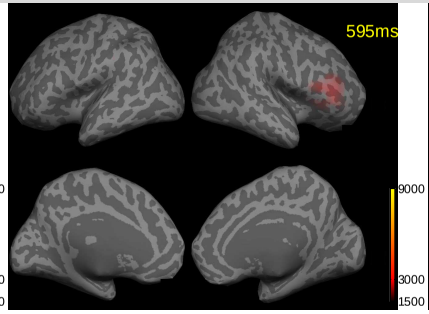		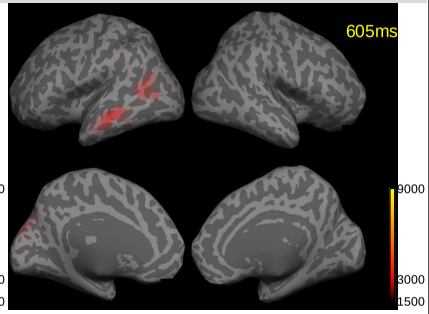	
Left	Right	Left	Right	Left	Right		
facial movement	ACC		ACC		inferior frontal gyrus	middle temporal gyrus	

610 ms		620 ms		630 ms		660ms	
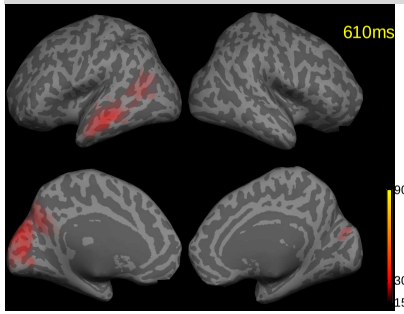		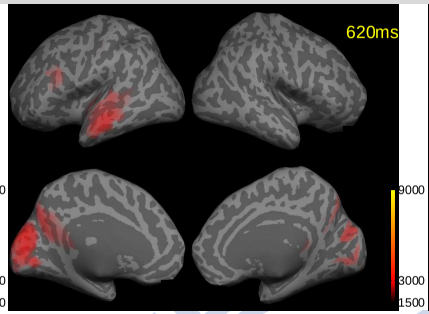		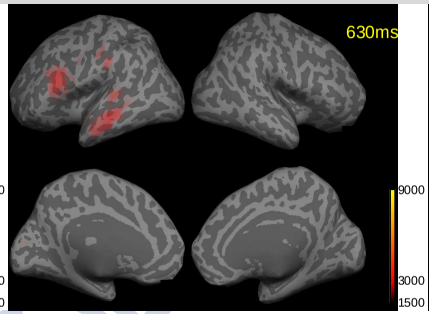		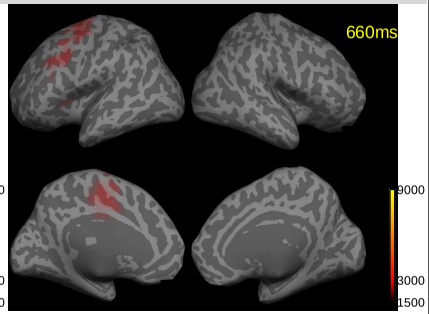	
Left	Right	Left	Right	Left	Right		
middle temporal gyrus		middle temporal gyrus	V1	middle temporal gyrus		SMA	
V2		inferior frontal gyrus		inferior frontal gyrus			
		V1					
		parieto-occipital fissure					

670 ms		680 ms		690 ms		695ms	
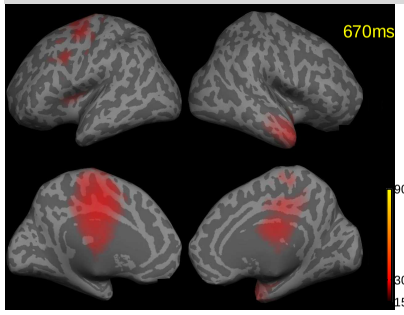		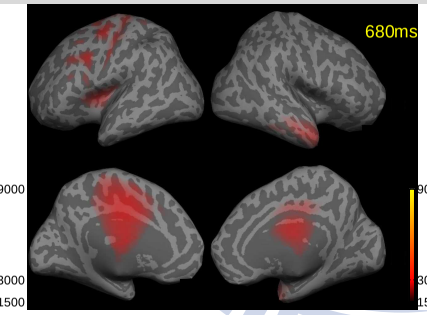		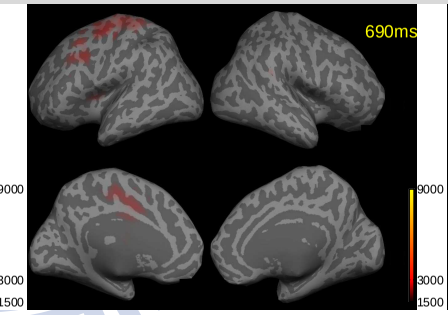		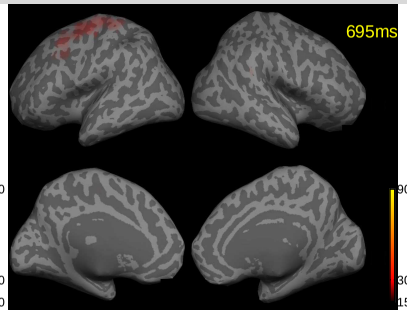	
Left	Right	Left	Right	Left	Right		
ACC	temporal pole	ACC	temporal pole	SMA		premotor	
SMA	ACC	SMA	ACC	premotor			

Execution condition The results were shown in Table 3.6.

Table 3.6: The correlation map and the significant correlation regions of the reference region at left inferior frontal gyrus on execution condition at different time interval.

The correlated brain region with left inferior gyrus of various time

125 ms		135 ms		140 ms		145 ms	
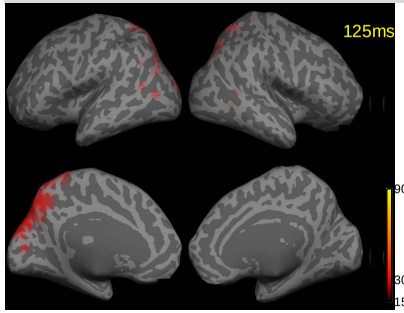		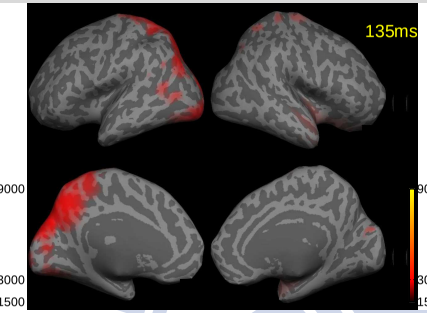		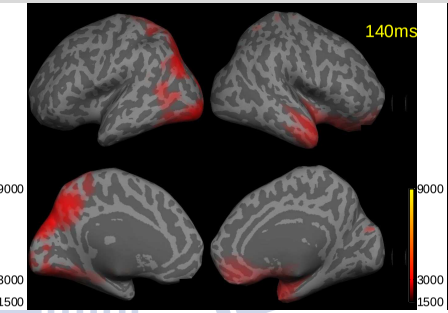		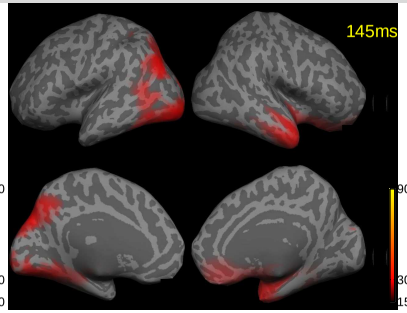	
Left	Right	Left	Right	Left	Right	Left	Right
dorsal stream		dorsal stream		dorsal stream	orbitofrontal cortex	dorsal stream	orbitofrontal cortex
		occipital arietal		ventral stream	amygdala	ventral stream	amygdala
				occipital arietal	temporal pole	occipital arietal	temporal pole
						fusiform gyrus	

155 ms		160 ms		170 ms		185 ms	
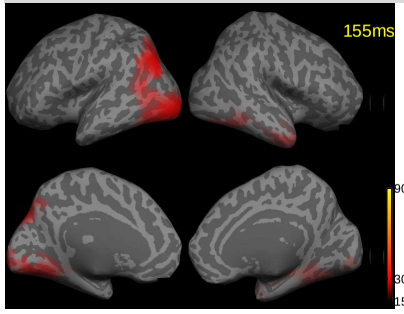		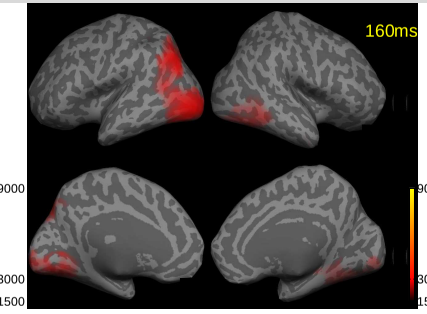		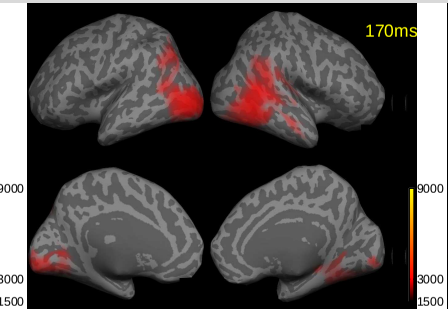		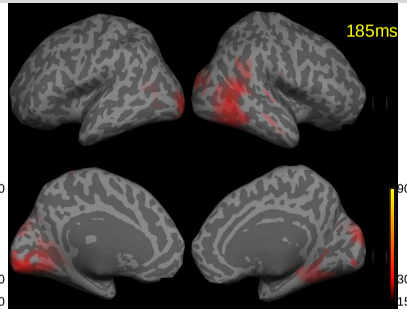	
Left	Right	Left	Right	Left	Right	Left	Right
occipital arietal	temporal pole	inferior temporal gyrus	occipital arietal	fusiform gyrus	inferior occipital gyrus	fusiform gyrus	
fusiform gyrus	fusiform gyrus occipital arietal		inferior occipital gyrus	superior temporal gyrus		superior temporal sulcus	
inferior temporal gyrus	fusiform gyrus						
	inferior occipital gyrus						

190 ms

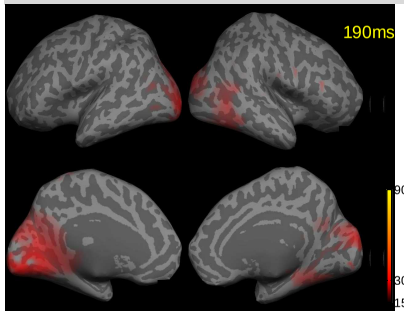

Left	Right
V2	fusiform gyrus
V3	

195 ms

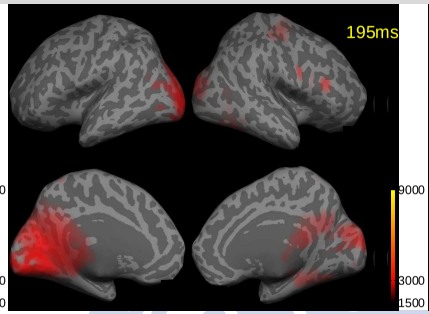

Left	Right
V2	V1
V3	posterior cingulate cortex
posterior cingulate cortex	middle temporal

205 ms

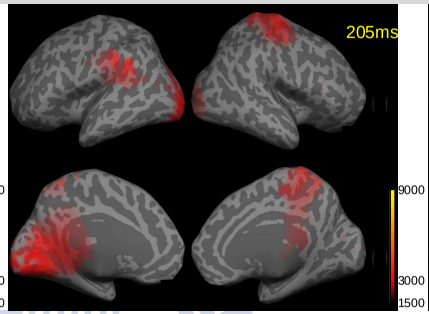

Left	Right
V2	central sulcus
V3	
posterior cingulate cortex	
inferior parietal	
supermarginal	

210 ms

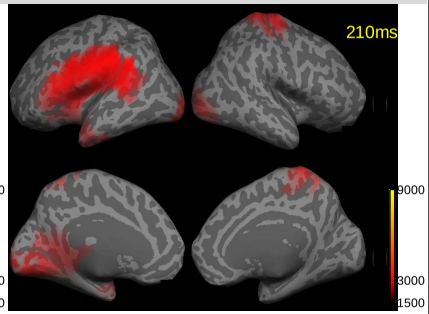

Left	Right
inferior frontal gyrus	central sulcus
temporal pole	

220 ms

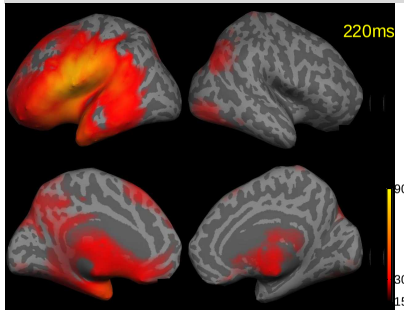

Left	Right
inferior frontal gyrus	caudate nucleus
temporal pole	poterior parietal gyrus
orbitofrontal cortex	inferior occipital gyrus
superior frontal gyrus	
middle temporal gyrus	

235 ms

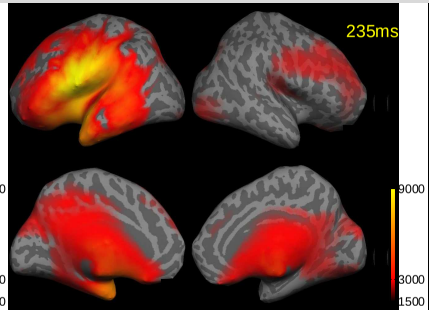

Left	Right
inferior frontal gyrus	inferior frontal gyrus
temporal pole	dorsal prefrontal gyrus
orbitofrontal cortex	premotor cortex
superior frontal gyrus	inferior occipital gyrus
middle temporal gyrus	posterior cingulate cortex
	orbitofrontal cortex

250 ms

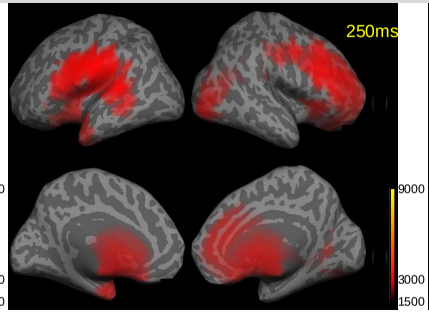

Left	Right
inferior frontal gyrus	inferior frontal gyrus
temporal pole	middle frontal gyrus
orbitofrontal cortex	premotor cortex
superior temporal gyrus	lateral occipital gyrus
caudate nucleus	anterior cingulate cortex
	orbitofrontal cortex

255 ms

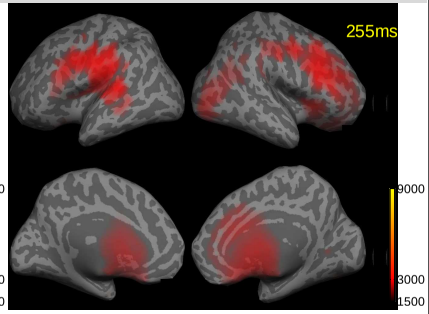

Left	Right
premotor cortex	middle frontal gyrus
superior temporal gyrus	premotor cortex
primary somatosensory cortex	lateral occipital gyrus
	anterior cingulate cortex
	orbitofrontal cortex

260 ms

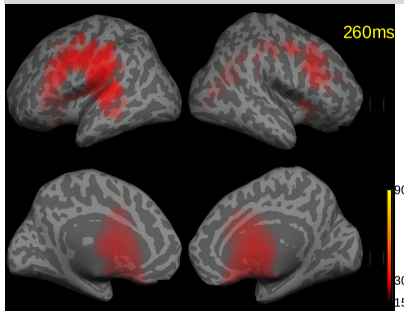

Left	Right
premotor cortex	dorsolateral prefrontal cortex
superior temporal gyrus	anterior cingulate cortex
primary somatosensory cortex	
anterior cingulate cortex	

265 ms

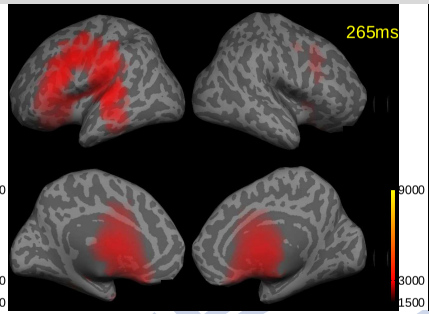

Left	Right
inferior frontal gyrus	premotor cortex
premotor cortex	anterior cingulate cortex
primary somatosensory cortex	
anterior cingulate cortex	
supurior temporal gyrus	

275 ms

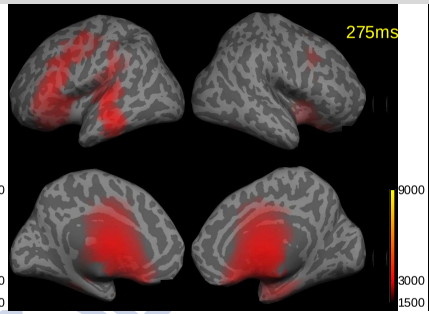

Left	Right
inferior frontal gyrus	anterior cingulate cortex
premotor cortex	amygdala
anterior cingulate cortex	premotor cortex
supurior temporal gyrus	
middle temporal gyrus	
orbitofrontal gyrus	

280 ms

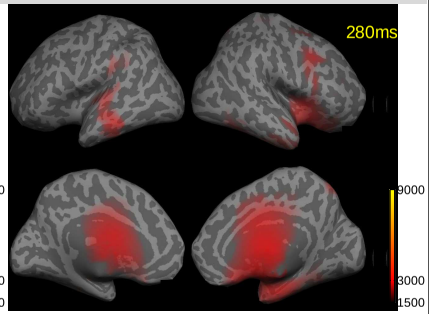

Left	Right
anterior cingulate cortex	anterior cingulate cortex
middle temporal gyrus	amygdala
	orbitofrontal cortex
	premotor cortex

290 ms

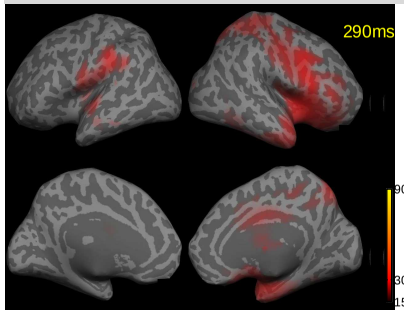

Left	Right
inferior partial	premotor cortex
	central culcus
	temporal pole
	superior parietal
	anterior insula

300 ms

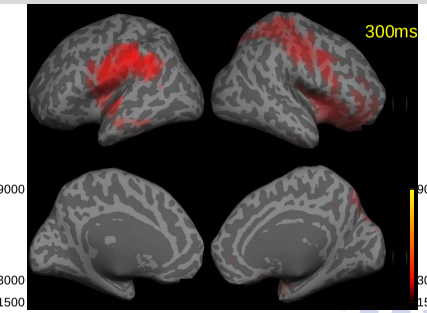

Left	Right
posterior insula	premotor cortex
supermarginal gyrus	central culcus
inferior parietal	superior parietal
sensorimotor cortex	anterior insula

310 ms

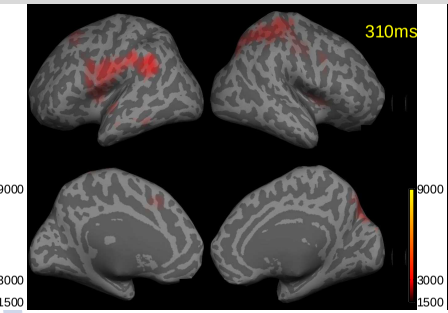

Left	Right
posterior insula	superior parietal
supermarginal gyrus	
sensorimotor	
inferior parietal	
preSMA	

315 ms

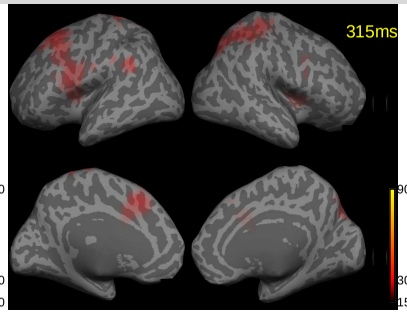

Left	Right
inferior frontal gyrus	superior parietal
SMA	
premotor	

320 ms		325 ms		330 ms		335 ms	
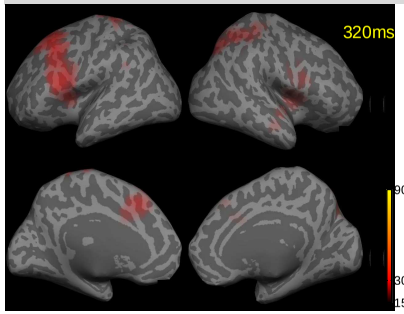		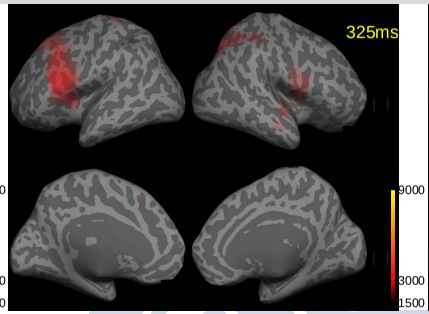		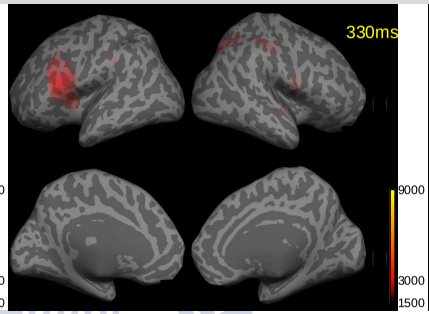		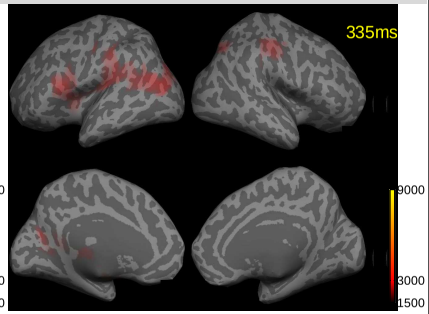	
Left	Right	Left	Right	Left	Right	Left	Right
inferior frontal gyrus	superior parietal	inferior frontal gyrus	superior parietal	inferior frontal gyrus		inferior forntal gyrus	primary somatosensory cortex
premotor		premotor		premotor		premotor	
SMA		SMA				superior temporal sulcus	
						inferior parietal gyrus	

340 ms		350 ms		360 ms		365ms	
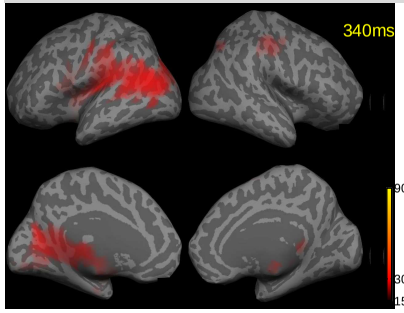		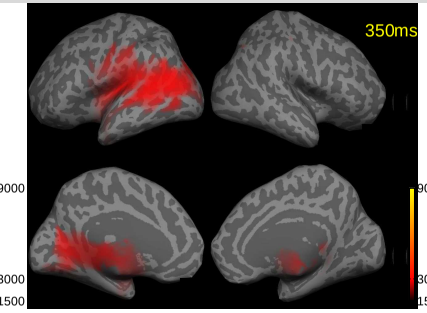		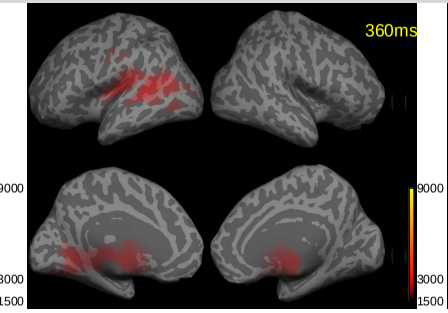		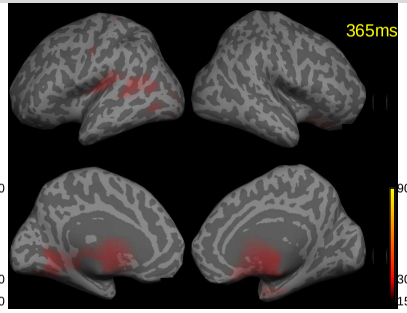	
Left	Right	Left	Right	Left	Right		
superior temporal sulcus		superior temporal sulcus		superior temporal sulcus		superior temporal sulcus	
middle temporal sulcus		middle temporal sulcus		posterior insula		posterior insula	
posterior insula		posterior insula					

375 ms

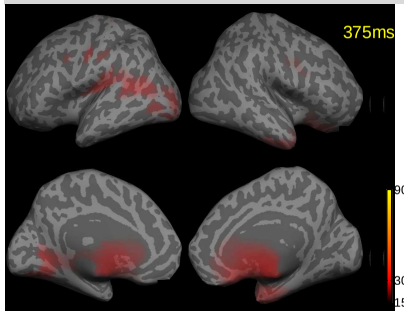

Left	Right
superior temporal sulcus	temporal pole
fusiform gyrus	orbitofrontal gyrrus

380 ms

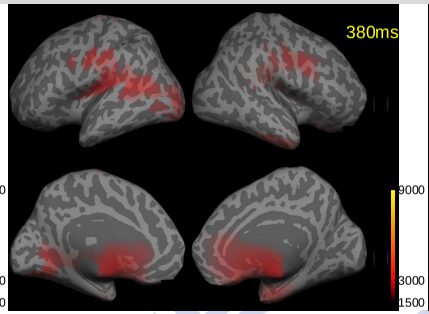

Left	Right
superior temporal sulcus	sensorimotor cortex
posterior insula	temporal pole
fusiform gyrus	orbitofrontal cortex
sensorimotor cortex	
orbitofrontal cortex	

385 ms

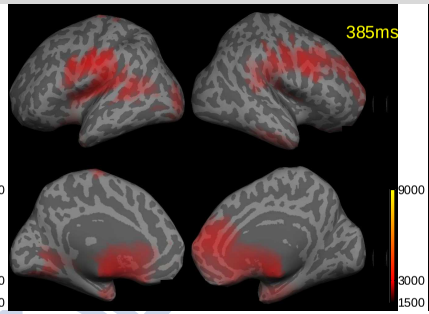

Left	Right
superior temporal sulcus	dorsolateral prefrontal cortex
posterior insula	premotor cortex
fusiform gyrus	sensorimortex cortex
sensorimotor cortex	orbitofrontal corte
orbitofrontal cortex	medile prefrontal cortex
	inferior temporal gyrus

390ms

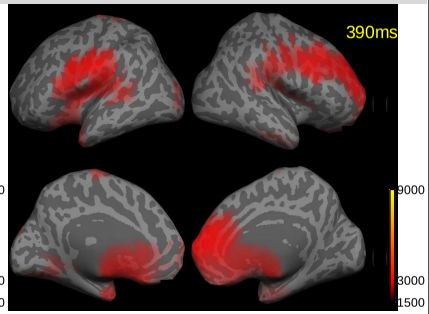

facial movement	premotor cortex
orbitofrontal cortex	anterior cingulate cortex
sensorimotor cortex	orbitofrontal cortex
premotor cortex	middle frontal cortex

400 ms

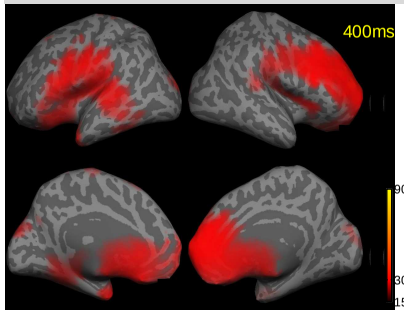

Left	Right
facial movement	premotor cortex
orbitofrontal cortex	anterior cingulate cortex
sensorimotor cortex	orbitofrontal cortex
premotor cortex	middle frontal cortex
inferior frontal gyrus	
temporal pole	
superior temporal gyrus	

410 ms

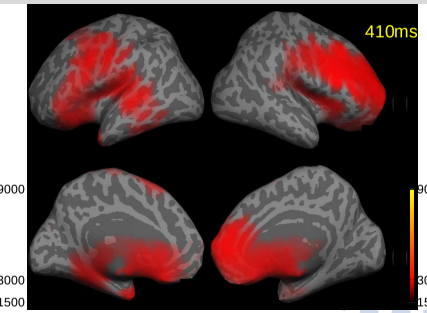

Left	Right
facial movement	premotor cortex
orbitofrontal cortex	anterior cingulate cortex
sensorimotor cortex	orbitofrontal cortex
premotor cortex	middle frontal cortex
inferior frontal gyrus	
temporal pole	
superior temporal gyrus	

420 ms

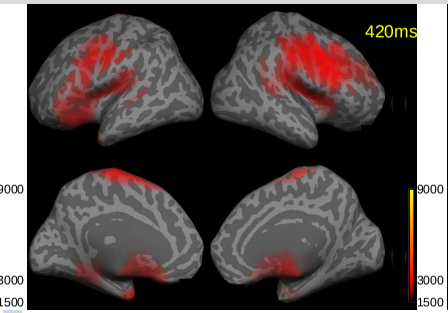

Left	Right
facial movement	premotor cortex
orbitofrontal cortex	orbitofrontal cortex
sensorimotor cortex	dorsolateral frontal cortex
premotor cortex	posterior insula
inferior frontal gyrus	
temporal pole	
superior temporal gyrus	

425ms

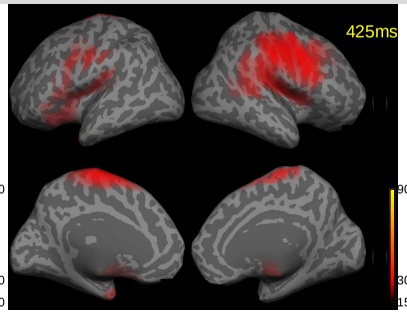

premotor cortex	premotor
inferior frontal gyrus	temporal parietal junction
sensorimotor cortex	sensorimotor cortex

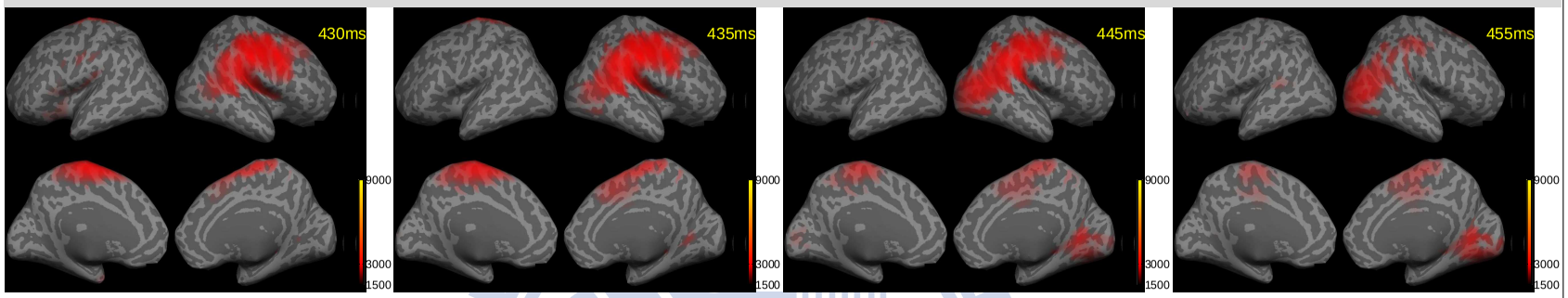

Left	Right	Left	Right	Left	Right		
sensorimotor cortex	premotor	sensorimotor cortex	premotor	central sulcus	premotor	central sulcus	temporal parietal junction
	temporal parietal junction		temporal parietal junction		temporal parietal junction		somatosensory cortex
	supermarginal		supermarginal		supermarginal		inferior parietal
	sensorimotor cortex		sensorimotor cortex		sensorimotor cortex		occipital
	inferior parietal		inferior parietal		inferior parietal		
	superior temporal sulcus		superior temporal sulcus		superior temporal sulcus		
					occipital		

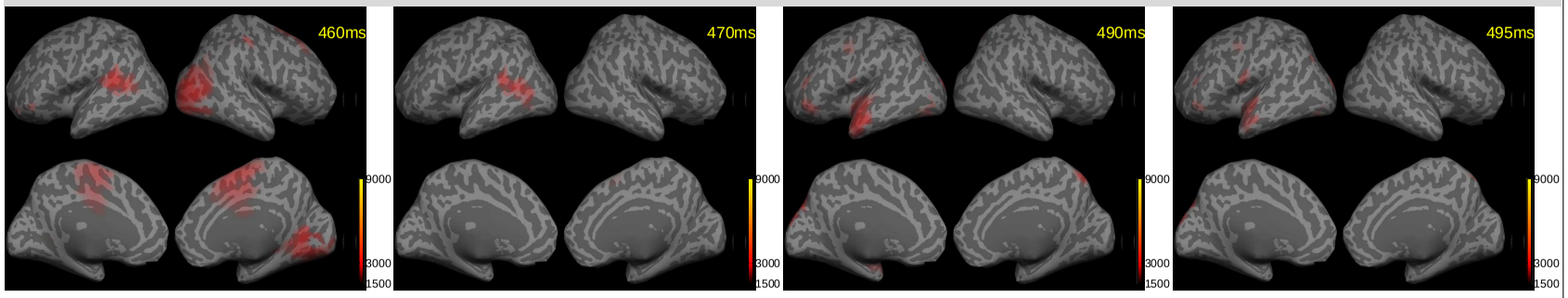

Left	Right	Left	Right	Left	Right
superior temporal sulcus	occipital	superior temporal sulcus	superior temporal sulcus	superior temporal sulcus	superior temporal sulcus
premotor	premotor				

515 ms		520 ms		525 ms		530ms	
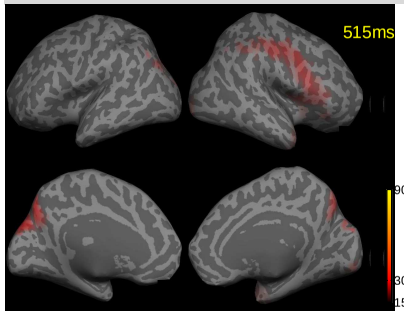		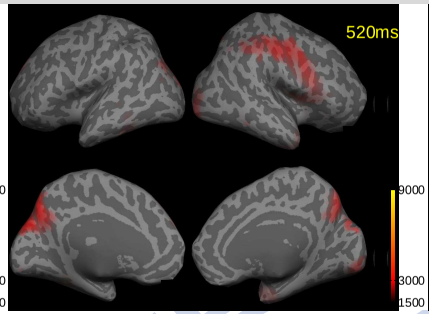		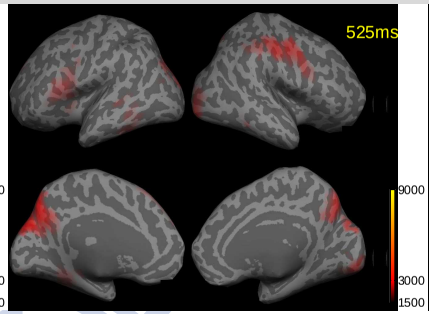		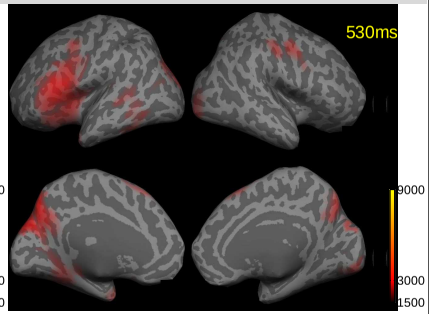	
Left	Right	Left	Right	Left	Right	Left	Right
posterior parietal	premotor cortex	posterior parietal	posterior parietal premotor cortex sensorimotor cortex	posterior parietal inferior frontal gyrus	posterior parietal premotor cortex sensorimotor cortex	posterior parietal inferior frontal gyrus premotor cortex	posterior parietal sensorimotor cortex

535 ms		540 ms		545 ms		550 ms	
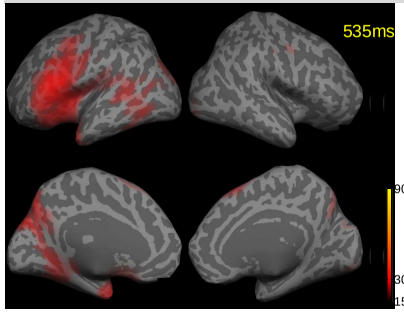		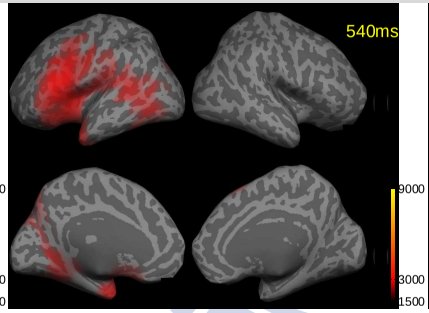		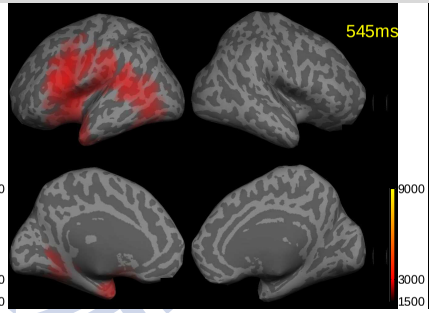		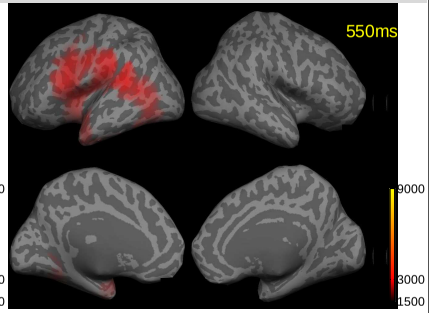	
Left	Right	Left	Right	Left	Right		
posterior parietal inferior frontal gyrus premotor cortex temporal pole superior temporal sulcus middle temporal sulcus		inferior frontal gyrus premotor cortex temporal pole superior temporal sulcus middle temporal sulcus		inferior frontal gyrus premotor cortex sensorimotor cortex temporal pole superior temporal sulcus middle temporal sulcus		inferior frontal gyrus premotor cortex sensorimotor cortex temporal pole superior temporal sulcus middle temporal sulcus	

555 ms

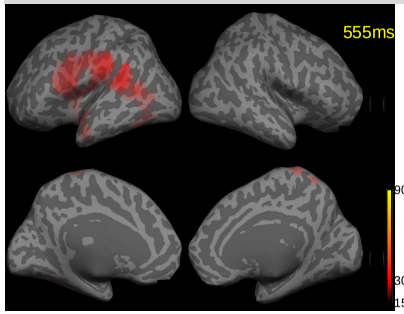

Left	Right
premotor cortex	
sensorimotor cortex	
inferior parietal gyrus	
superior temporal gyrus	

560 ms

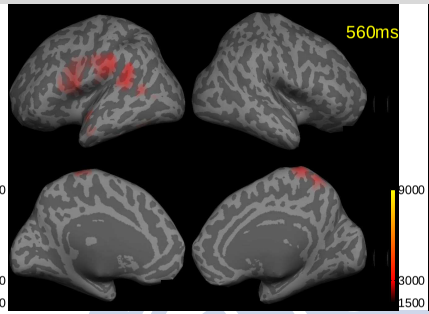

Left	Right
premotor cortex	central culcus
sensorimotor cortex	
inferior parietal gyrus	
superior temporal gyrus	

570 ms

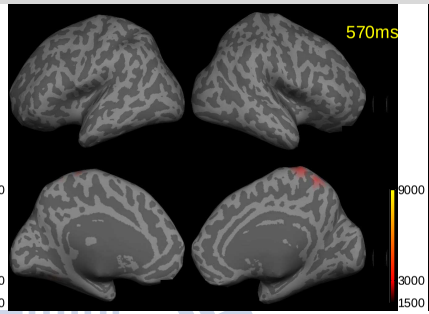

Left	Right
	central sulcus

580 ms

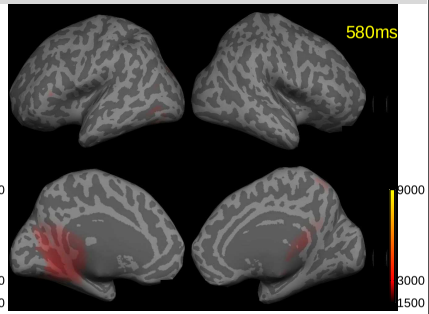

585 ms

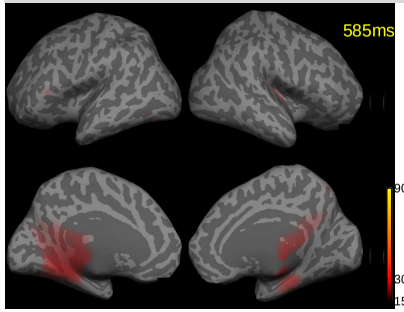

Left	Right
inferior temporal gyrus	

590 ms

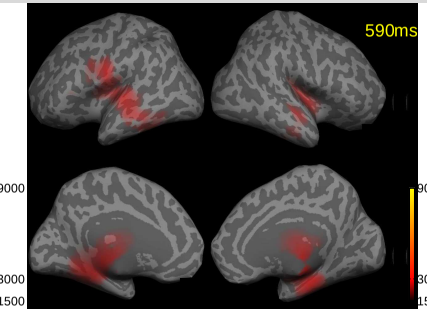

Left	Right
inferior temporal gyrus	inferior temporal gyrus
superior temporal gyrus	
meddile temporal gyrus	
facial movement	

600 ms

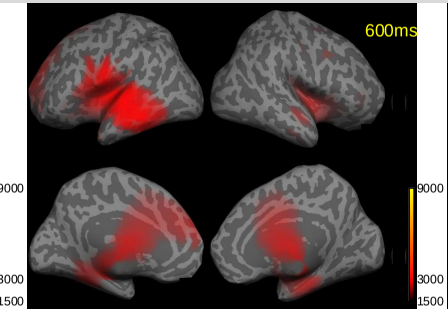

Left	Right
inferior temporal gyrus	inferior temporal gyrus
superior temporal gyrus	
meddile temporal gyrus	
facial movement	
superior frontal gyrus	

605 ms

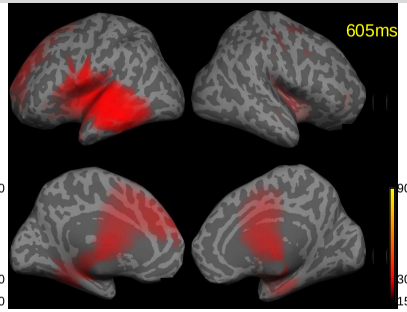

inferior temporal gyrus	inferior temporal gyrus
superior temporal gyrus	
meddile temporal gyrus	
facial movement	
superior frontal gyrus	

615 ms		620 ms		625 ms		630 ms	
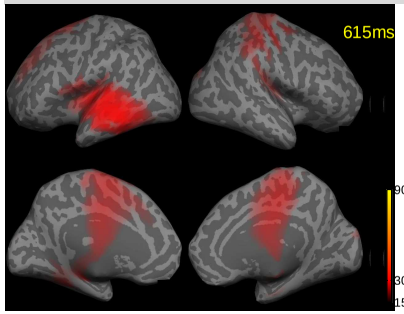		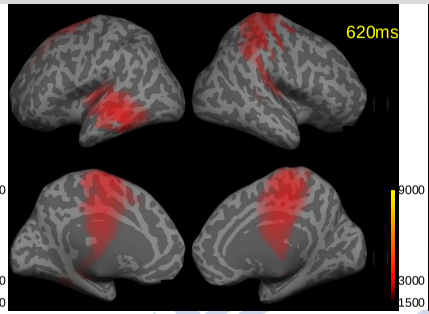		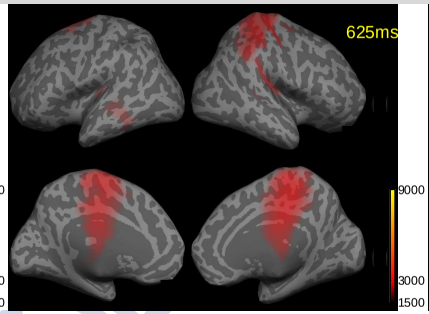		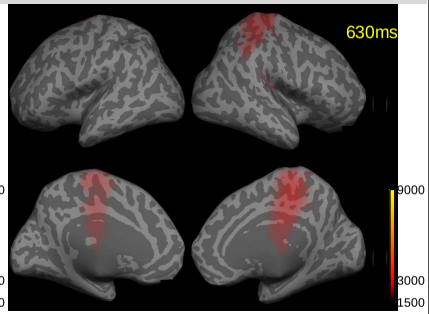	
Left	Right	Left	Right	Left	Right		
inferior temporal gyrus	sensorimotor cortex	superior temporal gyrus	sensorimotor cortex	sensorimotor cortex	sensorimotor cortex	sensorimotor cortex	sensorimotor cortex
superior temporal gyrus		middle temporal gyrus					
middle temporal gyrus		sensorimotor cortex					
facial movement							
superior frontal gyrus							

670 ms		680 ms		685 ms		695 ms	
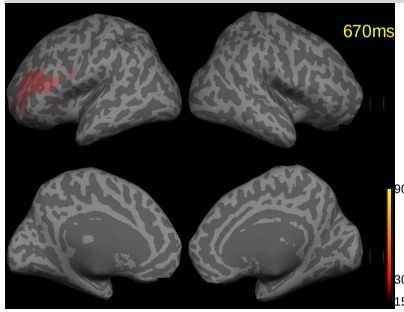		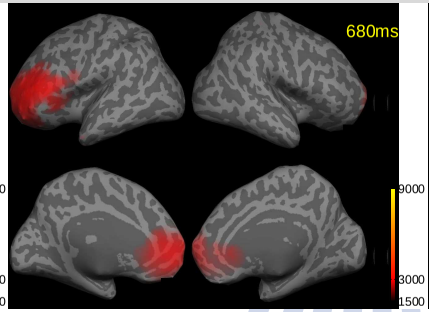		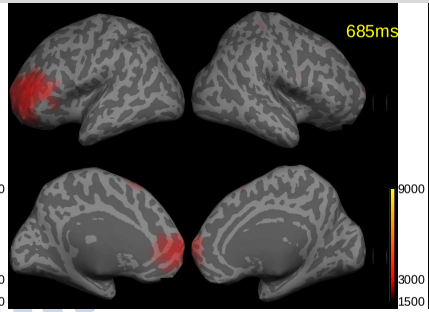		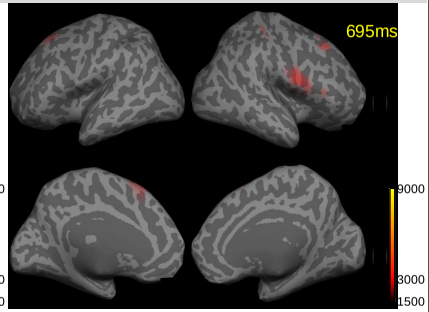	
Left	Right	Left	Right	Left	Right		
middle prefrontal gyrus		middle prefrontal gyrus		middle frontal gyrus			

Subject B

The anatomical position of left inferior frontal gyrus was shown in the first row of the Table 3.7. The axis of the volume was at (68,160,68) voxel. The source signals at the left inferior frontal gyrus of three conditions calculated by MCB was shown in the next row of the Table 3.7. In this reference position, We chose 120 to 220 ms were chosen as reference signal on imitation and observation conditions, and 180 to 2xz2180 ms was chosen as reference signal on execution condition.

Imitation condition The results were shown in Table 3.8. In addition, the result with different threshold were shown in Table 3.9 which included 400 ms to 670 ms. We can observe that at

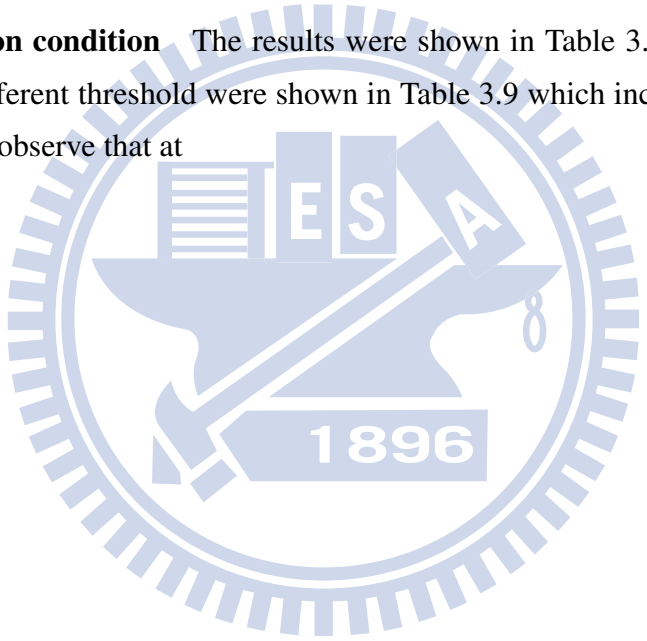

Table 3.7: The source signal of the left inferior frontal gyrus as reference signal which were calculated by MCB. The first row shows the position of the left inferior frontal gyrus. The next is the source signal of three condition - imitate, observation and execution.

the information of the reference – left inferior frontal gyrus		
the position (56,152,76)		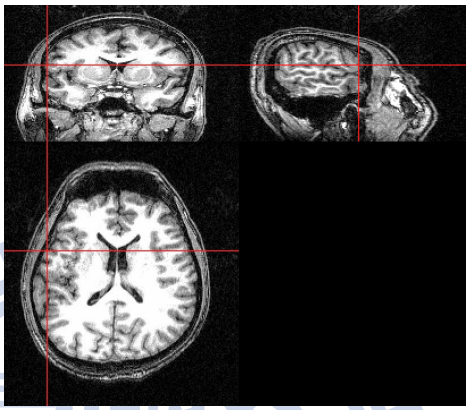
the signal	imitate	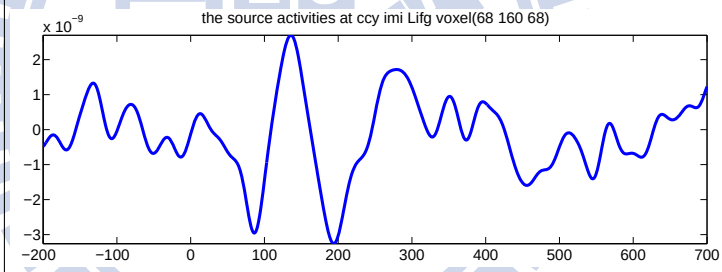
	observation	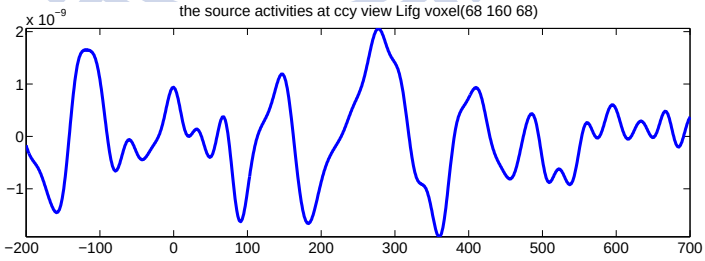
	execution	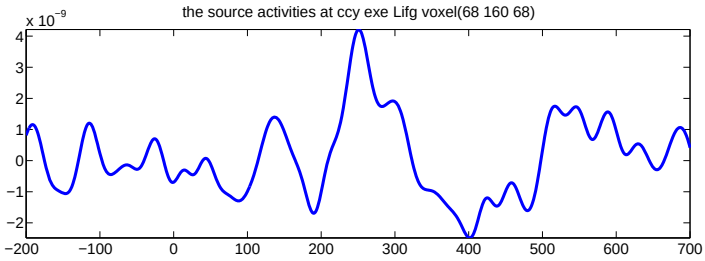

Table 3.8: The correlation map and the significant correlation regions of the reference region at left inferior frontal gyrus on imitation condition at different time interval.

The correlated brain region with left inferior gyrus of various time

80 ms		90 ms		110 ms		115 ms	
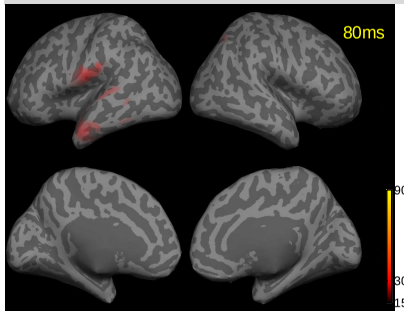		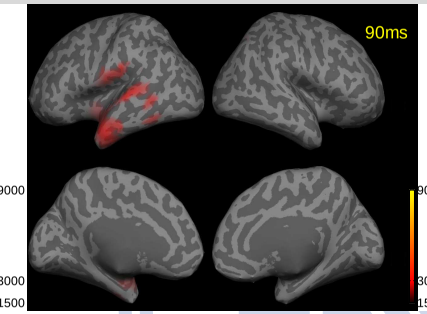		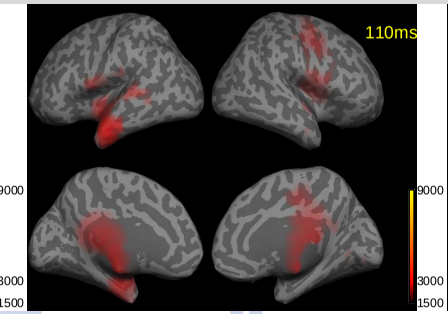		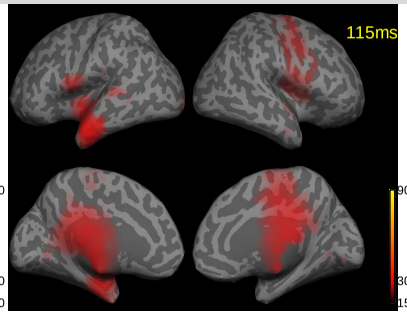	
Left	Right	Left	Right	Left	Right	Left	Right
middle temporal gyrus		middle temporal gyrus superior temporal gyrus		middle temporal gyrus superior temporal gyrus amygdala	premotor cortex	middle temporal gyrus superior temporal gyrus amygdala	premotor cortex central sulcus
120 ms		**250 ms**		**260 ms**		**265 ms**	
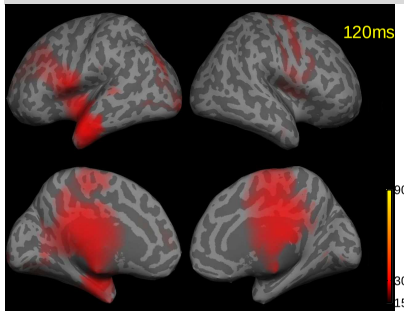		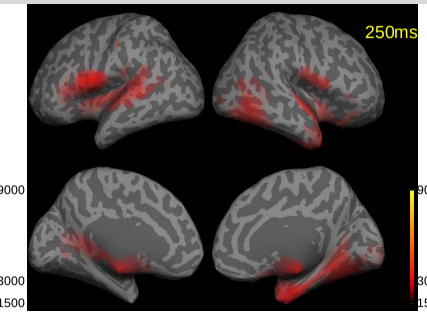		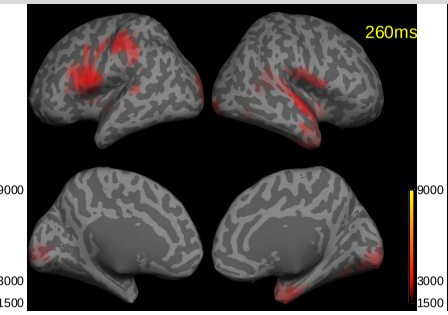		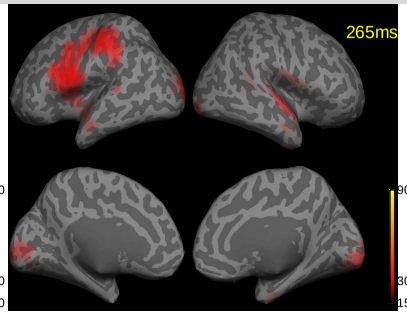	
Left	Right	Left	Right	Left	Right	Left	Right
middle temporal gyrus superior temporal gyrus amygdala	premotor cortex central sulcus	superior temporal gyrus facial movement	temporal pole occipital temporal facial movement	facial movement somatosensory cortex premotor	facial movement superior temporal gyrus temporal pole	facial movement somatosensory cortex sensorimotor cortex premotor	facial movement superior temporal gyrus

275 ms

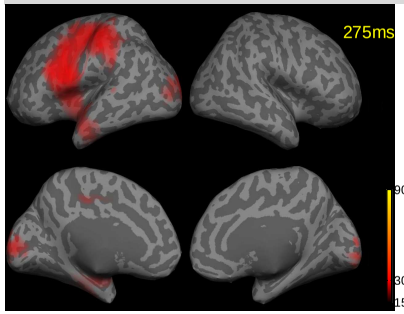

Left	Right
facial movement	
somatosensory cortex	
sensorimotor cortex	
premotor	

285 ms

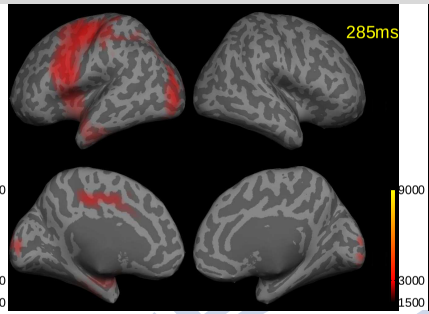

Left	Right
facial movement	
somatosensory cortex	
sensorimotor cortex	
premotor	
central sulcus	

295 ms

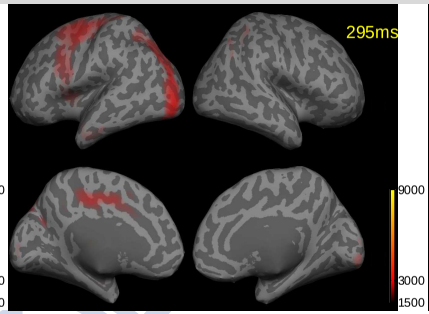

Left	Right
facial movement	
somatosensory cortex	
sensorimotor cortex	
premotor	
SMA	
central sulcus	

310 ms

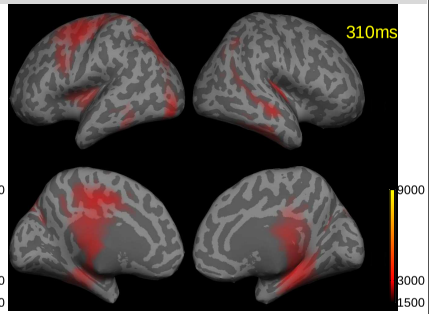

Left	Right
facial movement	
somatosensory cortex	
sensorimotor cortex	
premotor	

350 ms

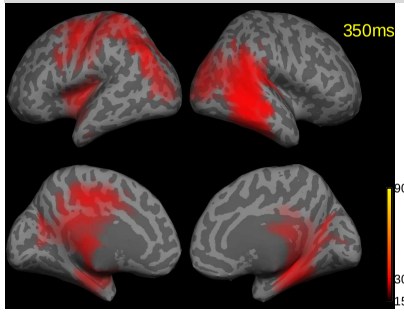

Left	Right
somatosensory cortex	angular gyrus
sensorimotor cortex	posterior insula cortex
premotor	superior temporal gyrus
inferior parietal	
superior parietal	

365 ms

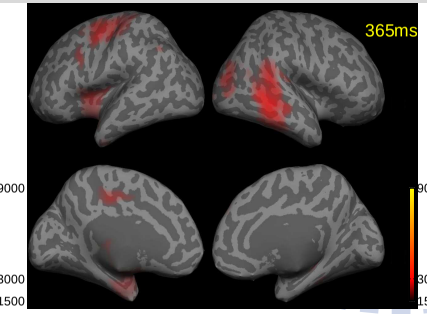

Left	Right
sensorimotor cortex	superior temporal gyrus

415 ms

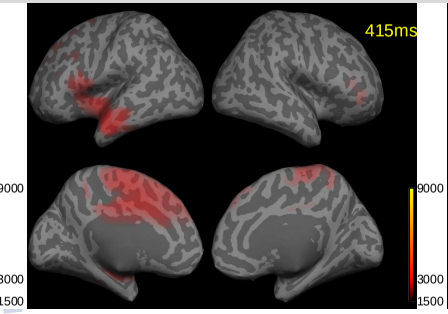

Left	Right
SMA	
inferior frontal gyrus	

435 ms

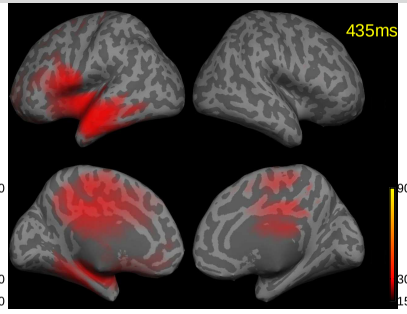

Left	Right
premotor cortex	
middle temporal gyrus	
amygdala	
SMA	

450 ms		470 ms		485 ms		505 ms	
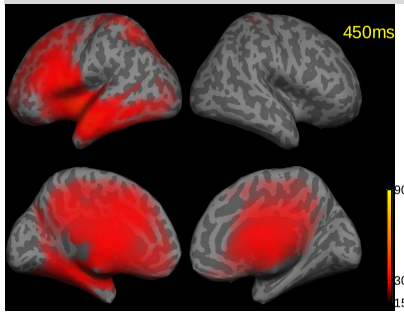		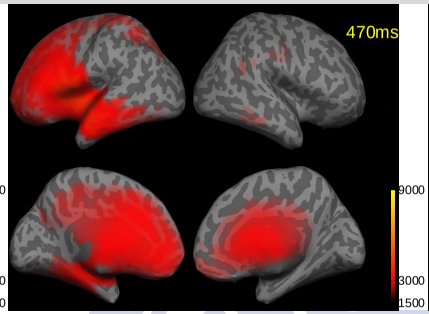		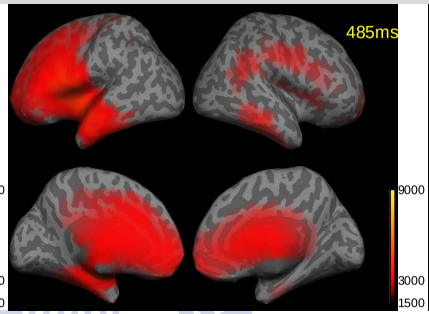		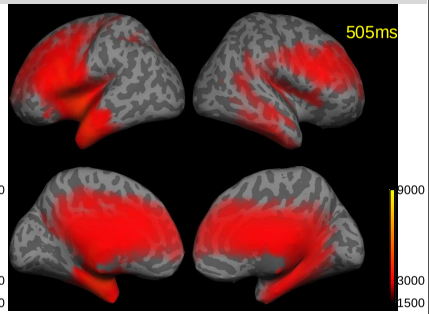	
Left	Right	Left	Right	Left	Right	Left	Right
facial movement		facial movement		facial movement	premotor cortex	facial movement	premotor cortex
orbitofrontal cortex		orbitofrontal cortex		orbitofrontal cortex	superior temporal gyrus	superior temporal sulcus	superior temporal gyrus
SMA		superior temporal sulcus		superior temporal sulcus	central sulcus	middle temporal sulcus	central sulcus
inferior frontal gyrus		middle temporal sulcus		middle temporal sulcus		ACC	middle prefrontal cortex
ACC		ACC		ACC		middle prefrontal cortex	
superior parietal				middle prefrontal cortex			
520 ms		**535 ms**		**565 ms**		**585 ms**	
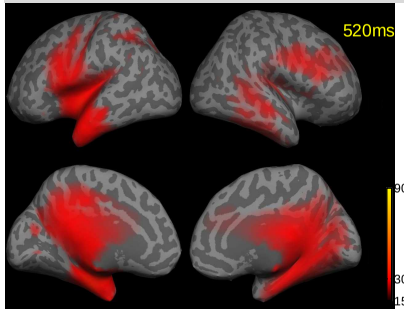		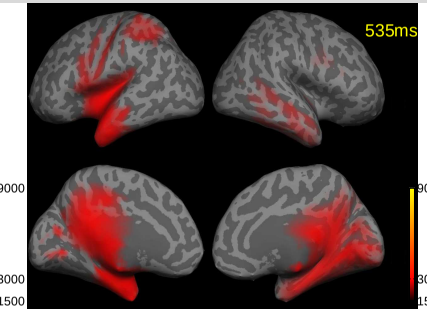		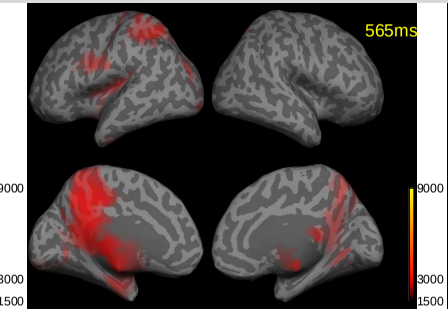		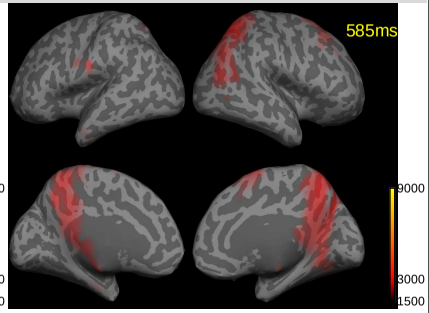	
Left	Right	Left	Right	Left	Right	Left	Right
facial movement	premotor cortex	temporal pole	middle temporal gyrus	superior parietal gyrus			superior parietal
somatosensory cortex	superior temporal sulcus	superior parietal gyrus					SMA
sensorimotor cortex	middle temporal sulcus	central sulcus					
premotor							

Left	Right
inferior frontal gyrus	

Left	Right
inferior frontal gyrus	

Left	Right
inferior frontal gyrus premotor temporal pole	

Left	Right
SMA	

Left	Right
inferior parietal	middle temporal sulcus

Left	Right
middle temporal gyrus	

Table 3.9: The correlation map with threshold [1800 - 3200 - 4070] and the significant correlation regions of the reference region at left inferior frontal gyrus on imitation condition at different time interval.

The correlated brain region with left inferior gyrus of various time			
400 ms	410 ms	420 ms	430 ms
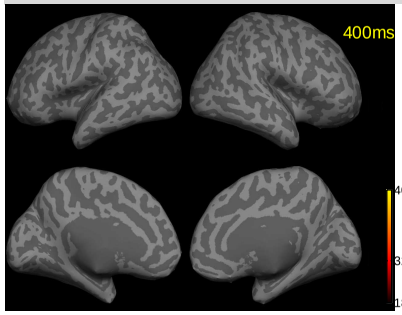	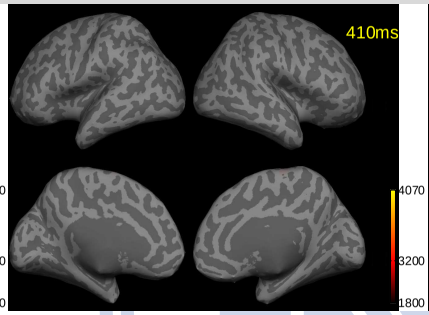	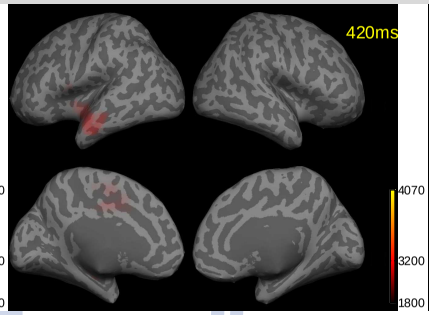	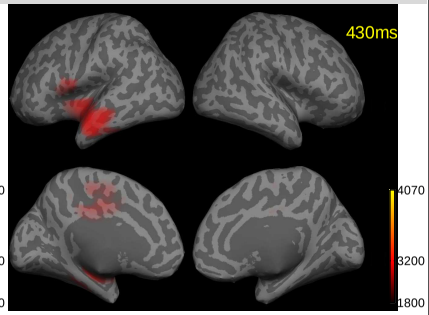
440 ms	450 ms	460 ms	470 ms
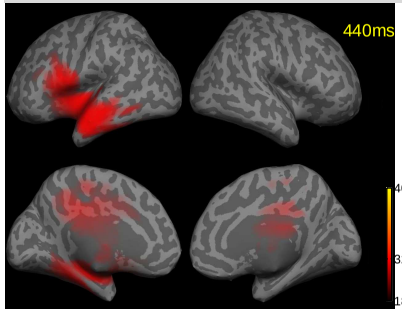	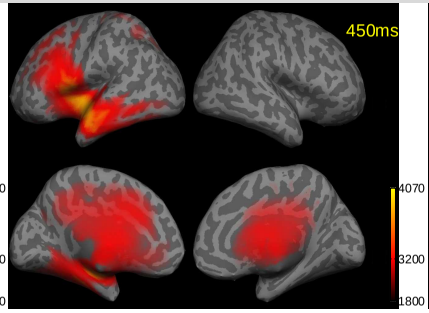	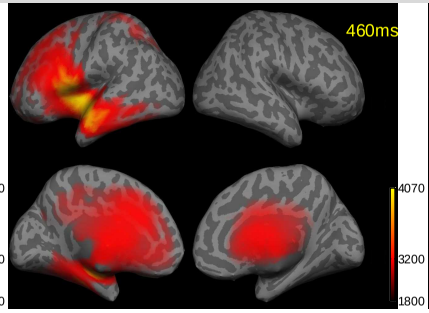	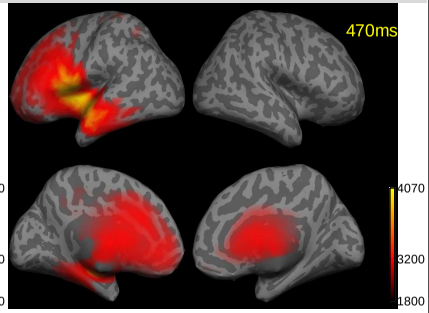

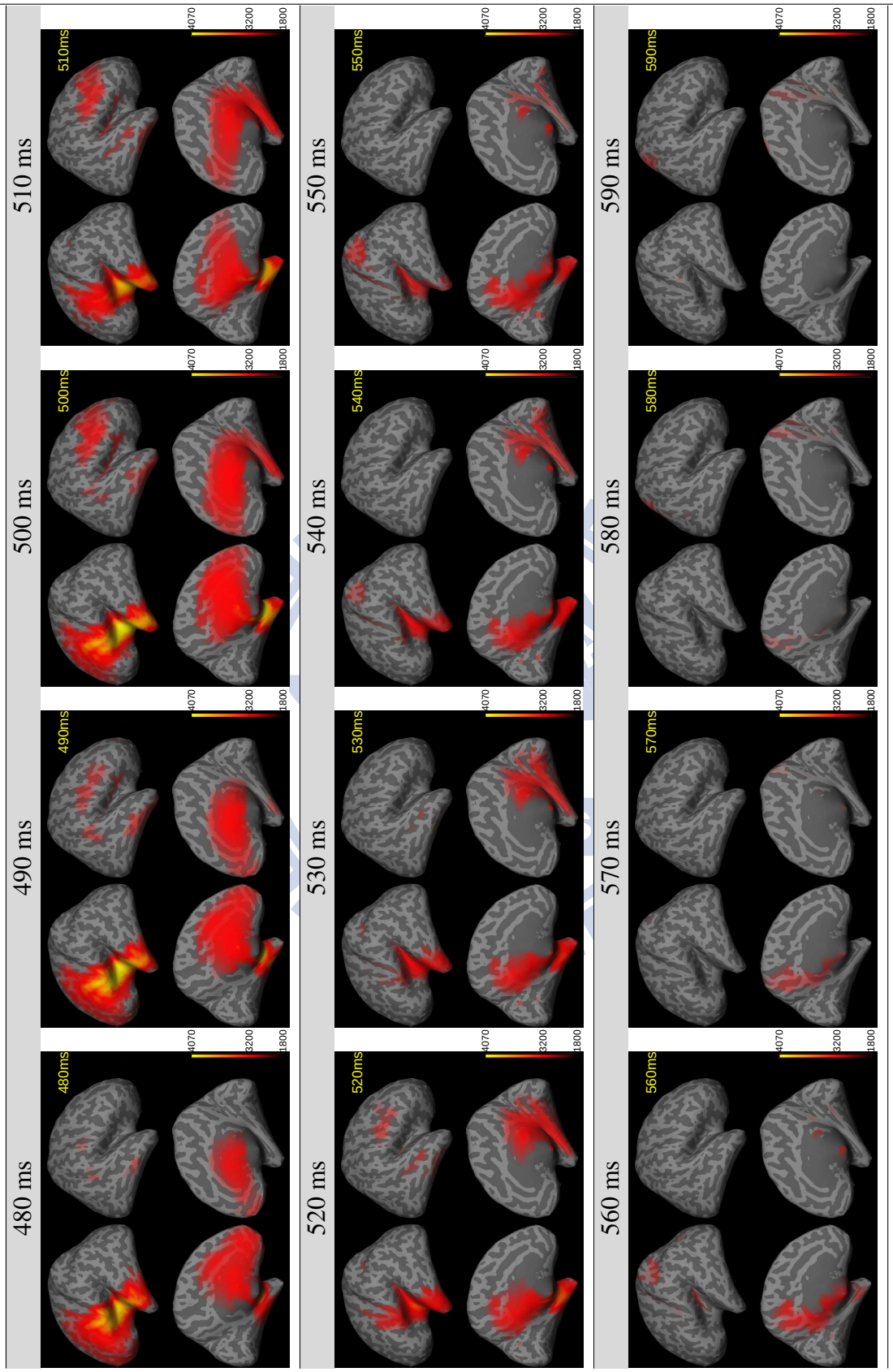
480 ms
480ms
490 ms
490ms
500 ms
500ms
510 ms
510ms
520 ms
520ms
530 ms
530ms
540 ms
540ms
550 ms
550ms
560 ms
560ms
570 ms
570ms
580 ms
580ms
590 ms
590ms
4070
3200
1800

600 ms
610 ms
620 ms
630 ms
640 ms
650 ms
660 ms
670 ms
600ms
610ms
620ms
630ms
640ms
650ms
660ms
670ms
4070
3200
1800
Left
Right
Left
Right
Left
Right
Left
Right
inferior parietal
middle temporal sulcus
middle temporal gyrus

Observation condition The results were shown in Table 3.10.

Table 3.10: The correlation map and the significant correlation regions of the reference region at left inferior frontal gyrus on observation condition at different time interval.

The correlated brain region with left inferior gyrus of various time

115 ms		125 ms		135 ms		140 ms	
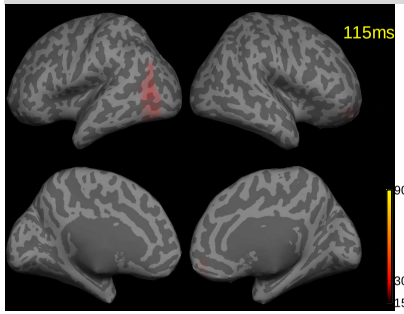		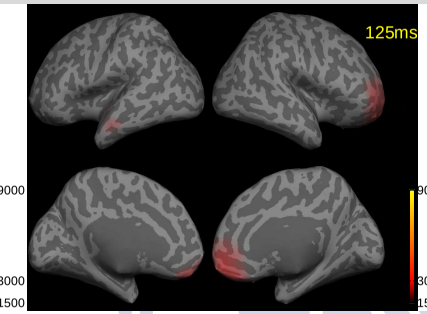		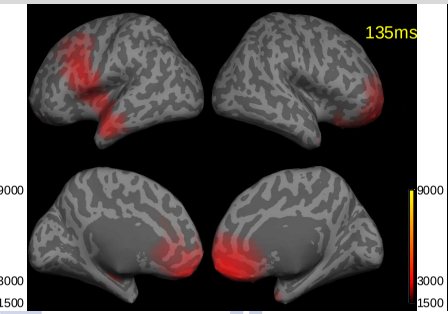		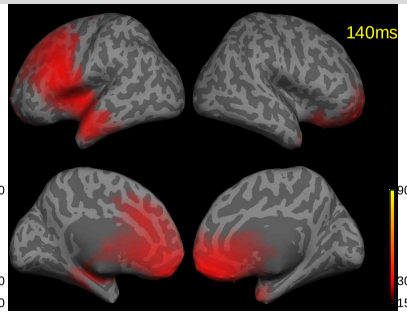	
Left	Right	Left	Right	Left	Right	Left	Right
occipital temporal			dorsolateral prefrontal cortex	inferior frontal gyrus obitalfrontal	obitalfrontal	premotor ACC amygdala inferior frontal gyrus obitalfrontal	obitalfrontal
205 ms		**235 ms**		**255 ms**		**265 ms**	
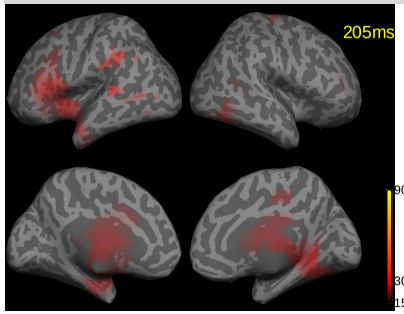		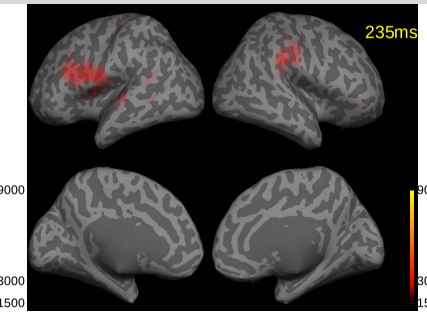		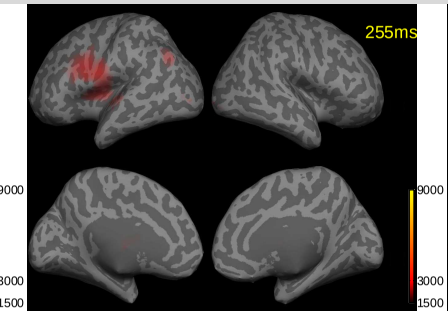		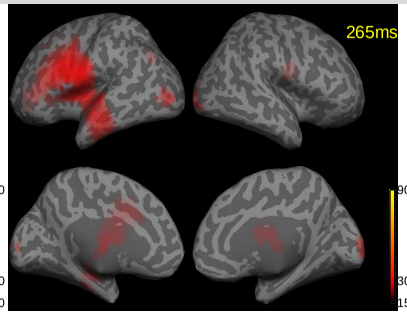	
Left	Right	Left	Right	Left	Right	Left	Right
premotor cortex inferior frontal gyrus amygdala	fusiform gyrus	premotor facial movement	central sulcus	premotor facial movement temporal parietal juction		premotor facial movement inferior frontal gyrus	facial movement

Left	Right	Left	Right	Left	Right
facial movement	facial movement	facial movement	facial movement	facial movement	inferior frontal gyrus
premotor		premotor		premotor	obitalfrontal
central sulcus		central sulcus		amygdala	dorsolateral prefrontal cortex
amygdala		amygdala		middle prefrontal cortex	

Left	Right	Left	Right	Left	Right	Left	Right
obitalfrontal	obitalfrontal	occipital	occipital	inferior frontal cortex	temporal cortex	occipitaltemporal	occipitaltemporal

495 ms		505 ms		515 ms		535 ms	
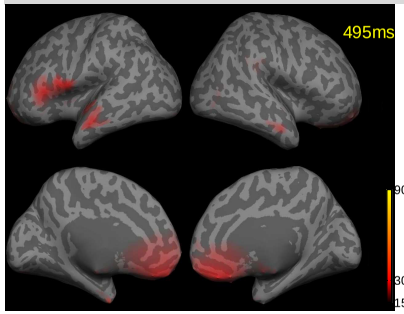		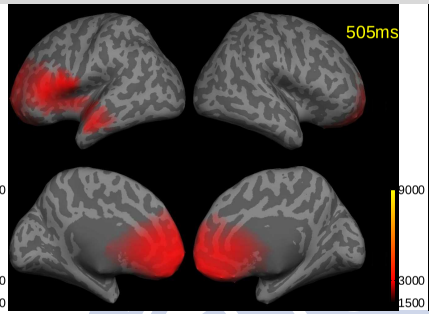		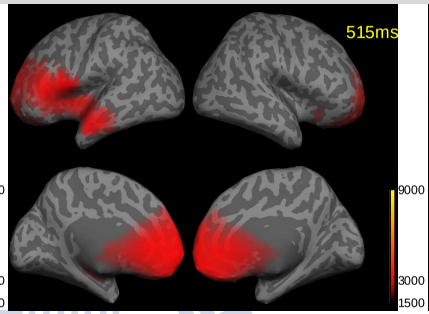		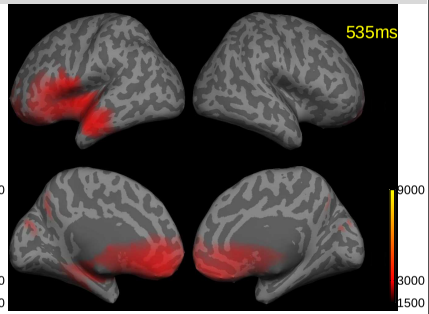	
Left	Right	Left	Right	Left	Right	Left	Right
obitalfrontal	obitalfrontal	obitalfrontal	obitalfrontal	obitalfrontal	obitalfrontal	obitalfrontal	obitalfrontal
inferior frontal cortex		inferior frontal cortex		inferior frontal cortex		inferior frontal cortex	

545 ms		550 ms		555 ms		585 ms	
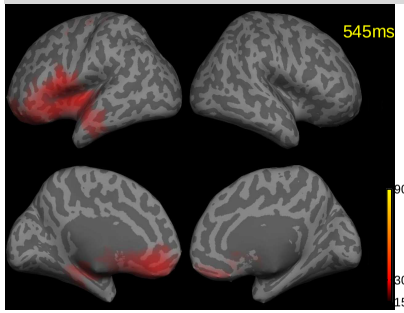		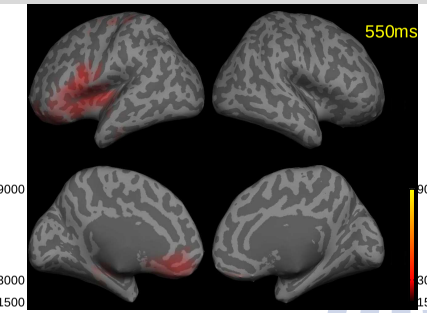		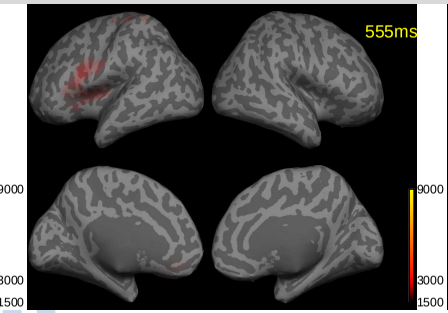		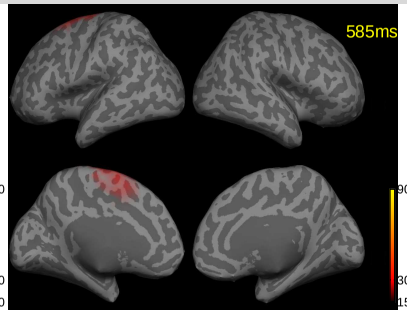	
Left	Right	Left	Right	Left	Right	Left	Right
obitalfrontal	obitalfrontal	obitalfrontal				SMA	
inferior frontal cortex		inferior frontal cortex					

595 ms		600 ms		605 ms		610 ms	
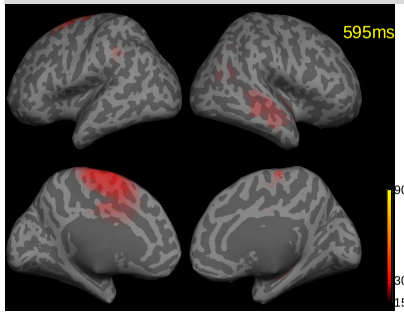		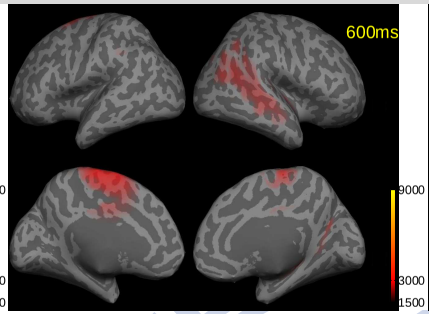		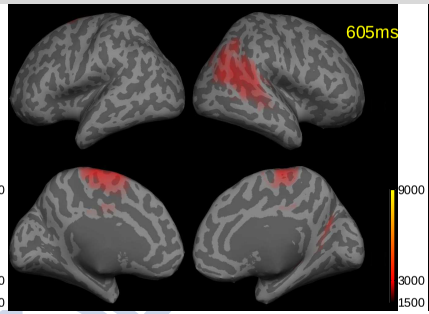		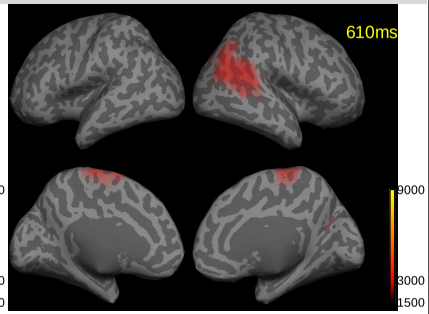	
Left	Right	Left	Right	Left	Right	Left	Right
SMA	middle temporal sulcus	SMA	middle temporal sulcus	SMA	middle temporal sulcus temporal parietal junction	SMA	middle temporal sulcus temporal parietal junction

670 ms		680 ms					
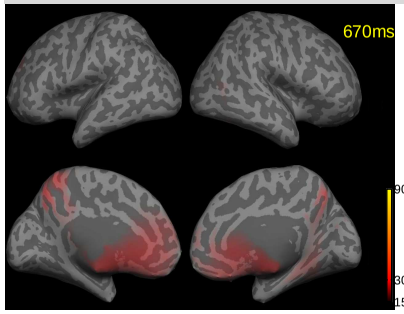		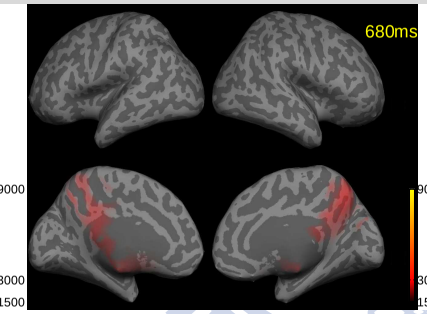					
Left	Right	Left	Right	Left	Right	Left	Right

Execution condition The results were shown in Table 3.11.

Table 3.11: The correlation map and the significant correlation regions of the reference region at left inferior frontal gyrus on execution condition at different time interval.

The correlated brain region with left inferior gyrus of various time

115 ms		120 ms		125 ms		135 ms	
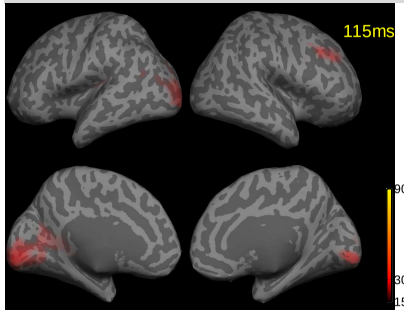		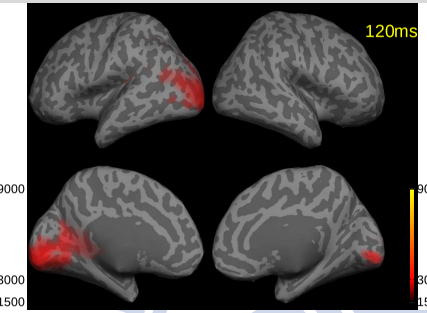		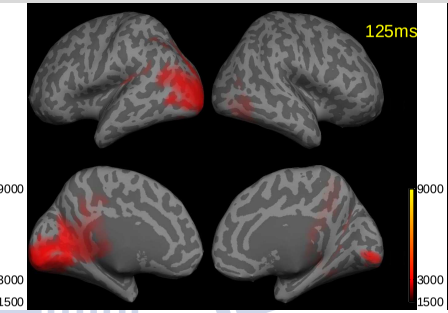		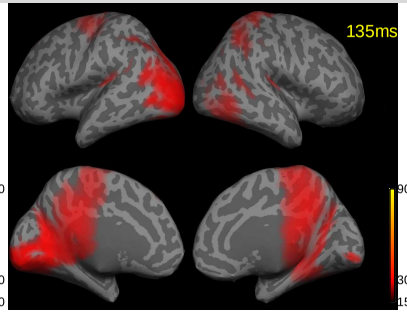	
Left	Right	Left	Right	Left	Right	Left	Right
occipital		occipital		ventral stream occipital		occipital dorsal stream	fusiform gyrus

150 ms		160 ms		170 ms		185 ms	
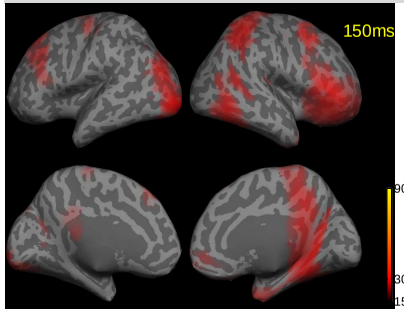		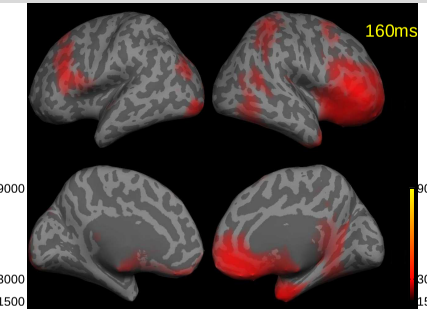		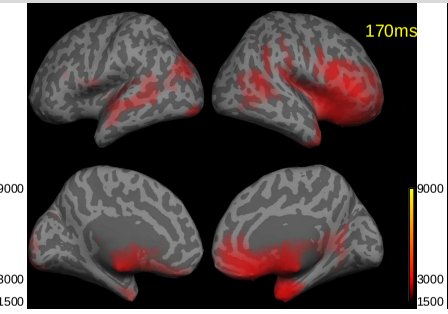		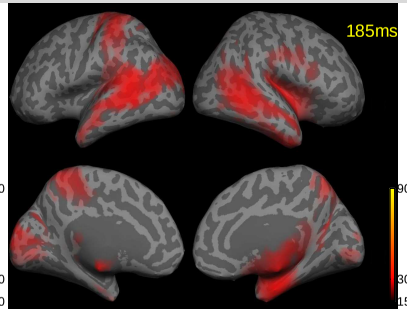	
Left	Right	Left	Right	Left	Right	Left	Right
occipital premotor cortex	dorsal lateral prefrontal superior parietal inferior temporal gyrus premotor	occipital premotor cortex	obitalfrontal dorsal lateral prefrontal superior parietal inferior temporal gyrus premotor temporal pole	occipital middle temporal sulcus	obitalfrontal dorsal lateral prefrontal temporal pole premotor	occipital superior parietal occipitaltemporal middle temporal sulcus	middle temporal gyrus amygdala

195 ms		205 ms		210 ms		255 ms	
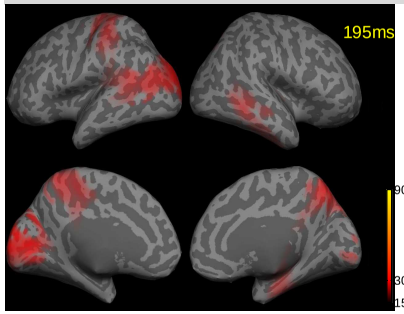		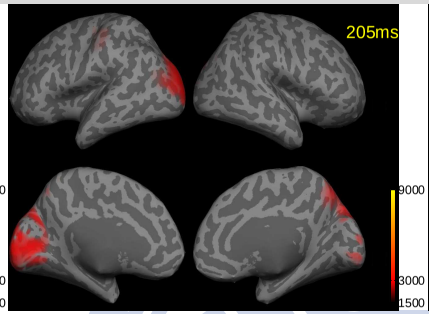		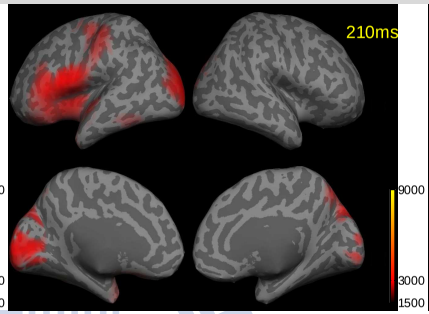		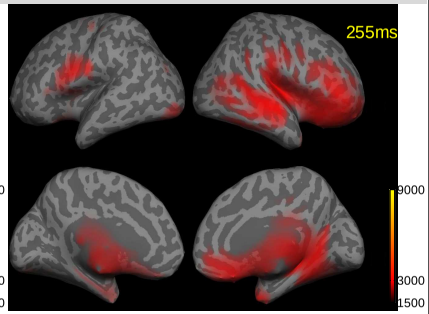	
Left	Right	Left	Right	Left	Right	Left	Right
occipital	occipital		inferior frontal gyrus		M1	obitalfrontal	
central sulcus			occipital			middle temporal sulcus	
						middle prefrontal cortex	

265 ms		285 ms		295 ms		305 ms	
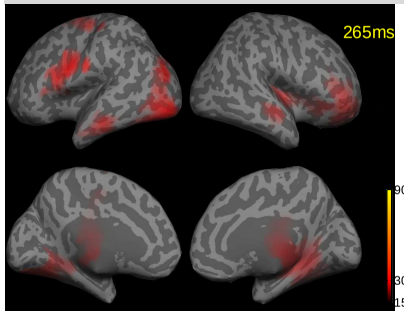		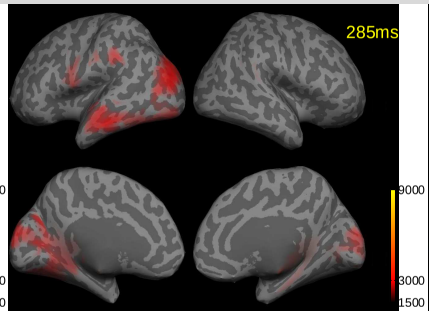		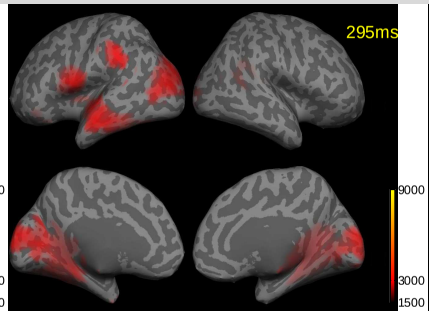		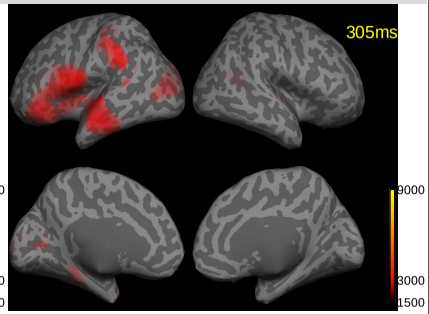	
Left	Right	Left	Right	Left	Right	Left	Right
M1	fusiform gyrus	inferior temporal sulcus		inferior frontal gyrus		inferior frontal gyrus	
fusiform gyrus	inferior frontal gyrus			occipital		inferior parietal	
				inferior parietal			

315 ms	330 ms	340 ms	350 ms
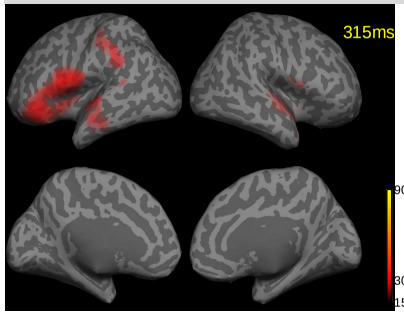	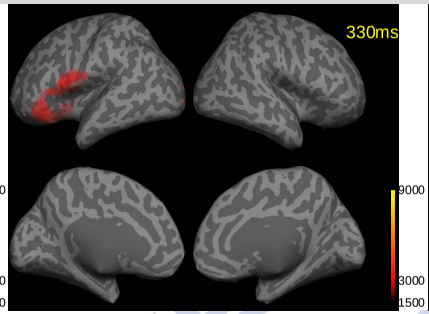	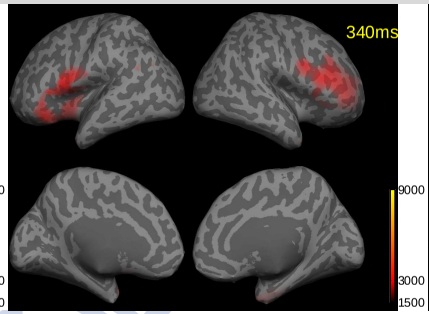	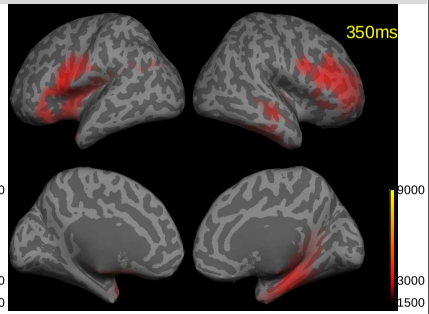
Left / Right	Left / Right	Left / Right	Left / Right
inferior frontal gyrus	inferior frontal gyrus	inferior frontal gyrus	inferior frontal gyrus
inferior parietal		inferior frontal gyrus	inferior frontal gyrus

360 ms	370 ms	380 ms	450 ms
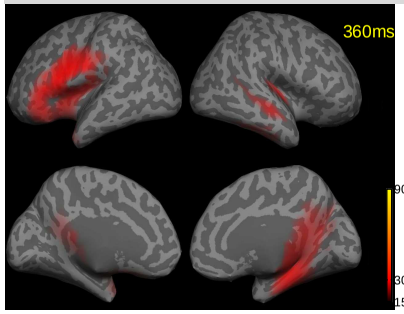	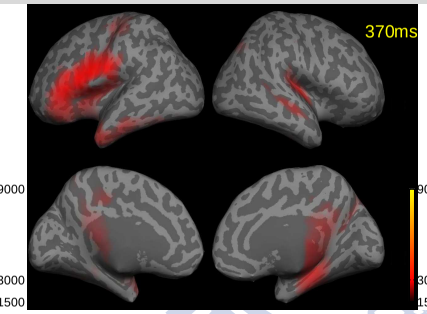	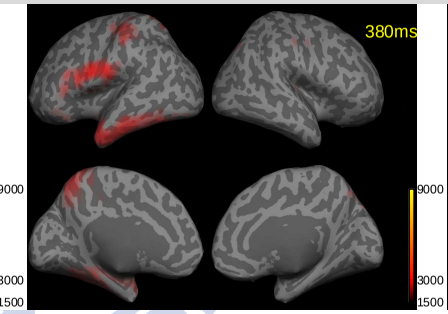	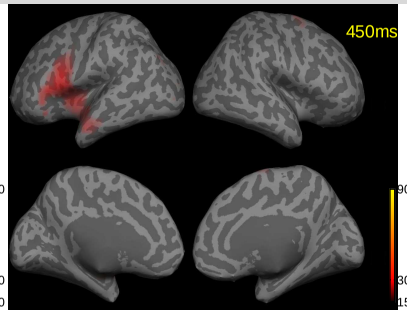
Left / Right	Left / Right	Left / Right	Left / Right
inferior frontal gyrus	inferior frontal gyrus	inferior frontal gyrus	inferior frontal gyrus
M1	M1	inferior temporal gyrus	premotor
		superior parietal	

485 ms		495 ms		510 ms		520 ms	
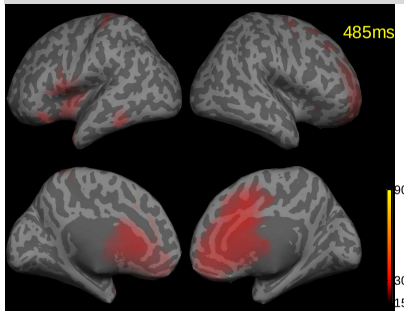		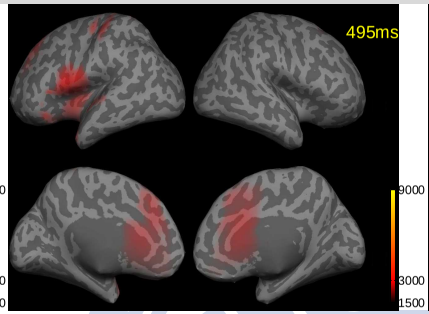		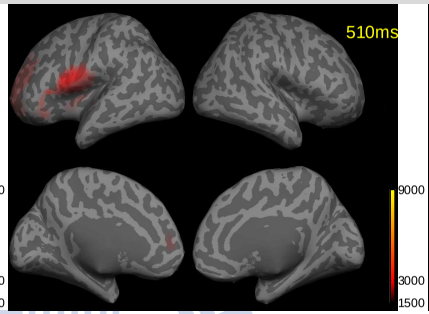		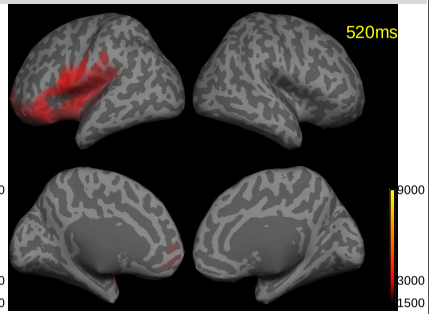	
Left	Right	Left	Right	Left	Right	Left	Right
ACC	ACC	inferior frontal gyrus		inferior frontal gyrus		insula	
	dorsal lateral prefrontal					prefrontal	

530 ms		550 ms		565 ms		580ms	
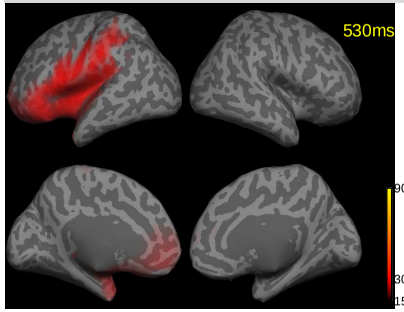		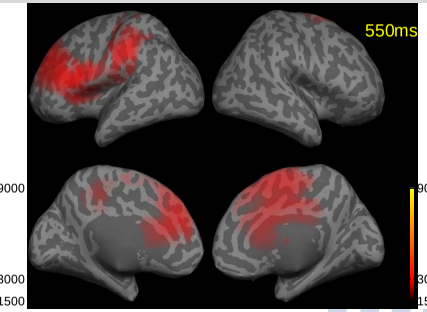		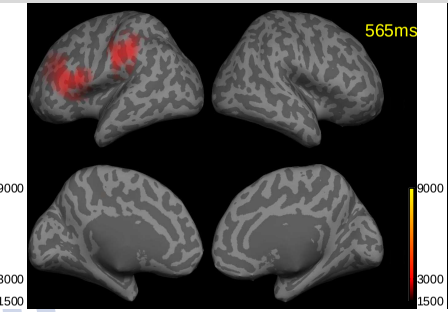		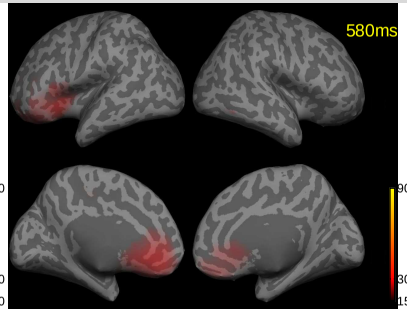	
Left	Right	Left	Right	Left	Right		
sensorimotor cortex		inferior parietal		inferior parietal		obitalfrontal	
somatosensory cortex		middle prefrontal gyrus		inferior frontal			
obitalfrontal							
amygdala							

595 ms
625 ms
655 ms
595ms
625ms
655ms
9000
3000
1500
Left
Right
middle prefrontal cortex
SMA
somatosensory cortex

Chapter 4

Discussion

4.1 Simulation data

We apply our method to the simulation data in Chapter 3.3.1 and Chapter 3.3.2, and the result is accurate. The correlation source localization error is zero mm. It can prove our method can correctly image the distribution.

Furthermore, The result in Figure 4.1(a) is the reconstructed signal at the highest correlation position when we used C2 as the reference signal. The filtered signal is similar to reference signal even there are two source signals at the position. When we used the conventional source localization technique, we can reconstruct the signal containing two sources. The Figure 4.1(b) is the result calculated by MCB. The reconstructed signal is not similar to what we focus on, that is why we need to develop the proposed method to reveal the correlated level according to a specified reference. The reference can be a component decomposed by ICA, a cortical activities inside the brain, or the peripheral signal such as EMG measurement.

4.2 Real data - happy mirror neuron

In the section3.3.3, those highly correlation region are important in the emotional face perception, mirror neuron system. The related emotional face perception regions which have suggested by the past studies are shown as Figure 4.2; And the related mirror neuron regions are shown as Figure 4.3

In Figure 4.2, the area in yellow represent regions about the processing identity and associated semantic information, the area in red represent region involved in emotion analysis, and those in blue represent regions involved in spatial attention. The solid lines mean cortical pathway and dashed lines represent the subcortical route for rapid processing.

At beginning, mirror neuron system is originally discovered in area F5 of the monkey premotor cortex, that discharge both when the monkey does a particular action and when it observes another individual. Later, some evidences show the mirror neuron system is also exit in humans. A large number of studies showed that the observation of actions done by another individual activates a neural network formed by occipital. temporal, parietal and rostral part of inferior parietal lobe and inferior frontal gyrus. These region form the core

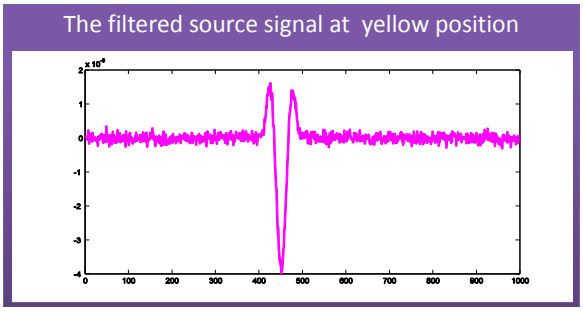

(a)

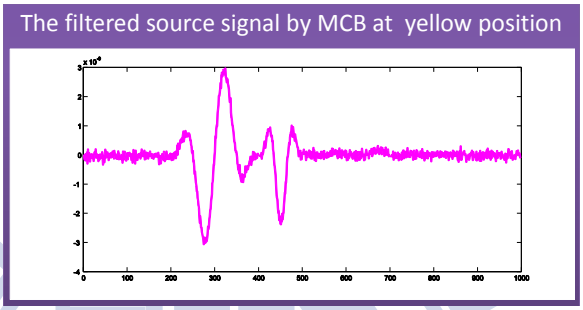

(b)

Figure 4.1: (a) The filtered signal at the yellow position obtained by our method (b) The filtered signal in the yellow position obtained by MCB.

of human mirror neuron system.

If the subject is asked to follow the action of what they see (imitation), some areas would activate more strong, such as left IFG, the right anterior parietal region, the right parietal operculum, and right STS. A study show superior parietal is not present when the subject just instruct to observe.

In Figure 4.3, it represents an extended mirror neuron system was proposed by Pineda [51]. The extended mirror neuron system include insula, middle temporal gyrus and somatosensory cortex. In general, the STS and parietal operculum are not thought as mirror neuron area. However, at the level of transformation performed on the data would make them important. Therefore they are included into extended mirror neuron system.

We collected the significant correlation regions from Table 3.4, Table 3.5 and Table 3.6 and listed them in Table 4.1. These regions are correlated to left inferior frontal gyrus

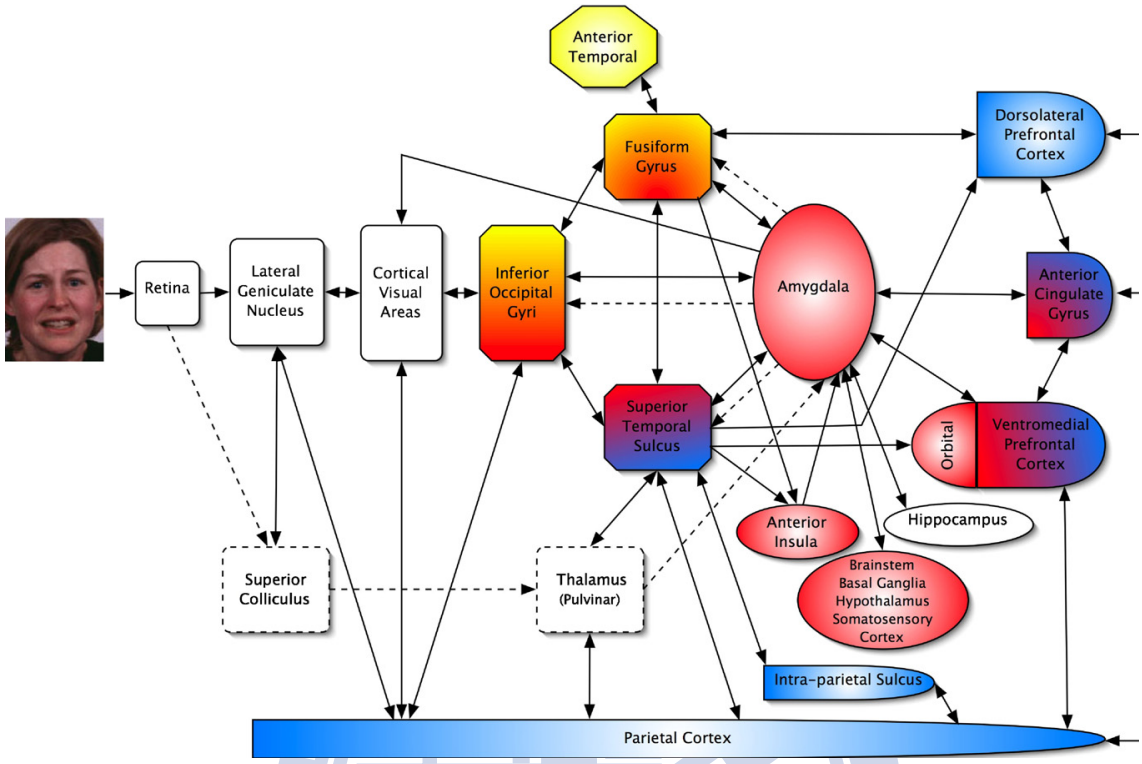

Figure 4.2: Anatomical view of a human brains showing areas involved with the mirror neuron system [50].

on corresponding condition. There correlation regions are highly coherent with previous finding of emotion processing, face perception and the mirror neuron task. The areas correlated the emotion processing and face are amygdala, dorsolateral prefontal cortex, ACC, orbitofrontal cortex, fusiform gyrus, anterior temporal, superior temporal sulcus, occipital and parietal cortex [50, 52–56]. The areas correlated the mirror neuron system are inferior frontal gyrus [51, 57–62], fronto-parietal [63], superior temporal sulcus [51, 59, 60, 64, 65], meddle temporal gyrus [60, 66], insula [51, 56, 60, 66, 67], superior parietal [66], inferior parital [51,59,65,66,68], SMA [51,66], sensorimotor cortex [51], premotor cortex [51,69].

Besides, in imitation and observation condition, we can reveal the automatic smiling at 240 ms and 275 ms respectively as suggested in a previous study suggested [60]. We also find the highly correlation between the left inferior frontal gyrus and the facial movement at 435 ms in the imitation condition, and it is the voluntary smiling. Furthermore,

in observation condition, the facial movement is also highly correlated with the left inferior frontal gyrus at 520 ms. This phenomenon matches the theory of the mirror neuron system [51, 57–59, 61].

Furthermore, a previous finding [70] pointed out the superior parietal lobe is typically not present when subjects are instructed to observe actions without the instruction to imitate them. In our study, we have the same finding. In imitation condition, the left superior parietal is highly correlated to left inferior frontal gyrus at 420 ms. And in execution condition the right superior parietal is highly correlated to the left inferior frontal gyrus at 310 ms. The impossible interpretation of this activation is that the request to imitate produces, through backward projections,sensory copies of the intended actions.

We also observe the correlation pattern in imitation and observation condition is more similar than the execution condition. A possible interpretation is the execution condition is a emotion expression interference effect, the subject has to smile at a neutral face. As [60] suggested, the right hemisphere would enhance at the expression interference effect.

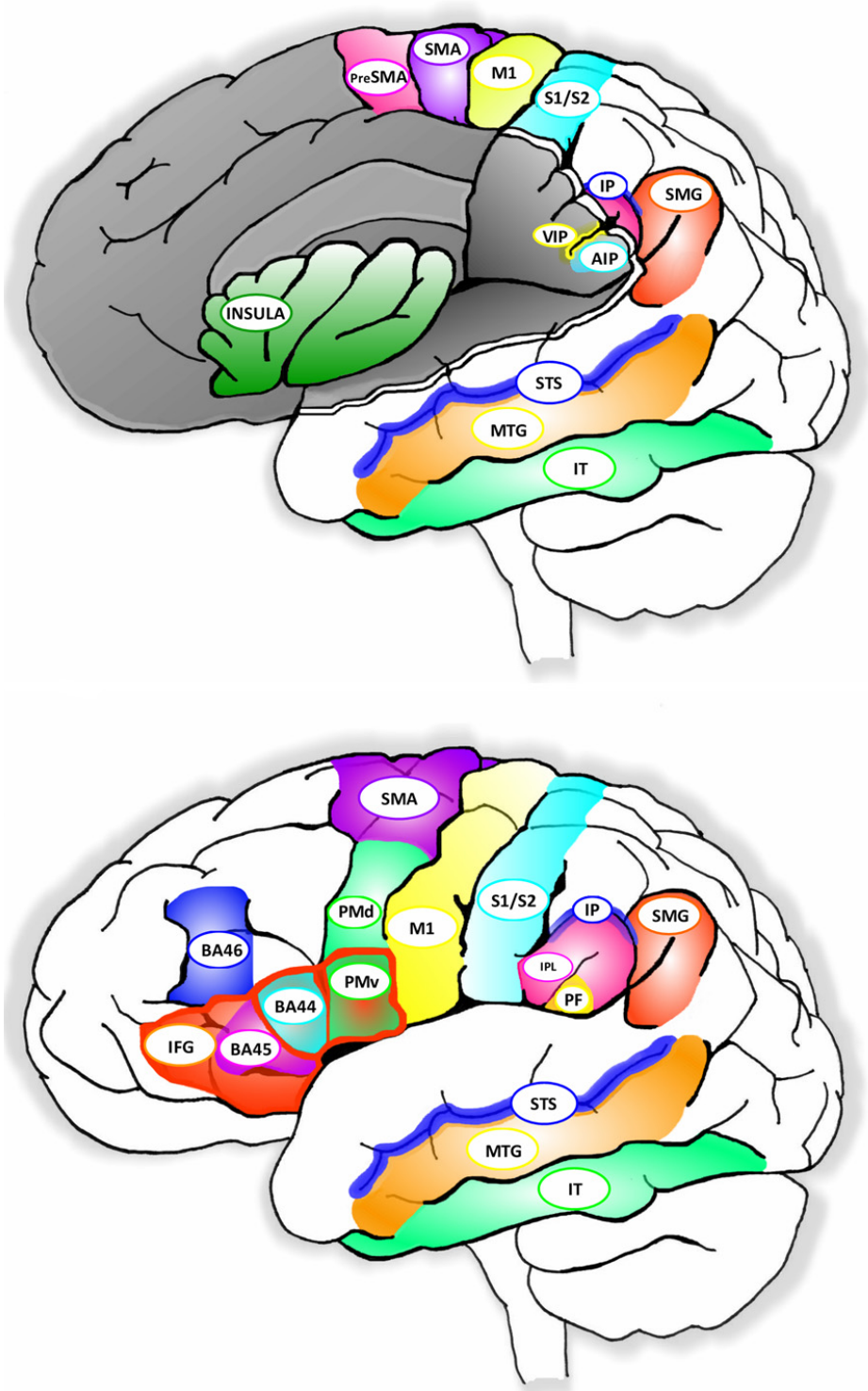

Figure 4.3: Anatomical view of a human brains showing areas involved with the mirror neuron system [51].

Table 4.1: The significant correlation regions of the reference region at left inferior frontal gyrus on imitation, observation and execution condition. If the region have exist at any time, it will be collected in the table.

imitation		observation		execution	
left	right	left	right	left	right
central sulcus	central sulcus	central sulcus	central sulcus	central sulcus	central sulcus
premotor cortex	premotor cortex	premotor cortex	premotor cortex	premotor cortex	premotor cortex
SMA	SMA	SMA	SMA	SMA	
middle prefrontal cortex	middle prefrontal cortex		middle prefrontal cortex	middle preforntal cortex	middle preforntal cortex
sensorimotor cortex		sensorimotor cortex	sensorimotor cortex	sensorimotor cortex	sensorimotor cortex
inferior frontal gyrus		inferior frontal gyrus	inferior frontal gyrus	inferior frontal gyrus	inferior frontal gyrus
middle temporal gyrus		middle temporal gyrus	middle temporal gyrus	middle temporal gyrus	middle temporal gyrus
somatosensory cortex		somatosensory cortex	somatosensory cortex	somatosensory cortex	somatosensory cortex
superior temporal sulcus		superior temporal sulcus	superior temporal sulcus	superior temporal sulcus	superior temporal sulcus
ACC		ACC	ACC	ACC	ACC
dorsolateral prefrontal cortex		dorsolateral prefrontal cortex	dorsolateral prefrontal cortex		dorsolateral prefrontal cortex
amygdala		amygdala	amygdala		amygdala
facial movement		facial movement		facial movement	

imitation		observation		execution	
left	right	left	right	left	right
temporal parietal junction		temporal parietal junction			temporal parietal junction
inferior parietal		inferior parietal		inferior parietal	inferior parietal
orbitofrontal cortex				orbitofrontal cortex	orbitofrontal cortex
superior pariatal					superior parietal
	superior temporal gyrus	superior temporal gyrus	superior temporal gyrus	superior temporal gyrus	
	temporal pole	temporal pole	temporal pole	temporal pole	temporal pole
	angular gyrus	angular gyrus			
	posterior insula cortex			posterior insula	posterior insula
		occipital	occipital	occipital	occipital
		posterior cingulate cortex	posterior cingulate cortex	posterior cingulate cortex	posterior cingulate cortex
			posterior parietal cortex	posterior parietal	posterior parietal
		occipital temporal	occipital temporal		
		occipital parietal	occipital parietal	occipital parietal	occipital parietal
		parieto-occipital fissure			
			inferior temporal gyrus	inferior temporal gyrus	inferior temporal gyrus

imitation		observation		execution	
left	right	left	right	left	right
			poterior insula		
				dorsal stream	
				ventral stream	
				supermarginal	
				superior frontal gyrus	
				supermarginal gyrus	
				medial prefrontal cortex	

E S A
1896

Chapter 5

Conclusion

In this thesis, we have proposed a beamformer-based imaging method of correlated brain activities that can reveal the neural network with similar temporal patterns for information exchange. The method can identify the regions correlated to a specified brain region, called the reference region. In principle, we can apply our method on all pairs of grid points to identify all possible the neural networks of correlated activities.

Our method exploits a maximum-correlation criterion that maximizes the significant level of correlation between the reference region and other regions inside the brain. The maximum correlation criterion helps to analytically and accurately determine the dipole orientation in a closed-form manner and thus determine the spatial filter very efficiently for each position. The correlation map can be calculated to reveal cortical regions with significant similarity to the reference position in the brain.

The experiments with simulation data demonstrated that our method can accurately determine the correlated region. Different from the conventional source localization method, we focus on the areas which have the similar temporal patterns with the reference signal. In the mirror neuron experiment, most of the regions we revealed are reported by the previous finding of emotional processing, face perception and the mirror neuron system. Moreover, we can provide the time information about when these regions are correlated to the neural network.

In summary, the proposed method can be used to directly study dynamic of correlation brain areas based on electromagnetic recordings of brain activities. Given the reference region as one of the areas in the neural network, our method can estimate the the correlated regions at each time point and thus reveal the dynamic behavior of the neural network.

Bibliography

[1] Marco Congedo. *Introduction to the Brain Electromagnetic Problem*.

[2] Clment F. Deriche R. Keriven R. Papadopoulo T. Roberts J. Viville T. Devernay F. Gomes J. Hermosillo G. Kornprobst P. Lingrand D. Faugeras, O. The inverse eeg and meg problems: The adjoint state approach i: The continuous case. Technical report, National Institute for Research in Informatics and Control (INRIA), 1999.

[3] Jan Scholz. The binding problem.

[4] Anne Treisman. The binding problem. *Current Opinion in Neurobiology*, 6:171–l 78, 1996.

[5] Adina L. Roskies. The binding problem. *Neuron*, 24:79, 1999.

[6] A. Engel and W. Singer. Temporal binding and the neural correlates of sensory awareness. *Trends Cogn Sci*, 5(1):16–25, Jan 2001.

[7] Bruno B Averbeck and Daeyeol Lee. Coding and transmission of information by neural ensembles. *Trends Neurosci*, 27(4):225–230, Apr 2004.

[8] E. Salinas and T. J. Sejnowski. Correlated neuronal activity and the flow of neural information. *Nat Rev Neurosci*, 2(8):539–550, Aug 2001.

[9] Christoph von der Malsburg. The correlation theory of brain function. Technical report, Max-Planck-Institute for Biophysical Chemistry, 1981.

[10] C. von der Malsburg. The what and why of binding: the modeler's perspective. *Neuron*, 24(1):95–104, 111–25, Sep 1999.

[11] W. Singer and C. M. Gray. Visual feature integration and the temporal correlation hypothesis. *Annu Rev Neurosci*, 18:555–586, 1995.

[12] A. K. Engel, P. Fries, P. Knig, M. Brecht, and W. Singer. Temporal binding, binocular rivalry, and consciousness. *Conscious Cogn*, 8(2):128–151, Jun 1999.

[13] P. Knig and A. K. Engel. Correlated firing in sensory-motor systems. *Curr Opin Neurobiol*, 5(4):511–519, Aug 1995.

[14] Wolf Singer. *Synchronization, binding and expectancy*. Cambridge, MA: The MIT Press,, 2003.

[15] Alfons Schnitzler and Joachim Gross. Normal and pathological oscillatory communication in the brain. *Nat Rev Neurosci*, 6(4):285–296, Apr 2005.

[16] Geraint Rees, Gabriel Kreiman, and Christof Koch. Neural correlates of consciousness in humans. *Nat Rev Neurosci*, 3(4):261–270, Apr 2002.

[17] S. Baillet, J. C. Mosher, and R. M. Leahy. Electromagnetic brain mapping. *Signal Processing Magazine, IEEE*, 18(6):14–30, 2001.

[18] J. Sarvas. Basic mathematical and electromagnetic concepts of the biomagnetic inverse problem. *Phys Med Biol*, 32(1):11–22, Jan 1987.

[19] J. C. Mosher, R. M. Leahy, and P. S. Lewis. Eeg and meg: forward solutions for inverse methods. *IEEE Trans Biomed Eng*, 46(3):245–259, Mar 1999.

[20] M. Scherg. Fundamentals of dipole source potential analysis. *Advances in audiology*, 6:40–69, 1990.

[21] R. M. Leahy, J. C. Mosher, M. E. Spencer, M. X. Huang, and J. D. Lewine. A study of dipole localization accuracy for meg and eeg using a human skull phantom. *Electroencephalogr Clin Neurophysiol*, 107(2):159–73, 1998.

[22] J. C. Mosher, P. S. Lewis, and R. M. Leahy. Multiple dipole modeling and localization from spatio-temporal meg data. *Biomedical Engineering, IEEE Transactions on*, 39(6):541–557, 1992.

[23] J. C. Mosher and R. M. Leahy. Recursive music: A framework for eeg and meg source localization. *Biomedical Engineering, IEEE Transactions on*, 45(11):1342–1354, 1998.

[24] J. C. Mosher and R. M. Leahy. Source localization using recursively applied and projected (rap) music. *Signal Processing, IEEE Transactions on [see also Acoustics, Speech, and Signal Processing, IEEE Transactions on]*, 47(2):332–340, 1999.

[25] M. S. Hamalainen and R. J. Ilmoniemi. Interpreting magnetic fields of the brain: minimum norm estimates. *Medical and Biological Engineering and Computing*, 32(1):35–42, 1994.

[26] K. Matsuura and Y. Okabe. Selective minimum-norm solution of the biomagnetic inverse problem. 42(6):608–615, June 1995.

[27] K. Uutela, M. Hmlinen, and E. Somersalo. Visualization of magnetoencephalographic data using minimum current estimates. *Neuroimage*, 10(2):173–180, Aug 1999.

[28] G. R. Barnes and A. Hillebrand. Statistical flattening of meg beamformer images. *Human Brain Mapping*, 18(1):1–12, 2003.

[29] B. D. Van Veen and K. M. Buckley. Beamforming: a versatile approach to spatial filtering. *ASSP Magazine, IEEE [see also IEEE Signal Processing Magazine]*, 5(2):4–24, 1988.

[30] B. D. VanVeen, W. vanDrongelen, M. Yuchtman, and A. Suzuki. Localization of brain electrical activity via linearly constrained minimum variance spatial filtering. *Ieee Transactions on Biomedical Engineering*, 44(9):867–880, 1997.

[31] S. E. Robinson and J. Vrba. Functional neuroimaging by synthetic aperture magnetometry (sam). *Recent Advances in Biomagnetism*, page 302V305, 1999.

[32] K. Sekihara, S. S. Nagarajan, D. Poeppel, and A. Marantz. Asymptotic snr of scalar and vector minimum-variance beamformers for neuromagnetic source reconstruction. *Ieee Transactions on Biomedical Engineering*, 51(10):1726–1734, 2004.

[33] J. Vrba and S. E. Robinson. Differences between synthetic aperture magnetometry (sam) and linear beamformers. *Biomag*, page 681V684, 2000.

[34] Arjan Hillebrand and Gareth R Barnes. The use of anatomical constraints with meg beamformers. *Neuroimage*, 20(4):2302–2313, Dec 2003.

[35] Y. S. Chen, C. Y. Cheng, J. C. Hsieh, and L. F. Chen. Maximum contrast beamformer for electromagnetic mapping of brain activity. *IEEE TRANSACTIONS ON BIOMEDICAL ENGINEERING*, 53(9):1765–1774, 2006.

[36] C. Andrew and G. Pfurtsheller. Ecent-related coherence as a tool for studying dynamic interaction of brain regions. *Electroencephalogr. Clin. Neurophysiol.*, 98:144–148, 1996.

[37] M. Kaminski, K. Blinowska, and W. Szelenberger. Topographic analysis of coherence and propagation of EEG activity during sleep and wakefulness. *Electroencephalogr. Clin. Neurophysiol.*, 102:216–227, 1997.

[38] R. Saab, M. J. McKeown, L. J. Myers, and R. Abu-Gharbieh. A wavelet based approach for the detection of coupling in EEG signals. In *Proceedings of the 2nd International IEEE EMBS Conference on Neural Engineering*, pages 616–620, Arlington, Virginia, March 2005.

[39] L. Leocani, C. Toro, P.Manganotti, P. Zuang, and M. Hallett. Event-related coherence and event-related desynchronization/synchronization in the 10 hz and 20 hz eeg during self-paced movements. *Electroencephalogr. Clin. Neurophysiol.*, 104:199–206, 1997.

[40] J. P. Lachaux, A. Lutz, D. Rudrauf, D. Cosmelli, M. L. V. Quyen, J. Martinerie, and F. Varela. Estimating the time-course of coherence between single-trial brain signals: an introduction to wavelet coherence. *Neurophysiol Clin.*, 32:175–174, 2002.

[41] T. H. Li and W. R. Klemm. Detection of cognitive binding during ambiguous figure tasks by wavelet coherence analysis of EEG signals. In *Proceedings of the 15th International Conference on Pattern Recognition*, Barcelona, Spain, September 2000.

[42] Arthur C. Leuthold Frederick J. P. Langheim and Apostolos P. Georgopoulos. Synchronous dynamic brain networks revealed by magnetoencephalography. *Proc Natl Acad Sci U S A*, 103:455–459, 2006.

[43] J.B. Deijen E.Ch. Wolters C.J. Stam D. Stoffers, J.L.W. Bosboom and H.W. Berendsea. Increased cortico-cortical functional connectivity in early-stage parkinson's disease: An meg study. *NeuroImage*, 41:212222, 2008.

[44] Ph. Scheltens B.W. van Dijk E.J. Jonkman H.W. Berendse, J.P.A. Verbunt. Magnetoencephalographic analysis of cortical activity in alzheimer's disease: a pilot study. *Clinical Neurophysiology*, 111:604–612, 2000.

[45] Sari Himanen and Joel Hasan. Limitations of rechtschaffen and kales. *Sleep Med Rev*, 4(2):149–167, Apr 2000.

[46] J. Gross, J. Kujala, M. Hamalainen, L. Timmermann, A. Schnitzler, and R. Salmelin. Dynamic imaging of coherent sources: Studying neural interactions in the human brain. *Proc Natl Acad Sci U S A*, 98(2):694–699, Jan 2001.

[47] E. N. Bruce. *Biomedical signal processing and signal modeling*. J. Wiley, 2001.

[48] M. A. Uusitalo and R. J. Ilmoniemi. Signal-space projection method for separating meg or eeg into components. *Medical and Biological Engineering and Computing*, 35(2):135–140, 1997.

[49] S. Taulu, M. Kajola, and J. Simola. Suppression of interference and artifacts by the signal space separation method. *Brain Topography*, 16(4):269–275, 2004.

[50] Romina Palermo and Gillian Rhodes. Are you always on my mind? a review of how face perception and attention interact. *Neuropsychologia*, 45(1):75–92, Jan 2007.

[51] Jaime A Pineda. Sensorimotor cortex as a critical component of an 'extended' mirror neuron system: Does it solve the development, correspondence, and control problems in mirroring? *Behav Brain Funct*, 4:47, 2008.

[52] Haxby, Hoffman, and Gobbini. The distributed human neural system for face perception. *Trends Cogn Sci*, 4(6):223–233, Jun 2000.

[53] Ingrid R Olson, Alan Plotzker, and Youssef Ezzyat. The enigmatic temporal pole: a review of findings on social and emotional processing. *Brain*, 130(Pt 7):1718–1731, Jul 2007.

[54] J. S. Morris, A. Ohman, and R. J. Dolan. Conscious and unconscious emotional learning in the human amygdala. *Nature*, 393(6684):467–470, Jun 1998.

[55] Chris D Frith. The social brain? *Philos Trans R Soc Lond B Biol Sci*, 362(1480):671–678, Apr 2007.

[56] Laurie Carr, Marco Iacoboni, Marie-Charlotte Dubeau, John C Mazziotta, and Gian Luigi Lenzi. Neural mechanisms of empathy in humans: a relay from neural systems for imitation to limbic areas. *Proc Natl Acad Sci U S A*, 100(9):5497–5502, Apr 2003.

[57] Gorana Pobric and Antonia F de C Hamilton. Action understanding requires the left inferior frontal cortex. *Curr Biol*, 16(5):524–529, Mar 2006.

[58] Jeremy D W Greenlee, Hiroyuki Oya, Hiroto Kawasaki, Igor O Volkov, Olaf P Kaufman, Christopher Kovach, Matthew A Howard, and John F Brugge. A functional connection between inferior frontal gyrus and orofacial motor cortex in human. *J Neurophysiol*, 92(2):1153–1164, Aug 2004.

[59] Nobuyuki Nishitani and Riitta Hari. Viewing lip forms: cortical dynamics. *Neuron*, 36(6):1211–1220, Dec 2002.

[60] Tien-Wen Lee, Raymond J Dolan, and Hugo D Critchley. Controlling emotional expression: behavioral and neural correlates of nonimitative emotional responses. *Cereb Cortex*, 18(1):104–113, Jan 2008.

[61] Istvan Molnar-Szakacs, Marco Iacoboni, Lisa Koski, and John C Mazziotta. Functional segregation within pars opercularis of the inferior frontal gyrus: evidence from

fmri studies of imitation and action observation. *Cereb Cortex*, 15(7):986–994, Jul 2005.

[62] Lisa Aziz-Zadeh, Lisa Koski, Eran Zaidel, John Mazziotta, and Marco Iacoboni. Lateralization of the human mirror neuron system. *J Neurosci*, 26(11):2964–2970, Mar 2006.

[63] Istvan Molnar-Szakacs, Jonas Kaplan, Patricia M Greenfield, and Marco Iacoboni. Observing complex action sequences: The role of the fronto-parietal mirror neuron system. *Neuroimage*, 33(3):923–935, Nov 2006.

[64] M. Iacoboni, L. M. Koski, M. Brass, H. Bekkering, R. P. Woods, M. C. Dubeau, J. C. Mazziotta, and G. Rizzolatti. Reafferent copies of imitated actions in the right superior temporal cortex. *Proc Natl Acad Sci U S A*, 98(24):13995–13999, Nov 2001.

[65] Laetitia Golay, Armin Schnider, and Radek Ptak. Cortical and subcortical anatomy of chronic spatial neglect following vascular damage. *Behav Brain Funct*, 4:43, 2008.

[66] Tien-Wen Lee, Oliver Josephs, Raymond J Dolan, and Hugo D Critchley. Imitating expressions: emotion-specific neural substrates in facial mimicry. *Soc Cogn Affect Neurosci*, 1(2):122–135, Sep 2006.

[67] Jennifer H Pfeifer, Marco Iacoboni, John C Mazziotta, and Mirella Dapretto. Mirroring others' emotions relates to empathy and interpersonal competence in children. *Neuroimage*, 39(4):2076–2085, Feb 2008.

[68] Leonardo Fogassi, Pier Francesco Ferrari, Benno Gesierich, Stefano Rozzi, Fabian Chersi, and Giacomo Rizzolatti. Parietal lobe: from action organization to intention understanding. *Science*, 308(5722):662–667, Apr 2005.

[69] Juha Jrvelinen, Martin Schrmann, and Riitta Hari. Activation of the human primary motor cortex during observation of tool use. *Neuroimage*, 23(1):187–192, Sep 2004.

[70] Luigi Cattaneo and Giacomo Rizzolatti. Themirror-neuron system. *Annu. Rev. Neurosci.*, 27:169–192, 2004.